

MULTICOMPONENT CRYSTALS OF NITROFURAZONE

by

KUDZAISHE NIGEL SHARARA

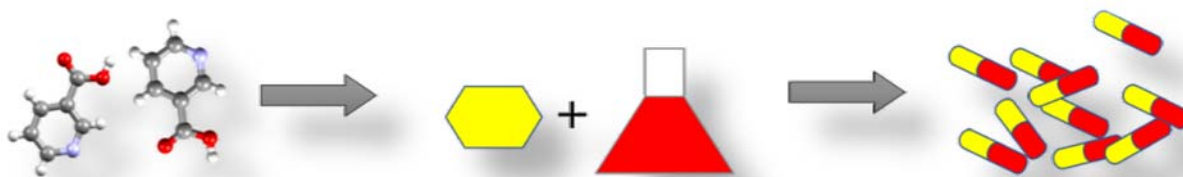
212279440

Thesis submitted in fulfilment of the requirements for the degree
Master of Applied Science in Chemistry
in the Faculty of Applied Sciences
at Cape Peninsula University of Technology

Supervisor: Prof Nikoletta B. Báthori

Co-Supervisor: Dr Merrill M. Wicht

2018



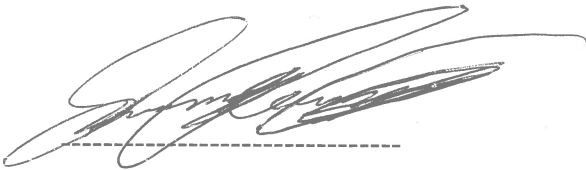
The financial assistance of the National Research Foundation towards this research is acknowledged. Opinions expressed in this thesis and the conclusions arrived at, are those of the author, and are not necessarily to be attributed to the National Research Foundation

CPUT copyright information

The thesis may not be published either in part (in scholarly, scientific or technical journals) or in whole (as a monograph), unless permission has been obtained from the University

Declaration

I, SHARARA KUDZAI SHE NIGEL, declare that the contents of this project represent my own unaided work and that the project has not been previously submitted for academic examination towards any qualification. Furthermore, it represents my own opinions and not necessarily those of Cape Peninsula University of Technology.



SIGNATURE

03/09/2018

DATE

Acknowledgements

Special thanks go to:

- My supervisor, Professor Nikoletta B. Báthori for guiding and overseeing my whole project.
- My co-supervisor Dr Merrill M. Wicht for overseeing my project.
- Dr Gerhard A. Venter (University of Cape Town) for the computational work
- Kudzanai Nyamayaro and Kelly Shunje for the continuous encouragement and academic input throughout my study.
- Tsitsi Dorcas Dhitima for all the support throughout the research period.
- My loving family for their support and care.

Despite the various setbacks I encountered as a student, working with them has been exciting and worthwhile.

Abstract

Physicochemical property enhancement of drugs is one of the focus areas of the pharmaceutical industry. This research demonstrates how crystal engineering methods offer a practical way to make systematic solid state modifications of active pharmaceutical ingredients.

Nitrofurazone ((5-nitro-2-furaldehydesemicarbazone), NFZ) was selected for multicomponent crystal formation, in order to improve its aqueous solubility without modification of its molecular structure. NFZ has both hydrogen bond donor and hydrogen bond acceptor groups on its semicarbazone chain; therefore, it seemed to be a suitable target to use synthon engineering principles to form a series of multicomponent crystals. Also, the torsional flexibility of the NFZ molecule suggested great adaptability of the molecule and thus good potential for forming a variety of crystalline solids with the selected co-formers. Surprisingly, 95% of the time the co-crystallisation experiments failed and the α -, β - or γ -polymorph of NFZ were obtained. The α -polymorph of NFZ was known since 1994. Parallel to this work, room temperature crystal structures of the β - and γ -polymorphs were reported by an independent research group. Although the crystal structures presented in this thesis were collected at 173 K, they are essentially the same as the already published ones with the obvious difference between the atomic thermal ellipsoids.

Multicomponent crystals of NFZ were formed only when the API was exposed to perchloric acid (HClO_4), phosphoric acid (H_3PO_4) and propionic acid (PA). These crystallisations resulted in the formation of $4\text{NFZ}\cdot[\text{H}_3\text{O}^+][\text{ClO}_4^-]$, $\text{NFZ}\cdot\text{H}_3\text{PO}_4$ and $\text{NFZ}\cdot\text{PA}$ crystals, respectively. The crystal structures were analysed with single crystal X-ray diffraction and the bulk properties of the material were analysed using powder X-ray diffraction, thermo-analytical methods and Fourier transform infrared spectroscopy.

The most significant observation of the project was the extreme difficulty of the multicomponent crystal formation of NFZ, even though the API has great hydrogen bonding capabilities associated with torsional flexibility. To understand this behaviour, the solid state behaviour of the semicarbazone moiety was analysed with the aid of data retrieved from the Cambridge Structural Database. The torsional flexibility of the semicarbazone moiety was also investigated and the most common conformers were identified; and these results were supported by the findings of computational methods.

Table of contents

Declaration.....	i
Acknowledgements.....	ii
Abstract.....	iii
List of figures.....	vi
Appendix figures.....	viii
List of tables.....	xi
Key terms.....	xii
List of symbols.....	xiii
Atom colour codes.....	xiv
Chapter 1.....	xv
1 Introduction.....	1
1.1 History of drugs.....	1
1.2 Advent of the pharmaceutical industry.....	2
1.3 Pharmaceutical design.....	3
1.4 Types of solids.....	3
1.5 Design stages.....	4
1.6 Crystal engineering.....	6
1.7 Polymorphism.....	8
1.8 Multicomponent systems.....	11
1.9 Pharmaceutical salts.....	12
1.10 Nitrofurazone (NFZ).....	14
1.11 Statement of research problem.....	15
1.12 Objectives of the research.....	15
1.13 Research hypothesis.....	16
References.....	17
Chapter 2.....	25
2 Materials and methods.....	26
2.1 Materials.....	26
2.2 Engineering multicomponent crystals.....	26
2.3 Methods of crystal growth.....	28
2.3.1 Crystallization in solution.....	28
2.3.2 Liquid-assisted grinding.....	29
2.4 Crystal growth.....	30
2.5 Analytical tools.....	32

2.5.1	Single crystal X-ray diffraction (SCXRD)	32
2.5.2	Powder X-ray diffraction (PXRD).....	34
2.5.3	Differential Scanning Calorimetry (DSC)	34
2.5.4	Thermogravimetric analysis (TGA).....	35
2.5.5	Fourier Transform Infra-Red Spectroscopy (FT-IR).....	35
2.5.6	Optical microscopy	35
References.....		36
Chapter 3.....		38
3	Polymorphs of NFZ.....	39
3.1	Crystal structures of NFZ polymorphs.....	42
3.2	Bulk property analysis of NFZ polymorphs.....	48
3.2.1	Powder X-ray diffraction of NFZ polymorphs	48
3.2.2	Thermal analysis of NFZ polymorphs	49
3.2.3	FTIR spectroscopy of NFZ polymorphs.....	52
References.....		55
Chapter 4.....		56
4	Multicomponent crystals of nitrofurazone	57
4.1	Crystal structure of 4NFZ·[H ₃ O ⁺][ClO ₄ ⁻]	58
4.2	Crystal structure of NFZ·H ₃ PO ₄	63
4.3	Crystal structure of NFZ·PA	67
4.4	Bulk property analysis of multicomponent crystals of NFZ.....	71
4.4.1	Powder X-ray diffraction of multicomponent crystals of NFZ	71
4.4.2	Thermal analysis of multicomponent crystals of NFZ	74
4.4.3	FTIR analysis of the multicomponent crystals of NFZ	78
References.....		82
Chapter 5.....		83
5	CSD analysis of the semicarbazone moiety	84
5.1	Hydrogen bonding of the semicarbazone fragment	84
5.2	Conformational analysis.....	88
References.....		96
Chapter 6.....		97
6	Summary and conclusion.....	98
Appendix.....		100

List of figures

Figure 1.1 Classic examples of pharmaceutical compounds from antiquity	1
Figure 1.2 One of the first drugs to be utilized in the pharmaceutical industry	3
Figure 1.3 Characteristic supramolecular synthons involved in multicomponent crystal systems	7
Figure 1.4 Typical synthon polymorphism (left: heterosynthon and acid-acid homosynthon; right: heterosynthon and hydroxyl-acid heterosynthon) exhibited in crystals of 4-hydroxybenzoic acid and 2,3,5,6-tetramethylpyrazine (figure re-made)	9
Figure 1.5 Packing diagram of the artemisinin orthorhombic (left) and triclinic (right) cell viewed down the crystallographic <i>c</i> axis	9
Figure 1.6: Conformational polymorphism demonstrated in bezafibrate. The two structurally differ at the carboxylic acid hydrogen	10
Figure 1.7 Pharmaceuticals that failed on the market due to polymorphic tendencies	11
Figure 1.8 HCl pharmaceutical salts	13
Figure 1.9 Nitrofurazone (5-nitro-2-furaldehydesemicarbazone, NFZ)	16
Figure 2.1 Flow chart of crystallisation work	27
Figure 3.1 Differences in morphology and colour for the three polymorphs	42
Figure 3.2 Eight possible conformers arising from the <i>sp</i> and <i>ap</i> torsion combinations. Newly found conformer in NFZ•H ₃ PO ₄ molecule is circled in red	44
Figure 3.3 Conformers observed in the known polymorphs	45
Figure 3.4 Hydrogen bonded interactions between the NFZ tapes	46
Figure 3.5 Representation of the slight difference in the NFZ conformers in the β- and γ-polymorphs	46
Figure 3.6 Packing of the parallel sheets in the NFZ polymorphs	47
Figure 3.7 Generated SCXRD patterns of α-, β- and γ-polymorphs and PXRD pattern of NFZ starting material	48
Figure 3.8 DSC curves of α form against the starting material (β form)	51
Figure 3.9 DSC curves of γ form against starting material (β form)	51
Figure 3.10 IR spectra of the three polymorphic forms	53
Figure 4.1 The pKa values of NFZ calculated with Marvin	57

Figure 4.2 Photograph of uncut $4\text{NFZ}\cdot[\text{H}_3\text{O}^+][\text{ClO}_4^-]$ co-crystal salt	58
Figure 4.3 ASU of $4\text{NFZ}\cdot[\text{H}_3\text{O}^+][\text{ClO}_4^-]$ showing the hydrogen bonds between the four symmetry independent NFZ molecules (labelled as A-D) and the hydronium ion (perchlorate anion is omitted for clarity).....	59
Figure 4.4 Hydrogen bonds between the neighbouring NFZ molecules to hold the tetramers together. (The hydronium ions and the perchlorate anions are omitted for clarity).....	59
Figure 4.5 Embedded perchlorate ions in the layer of tetramers. (Perchlorate ions are presented in space fill view)	62
Figure 4.6 Hydrogen bonding of ClO_4^- between the layers of tetramers.....	63
Figure 4.7 An uncut crystal of $\text{NFZ}\cdot\text{H}_3\text{PO}_4$	63
Figure 4.8 The asymmetric unit of $\text{NFZ}\cdot\text{H}_3\text{PO}_4$	64
Figure 4.9 Hydrogen bonding between the coplanar NFZ molecules and the adjacent phosphoric acids	65
Figure 4.10 Hydrogen bonding between adjacent phosphoric acid molecules in $\text{NFZ}\cdot\text{H}_3\text{PO}_4$	66
Figure 4.11 The packing of $\text{NFZ}\cdot\text{H}_3\text{PO}_4$ viewed down a (a) and showing the layered nature of the structure (b).....	67
Figure 4.12 Uncut crystal of $\text{NFZ}\cdot\text{PA}$	67
Figure 4.13 Asymmetric unit of $\text{NFZ}\cdot\text{PA}$. Molecular units are labelled as A, B, C and D. Full numbering scheme of non-hydrogen atoms for unit A is shown.....	69
Figure 4.14 The complex hydrogen bond network in the ASU.....	69
Figure 4.15 Packing of hydrogen bonded tetramers of $\text{NFZ}\cdot\text{PA}$ viewed down b (a) and down a (b).....	71
Figure 4.16 PXRD patterns of the samples prepared with different methods of $4\text{NFZ}\cdot[\text{H}_3\text{O}^+][\text{ClO}_4^-]$	72
Figure 4.17 PXRD patterns of the samples prepared with different methods of $\text{NFZ}\cdot\text{H}_3\text{PO}_4$	73
Figure 4.18 PXRD patterns of the samples prepared with different methods of $\text{NFZ}\cdot\text{PA}$	73
Figure 4.19 DSC curves of $4\text{NFZ}\cdot[\text{H}_3\text{O}^+][\text{ClO}_4^-]$ bulk material and samples obtained from LAG	74
Figure 4.20: Thermal analysis curve showing steps of mass loss of $4\text{NFZ}\cdot[\text{H}_3\text{O}^+][\text{ClO}_4^-]$	75
Figure 4.21 DSC curve of NFZ starting material, $4\text{NFZ}\cdot[\text{H}_3\text{O}^+][\text{ClO}_4^-]$ and $\text{NFZ}\cdot\text{H}_3\text{PO}_4$ bulk material	76
Figure 4.22 Thermal analysis curve showing weight loss in $\text{NFZ}\cdot\text{H}_3\text{PO}_4$ bulk material	76

Figure 4.23 DSC and DTA curves of NFZ•PA	77
Figure 4.24 FTIR spectra of NFZ and 4NFZ•[H ₃ O ⁺][ClO ₄ ^-].....	79
Figure 4.25 FTIR spectra of NFZ and NFZ•H ₃ PO ₄	80
Figure 4.26 FTIR spectra of NFZ and NFZ•PA	81
Figure 5.1 Possible bonding sites in the semicarbazone functionality. Site 1-4 are hydrogen bond donors and 5* and 6* are hydrogen bond acceptor	84
Figure 5.2 CSD hits for the selected fragments	85
Figure 5.3 Hits obtained from the hydrogen bond motif search, where X is any atom.....	87
Figure 5.4 Polar histogram showing τ_1 frequency distribution.....	89
Figure 5.5 Polar histogram showing τ_2 frequency distribution.....	89
Figure 5.6 Polar histogram showing τ_3 frequency distribution.....	90
Figure 5.7 Occurrence of semicarbazone conformers in the CSD.....	94
Figure 5.8 Low energy molecular conformations of NFZ obtained from gas phase calculations	95

Appendix figures

Figure A 1 PXRD patterns of α , β , and γ -polymorphs and the crystal obtained from methanol	101
Figure A 2 PXRD patterns of α , β , and γ -polymorphs and the crystal obtained from acetone	101
Figure A 3 PXRD patterns of α , β , and γ -polymorphs and the crystal obtained from dimethylformamide	102
Figure A 4 PXRD patterns of α , β , and γ -polymorphs and the crystal obtained from tetrahydrofuran	102
Figure A 5 PXRD patterns of α , β , and γ -polymorphs and the crystal obtained from 2-picoline	103
Figure A 6 PXRD patterns of α , β , and γ -polymorphs and the crystal obtained from 4-picoline	103
Figure A 7 PXRD patterns of α , β , and γ -polymorphs and the crystal obtained from 3,4-lutidine	104

Figure A 8 PXRD patterns of α , β , and γ -polymorphs and the crystal obtained from dioxane	104
Figure A 9 PXRD patterns of α , β , and γ -polymorphs and the crystal obtained from pyridine	105
Figure A 10 PXRD patterns of α , β , and γ -polymorphs and the crystal obtained from dimethylacetamide.....	105
Figure A 11 PXRD patterns of α , β , and γ -polymorphs and the crystal obtained from isopropanol	106
Figure A 12 PXRD patterns of α , β , and γ -polymorphs and the crystal obtained from 2-aminopyridine.....	106
Figure A 13 PXRD patterns of α , β , and γ -polymorphs and the crystal obtained from acetonitrile	107
Figure A 14 PXRD patterns of α , β , and γ -polymorphs and the crystal obtained from aspirin:isopropanol:H ₂ O	107
Figure A 15 PXRD patterns of α , β , and γ -polymorphs and the crystal obtained from acetamide:cetonitrile.....	108
Figure A 16 DSC curves showing NFZ starting material and NFZ crystals obtained from dimethylformamide	108
Figure A 17 DSC curves showing NFZ starting material and NFZ crystals obtained from acetone.....	109
Figure A 18 DSC curves showing NFZ starting material and NFZ crystals obtained from tetrahydrofuran	109
Figure A 19 DSC curves showing NFZ starting material and NFZ crystals obtained from picoline	110
Figure A 20 DSC curves showing NFZ starting material and NFZ crystals obtained from 2-aminopyridine-ethanol.....	110
Figure A 21 DSC curves showing NFZ starting material and NFZ crystals obtained from isopropanol	111
Figure A 22 DSC curves showing NFZ starting material and NFZ crystals obtained from methanol	111
Figure A 23 DSC curves showing NFZ starting material and NFZ crystals obtained from methylethylketone	112
Figure A 24 DSC curves showing NFZ starting material and NFZ crystals obtained from 4-picoline	112

Figure A 25 DSC curves showing NFZ starting material and NFZ crystals obtained from pyridine.....	113
Figure A 26 DSC curves showing NFZ starting material and NFZ crystals obtained from 2-aminopyridine-isopropanol.....	113
Figure A 27 DSC curves showing NFZ starting material and NFZ crystals obtained from 3,4-lutidine.....	114
Figure A 28 DSC curves showing NFZ starting material and NFZ crystals obtained from 2,3-lutidine.....	114
Figure A 29 DSC curves showing NFZ starting material and NFZ crystals obtained from dimethylacetamide.....	115
Figure A 30 DSC curves showing NFZ starting material and NFZ crystals obtained from acetamide:acetonitrile.....	115
Figure A 31 DSC curves showing NFZ starting material and NFZ crystals obtained from aspirin:isopropanol:H ₂ O.....	116
Figure A 32 Thermal analysis curve of NFZ starting material (β -polymorph).....	116
Figure A 33 Thermal analysis curve of NFZ_acetone crystals (α -polymorph).....	117
Figure A 34 Thermal analysis curve of NFZ_tetrahydrofuran crystals (β -polymorph).....	117
Figure A 35 Thermal analysis curve of NFZ_IPrOH crystals (γ -polymorph).....	118
Figure A 36 Infra-red spectra of NFZ starting material and NFZ crystals obtained from acetone.....	118
Figure A 37 Infra-red spectra of NFZ starting material and NFZ crystals obtained from.....	119
Figure A 38 Infra-red spectra of NFZ starting material and NFZ crystals obtained from.....	119
Figure A 39 Infra-red spectra of NFZ starting material and NFZ crystals obtained from.....	120

List of tables

Table 1.1 Properties of a crystalline solid.....	4
Table 1.2 Characteristics and properties of hydrogen bonds.....	6
Table 1.3 Predicted properties of nitrofurazone	16
Table 2.1 List of solvents/co-formers applied in cocrystallization experiments	27
Table 2.2 Typical crystallisation methods	29
Table 3.1 Crystallographic data of the three polymorphic forms collected at low (LT) or room temperature (RT).	40
Table 3.2 List of general solvents used and their respective crystallizations	41
Table 3.3 Torsion angle classes	43
Table 3.4 Torsion angles of polymorphs α , β and γ	45
Table 3.5 Geometric parameters for the intermolecular interactions in the three polymorphs	47
Table 3.6 DSC data for NFZ crystals obtained from crystallizations.....	50
Table 3.7 Molecular vibrations observed in the FTIR spectra of the polymorphic forms.....	54
Table 4.1 List of acid solvents used and their respective crystallizations	57
Table 4.2 Crystallographic data of the three multicomponent crystals of NFZ.....	60
Table 4.3 The geometric parameters for intermolecular interactions in $4\text{NFZ}\cdot[\text{H}_3\text{O}^+][\text{ClO}_4^-]$	61
Table 4.4 The geometric parameters for intermolecular interactions in $\text{NFZ}\cdot\text{H}_3\text{PO}_4$	66
Table 4.5 Hydrogen bonds in $\text{NFZ}\cdot\text{PA}$	70
Table 4.6 DSC data of multicomponent crystals of NFZ	77
Table 4.7 TGA data of multicomponent crystals of NFZ.....	77
Table 4.8 Molecular vibrations observed in the spectra of ClO_4^- , H_3PO_4 and PA.....	81
Table 5.1 Frequency of occurrence for each synthon pair, where X is any atom.....	88
Table 5.2 Relevant torsion angles and their resulting conformation (continued to page 94) ..	90

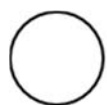
Key terms

Co-crystal	crystalline complex of two or more solid components that are held together by non-covalent interactions, mostly hydrogen bonding
Conformation	one of the spatial arrangements of atoms in a molecule that can come about through free rotation of the atoms about a single chemical bond
Co-former	the compound used for co-crystallisations
Bioavailability	refers to the extent and rate at which the active drug or metabolite enters to the systemic circulation, thereby accessing the site of action
Supramolecular	chemical systems made up of a discrete number of molecular subunits held together with intermolecular forces varying from weak to strong
Amorphous	solid form of a material which lacks positional order on the molecular scale
Polymorph	one of two or more different crystal structures of the same compound
Synthon	a structural unit within a molecule which presents predictable ability to form interactions with complementary functional groups
Salt	the product of a neutralization reaction between an acid and a base
Hydrate	a compound, typically a crystalline one, in which water molecules are chemically bound to another compound or an element
Solvate	a chemical compound formed by an interaction between a solvent and a solute

List of symbols

a, b, c	unit cell axes (Å)
α	designates angle between unit cell b and c axes (°) also alpha polymorph of nitrofurazone (CSD code: WERVEU)
β	designates angle between unit cell a and c axes (°) also beta polymorph of nitrofurazone (CSD code: WERVEU01)
γ	designates angle between unit cell a and b axes (°) also gamma polymorph of nitrofurazone (CSD code: WERVEU02)
τ	torsion angle (°)
API	Active Pharmaceutical Ingredient
bp	Boiling point (°C)
CSD	Cambridge Structural Database
DSC	Differential Scanning Calorimetry
LAG	Liquid Assisted Grinding
mp	Melting point (°C)
Mr	Molecular mass (g mol ⁻¹)
NFZ	Nitrofurazone
PA	Propionic acid
PXRD	Powder X-ray diffraction
SBC	Solvent Based Crystallization
SCXRD	Single Crystal X-Ray Diffraction
T _{onset}	Onset temperature (°C)
T _{peak}	Peak temperature (°C)
TG	Thermogravimetry
V	Unit cell volume (Å ³)
Z	number of formula units per unit cell

Atom colour codes



Hydrogen



Carbon



Nitrogen



Oxygen




Sulfur



Chlorine

CHAPTER 1

A blue decorative graphic consisting of a solid blue rectangle on the left that tapers to a point on the right, with a lighter blue gradient overlaying it.

Chapter 1 introduces the area of research by giving a contextual history of drugs and the pharmaceutical industry and motivates the reason for the study of solid state chemistry and application of synthon engineering principles in the same field.

1 Introduction

1.1 History of drugs

Drugs and medicines, from as early as 300 BC, were already being manipulated and contributing to human health and welfare.¹ First known reports on medicines were documented by Mesopotamians way before that, which suggests their prehistoric origin. Greek scientists and thinkers such as Hippocrates and Theophrastus dominated the medical and pharmaceutical arenas. Hippocrates is said to have written many books explaining how diseases might be treated using certain natural products. His use of the aspen tree bark for alleviating pain has been reported.² It was only in the nineteenth century that Leroux³ extracted the active ingredient from aspen bark.⁴ Aspirin is derived from this naturally occurring glucoside, known as salicin (Figure 1.1).⁴ Figure 1.1 shows various compounds used as medicine in the ancient world.

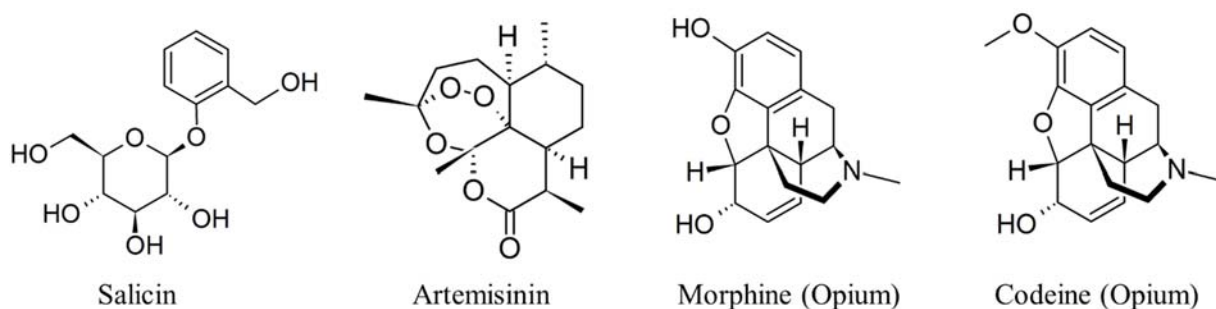


Figure 1.1 Classic examples of pharmaceutical compounds from antiquity

Another interesting medicinal compound is Artemisinin from East Asia; obtained from the Annual Mugwort plant. Artemisinin is built from three isoprene units and a rare peroxide linkage.⁵ Tu Youyou became the 2015 Nobel Prize laureate in Medicine for discovering and isolating artemisinin. She managed to obtain the drug from the herb by performing her isolation experiments at cold temperatures.^{6,7} Youyou is not the first to handle the Mugwort since it was reported ca. two millennia ago. The plant provided medicine for treating febricity and other temperature-related diseases.⁷ Around the 7th century A.D, further documentation was found in Asia where at least 800 drugs were logged.⁸ Among the medicines from antiquities was opium, a sedative extracted from the opium poppy pod. The ancient Greeks used it as an analgesic while the Middle Easterners resolved to not use it because of its unfavourable side effects.⁸ Opium is the mother plant from which many opiate alkaloids are obtained, but the two main active compounds in opium are morphine and codeine.⁸⁻¹⁰ Morphine and codeine were

separately isolated in the 19th century and caused a breakthrough in analgesia studies.¹¹ In the 20th century, Alexander Fleming revolutionized science when he discovered penicillin¹², a biological substance produced by *Penicillium notatum*.¹³ His work demonstrated its action against *Staphylococci*. Contemporary antibiotic drug families like sulfonamides and tetracyclines also gained reputation after penicillin's discovery. Antimicrobial drugs gained relevancy in this period because they combatted bacterial infections on injured soldiers during the Great War (World War I).¹⁴

Scientists were motivated to work with academic institutions to find efficient ways to isolate more natural products. The number of identified active natural compounds now passes 10⁶. Over half of those discovered active ingredients are obtained from vegetation. Only a small fraction is obtained from microorganisms. Approximately one quarter of all naturally occurring compounds have been found to possess therapeutic properties.¹⁵ All this has been made possible by the technological advancement in the natural compound screening systems since the industrial rise in Europe.

1.2 Advent of the pharmaceutical industry

The emergence of the pharmaceutical industry was concomitant with the industrial revolution in Europe. Most companies grew from trivial apothecaries into nationwide suppliers of medicines. Merck of Germany commenced extensive production in the 19th century after hundreds of years of operation as a local dispensary in the town of Darmstadt. By the late 1800s, they were supplying remedies like morphine ((4*R*,4*aR*,7*S*,7*aR*,12*bS*)-3-Methyl-2,3,4,4*a*,7,7*a*-hexahydro-1*H*-4,12-methanobenzofuro[3,2-*e*] isoquinoline-7,9-diol) and quinine ((*R*)-(6-Methoxyquinolin-4-yl)[(1*S*,2*S*,4*S*,5*R*)-5-vinylquinuclidin-2-yl]-methanol).

Other companies were evolving from supplying simple chemicals to pharmaceuticals. Among them are Bayer and Sandoz of Germany and Switzerland, respectively. Chemists were already isolating naturally occurring compounds like quinine, a cinchona alkaloid extracted from the cinchona tree. (Figure 1.2) The pharmaceutical industry has since evolved from producing simple natural extracts to more specific and complex drug forms¹⁶ to resolve poor solubility and shorter shelf life. One of the fundamental tools which has developed in solid state design is crystal engineering.¹⁷ Due to this development, medicines have seen a turnaround.

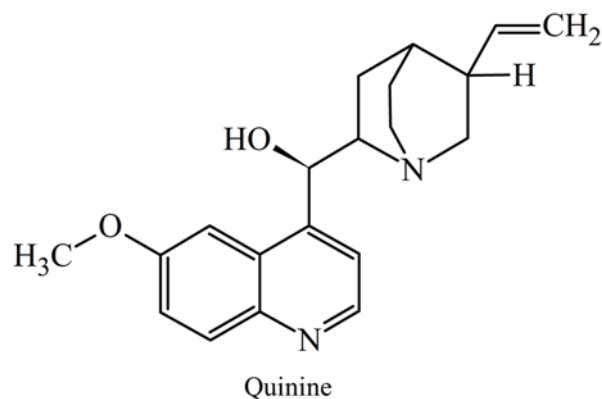


Figure 1.2 One of the first drugs to be utilized in the pharmaceutical industry

1.3 Pharmaceutical design

Formulation of a pharmaceutical product is relevant in drug technological advancement and provides new understandings and theories concerning medicines.¹⁸ In recent years, scientific interest turned toward the design and production of new forms of already existing drugs to improve dissolution rates,¹⁹ stability²⁰ during storage, as well as other properties, without alteration of their molecular structure.^{21, 22} This has brought insight into drug modification and tackled the problems of bioavailability.²³

1.4 Types of solids

Solids may be divided into two main classes: crystalline and amorphous. Crystalline solids are composed of well-ordered atoms, ions or molecules while amorphous solids do not have a uniformity in their particles.^{24,25,26} The repeating units of crystalline solids are known as unit cells. Crystalline solids are further divided into ionic solids (e.g. salts), molecular (e.g. sucrose), covalent (e.g. diamond) and metallic solids (e.g. iron metal).²⁷ Ionic solids are characterized by high melting points and are also known to be good electrolytes. Molecular solids have relatively low melting points and their molecules or atoms are held together by London forces, dipole-dipole interactions or hydrogen bonds.²⁸ Covalent solids are made up of atoms connected by covalent bonds. They are generally poor electrolytes and naturally hard. The strong covalent bonds give them their high melting points. Metallic solids have higher melting points and good electrical conductivity because of their free electrons in their structure. There are endless pure crystalline solids²⁹ that exist at room temperature and normal pressure. Table 1.1 summarizes the kinetic and packing properties of a crystalline solid.

Table 1.1 Properties of a crystalline solid^{27, 30}

Thermodynamic and kinetic properties	Packing properties
Melting/sublimation temperatures, vapour pressure	Molar volume and density
Dissolution rate	Hygroscopicity
Rates of solid state reaction	Particle morphology
Physical/chemical stability	Colour

Amorphous solids do not have ordered particles. Some of the used amorphous materials are fibres and plastics and other pure substances also exist in amorphous forms, such as phosphorus or sulphur.

1.5 Design stages

Drug discovery and development can be sectioned into three distinct stages, the first phase being therapeutic chemistry for the finding and screening of novel pharmaco-chemical substances. The second stage is popularly known as pre-formulation stage. This step centres on the discovery of a medicine as well as the inert substance, usually a solid, appropriate for use as a material in the final product. The last stage is the formulation phase which combines the sedentary components with the Active Pharmaceutical Ingredient (API) into a capsule or a tablet typically.³¹ Potentially active compounds in stage one, discovery of appropriate materials to couple with API in stage two and, finally, capsule products of formulation.

Solid-state formulation employs crystalline or amorphous systems. Formulation methods including multicomponent systems, micronization, oil encapsulation and solid dispersion have been used to enhance bioavailability of drug substances to significant extents.³² Micronization focuses on reducing particle size using mechanical means to alter solid dissolution rates.³² The disadvantage of using mechanical means is that the form of the particle may be unretainable. Shiraki *et al.* report the use of micronization on cancer drugs Megestrol acetate (17-alpha-acetoxy-6-methylpregna-4,6-diene-3,20-dione) and Exemestane (6-methylenandrosta-1,4-diene-3,17-dione). They state that micronization is a necessary procedure for improving bioavailability of Megestrol.³²

A drug substance can be administered orally as a solid, liquid, or gas, or injected as a serum. It can also be applied on skin as a cream or paste. Liquid formulations are now becoming significant due to the failure of some solid drug forms. Crystal engineering principles can be

applied in co-crystallization experiments where a co-former molecule is introduced to obtain multicomponent crystals. New chemistry has developed around formation of these multicomponent crystals as well as the peak performance of the Active Pharmaceutical Ingredient (API).^{28, 33, 34} Literature also focuses on intermolecular associations of drug co-crystals and their importance.

Regardless of the extent of study of multicomponent systems, there remains a concern towards them and how they can make a major pharmaceutical breakthrough. The persisting challenge with this inventive pharmaceutical solution is their regulatory ambiguity: this involves control of (i) how much of the effective drug substance enters the human body system, (ii) how much is assimilated and (iii) how much is excreted. The subsequent setback during laboratory investigation is the failure of these multicomponent systems to provide reassurance that they are effective within the human body. Other industrial challenges posed include large scale production problems as well as storage or shelf life.

Despite the challenges which solid drugs may pose to the scientist, the exclusiveness of drugs taken by oral ingestion is that they are almost always in solid form. When we talk of solid form we do not ignore purity and thermal stability of these drug substances among other properties. Strictly speaking, crystalline drug forms are preferred to amorphous forms for one reason or the other.³⁵ Such problems have stirred up pharmaceutical scientists to deal with these imperative factors.

1.6 Crystal engineering

Jonathan Steed defines crystal engineering as “...the design and preparation of a crystalline material based on a knowledge, or at least a consideration, of the steric, electronic, topological and intermolecular bonding capabilities of the constituent building blocks.”³³ Gautam Desiraju describes it as “the understanding of intermolecular interactions in the context of crystal packing and the utilization of such understanding in the design of new solids with desired physical and chemical properties”.²⁴ It is an essential instrument in the following disciplines: supramolecular chemistry,³³ solid state chemistry, materials science and crystallography.¹⁶ Also, it is applied in protein-ligand recognition design.³⁶ Crystal engineering offers tactical ways of solving poor oral bioavailability of medicines and other challenges which are encountered in drug delivery.^{35, 37} One basic quality a supramolecular chemist must possess is the ability to manipulate intermolecular interactions within organic molecular structures for formulating novel crystalline drug forms.²¹ While cement acts as an adhesive material in mechanical engineering, intermolecular interactions act as the reinforcement in crystals.³⁸ The most prevalent interaction is the hydrogen bond. Hydrogen bonds are non-covalent forces³⁹ that result from interaction between hydrogen donating and hydrogen accepting species.⁴⁰ Table 1.2 summarizes properties of hydrogen bonds.

Table 1.2 Characteristics and properties of hydrogen bonds⁴¹

Hydrogen bonds D•••A)	Strong	Moderate	Weak
Nature	mostly covalent	most electrostatic	electrostatic
Bond lengths	D•••H \approx H•••A	D•••H < H•••A	D•••H \ll H•••A
H•••A (Å)	~1.2-1.5	~1.5-2.2	2.2-3.2
D•••A (Å)	2.2-2.5	2.5-3.2	3.2-4.0
Bond angles (°)	175-180	130-180	90-150
Bond energy (kcal mol ⁻¹)	14-40	4-15	<4
Percentage IR vibration shift (shift in the OH frequency from 3400 cm ⁻¹)	25% shift	10-25% shift	<10% shift
Examples	strong acids bases salts	hydrates acids- bases all biological molecules	weak acids weak bases

Functional groups like carboxylic acids and amides may form supramolecular synthons as shown in Figure 1.3. Synthons with two different components like the nitro-iodo association are known as heterosynthons, while homosynthons form between the same functional groups.

The hydrogen bonding motifs in these multicomponent systems have been defined using a simple set by Margaret Etter.⁴² The naming system is called graph set notation.⁴² Graph set analysis explains and classifies hydrogen bonds of multicomponent crystal systems in the following groups: Chains (C), Discrete (D), Self (S) and Rings (R).³³ Hydrogen bonding motifs may not always have a single descriptor but will have the major notation ascribed to it.⁴²

The general graph set notation is $G_d^a(n)$,⁴² where,

G=descriptor (C, D, S or R)

a= number of hydrogen acceptors

d= number of hydrogen bond donors

n= number of atomic participants in the ring⁴²

The 8-membered homosynthon rings of acid and amide have graph set descriptor $R_2^2(8)$ alike (Figure 1.6).⁴² Nitro-iodo and nitro-amide heterosynthons both have graph set descriptor $R_1^2(4)$. Chloride/chloride and carboxylic acid synthons both have graph set descriptor D since they have a finite intermolecular pattern.³³

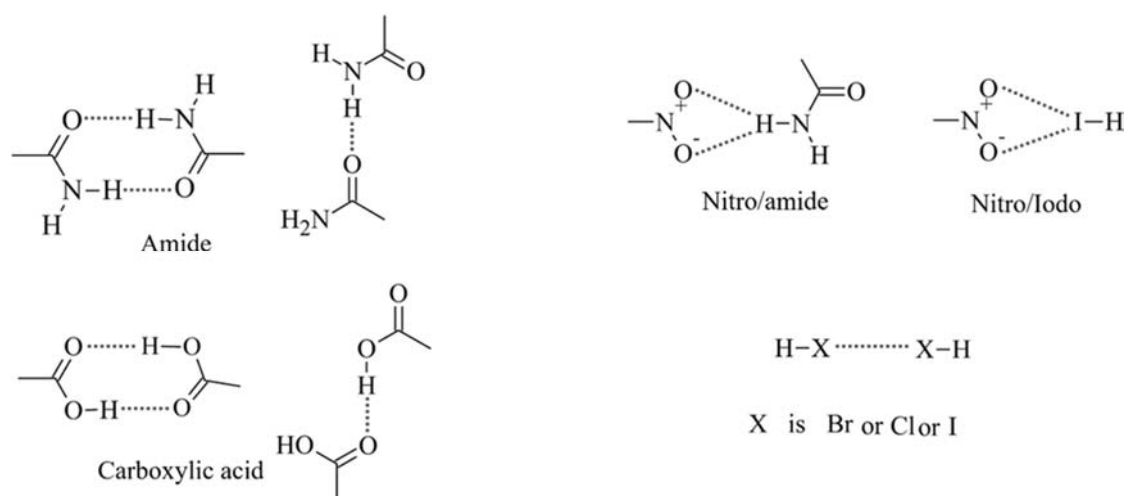


Figure 1.3 Characteristic supramolecular synthons involved in multicomponent crystal systems³³

The energy values of strong hydrogen bonds are calculated at 14-40 kcal mol⁻¹. Since these interactions are robust, they are utilized via supramolecular synthons or secondary building units⁴³ in crystal packing of carbon-based compounds.⁴⁴ Moderate hydrogen bonds are measured at 4-15 kcal mol⁻¹ while weaker hydrogen bond energy goes below 4 kcal mol⁻¹. The reason hydrogen bonds are applied in crystal engineering is that they can be manipulated in such a way that can estimate structure outcomes of multicomponent systems. We can also

project structure outcomes by studying other weaker interactions. It is also interesting that one molecule can have H-bond donor and acceptor groups at the same time, and this provides good ground for crystal engineering.⁴⁴

Another possible classification of hydrogen bonds are based on their formation: intra-molecular and intermolecular interactions.³⁹ Hydrogen-donating species act as Brønsted-Lowry acids when interacting with molecules of basic nature. Although hydrogen bonds are not the only forces that are at work between molecules in chemistry,³⁹ they play a significant role in many ways, namely, molecular recognition and self-assembly.⁴⁵ Some non-covalent forces include halogen bonds, pi-pi-interactions and electrostatic attractions.⁴⁶ Literature echoes that the study of these intermolecular interactions is increasingly being used to address many challenges in crystal engineering. Scientists support the minimization of intermolecular interactions within molecules so that study of one type of force is done in depth before conclusions can be made about their influence in crystal systems.²⁸

1.7 Polymorphism

The term polymorphism was first used by other disciplines of study before it was borrowed by crystal engineers. Joel Bernstein records that the first application of the term was by a chemist named Mitscherlich,⁴⁷ known for observing this phenomenon in two crystalline hydrates of $\text{NaH}_2\text{PO}_4 \cdot \text{H}_2\text{O}$ and NaH_2AsO_4 .⁴⁸ We now know from McCrone that “*A polymorph is a solid crystalline phase of a given compound resulting from the possibility of at least two different arrangements of the molecule of that compound in the solid state*”.⁴⁹ The reason why polymorphism is a major topic in solid state chemistry is that it offers insight into the fundamental forces that make inter-structural assembly possible, and their resultant physico-chemical properties.⁵⁰ In past years, scientists tried to avoid polymorphic tendencies of pharmaceutical solids by using more predictable multicomponent systems. This precaution was futile because multicomponent crystals also presented polymorphism.⁵¹ Polymorphism falls into three basic categories: conformational, packing and synthon polymorphism. Conformational polymorphism describes the geometric orientation in space a molecule assumes due to its flexibility. Packing polymorphism is the resultant arrangement of molecular tapes in higher dimensionality of the crystal system.⁵¹ Figure 1.4 shows characteristic examples of synthon polymorphism, when the difference of the crystal structures can be described with the manner the supramolecular synthons are formed.

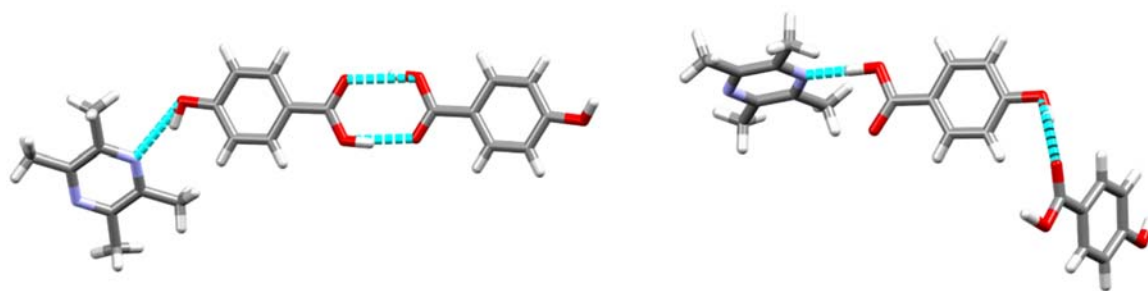


Figure 1.4 Typical synthon polymorphism (left: heterosynthon and acid-acid homosynthon; right: heterosynthon and hydroxyl-acid heterosynthon) exhibited in crystals of 4-hydroxybenzoic acid and 2,3,5,6-tetramethylpyrazine (figure re-made)⁵²

Artemisinin, (see Figure 1.1) was investigated for polymorphism. Two polymorphic forms of the anti-malarial drug have been recorded in detail by Chan *et al.*⁵³ The forms show enantiotropism with a critical temperature of ca. 403.15 K. The first form was solved in the triclinic space group $P1$. The other crystal was solved in the orthorhombic space group $P2_12_12_1$. Figure 1.5 shows a comparison of the packing of the two polymorphs.

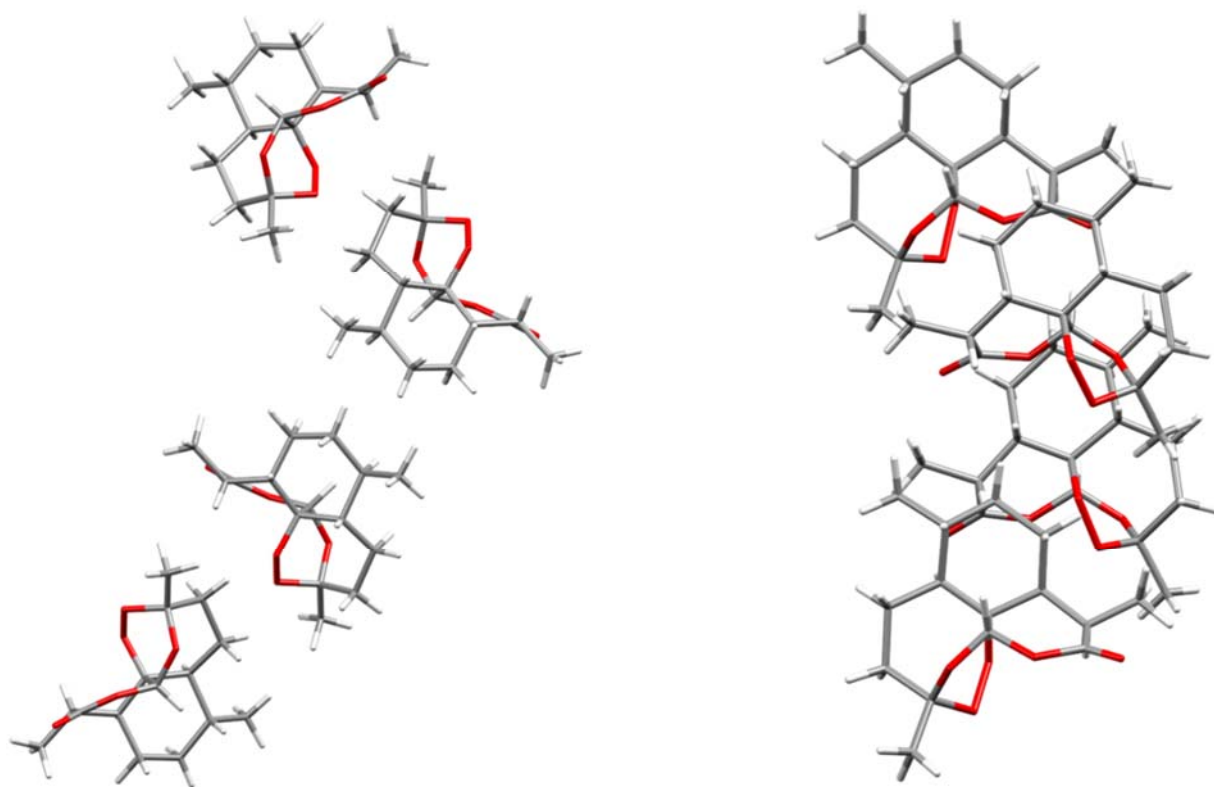


Figure 1.5 Packing diagram of the artemisinin orthorhombic (left) and triclinic (right) cell viewed down the crystallographic c axis

Lemmerer *et al.* investigated concomitant polymorphism in 2-[4-[2-(4-chlorobenzamide)ethyl]-phenoxy]-2-methylpropanoic acid (bezafibrate). They reported two polymorphic forms, a *syn* conformation of the carboxylic acid proton in one form and an *anti* conformation in the other.⁵⁴ The two forms are represented in Figure 1.6.

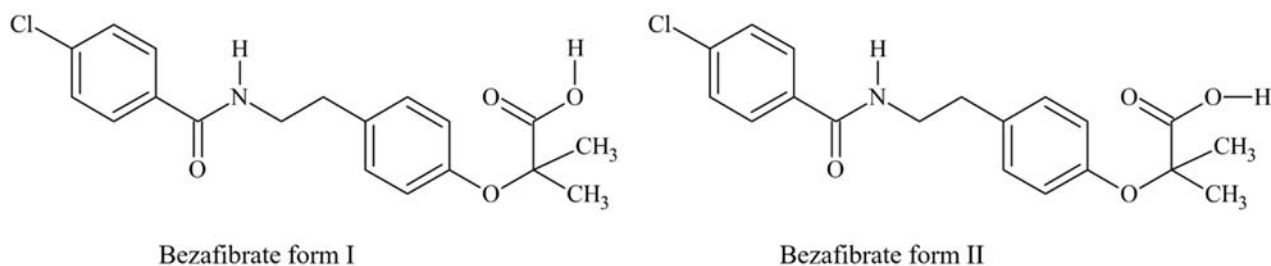


Figure 1.6: Conformational polymorphism demonstrated in bezafibrate. The two structures differ at the carboxylic acid hydrogen

5-Methyl-2-[(2-nitrophenyl)amino]-3-thiophenecarbonitrile, commonly known as ROY, shows excessive polymorphism which co-occur at room temperature and pressure.⁵⁵ Although the compound is an impurity of Olanzapine, it is largely used in proteomics. It is also a good foundation for polymorphism investigation since polymorphs are usually prone to phase transition from the metastable to the stable form.⁵⁶

Many more prominent drugs have had unsuccessful introductions in the market because of polymorphism. This was the case with Ritonavir⁵⁷, an antiretroviral drug that prevents protease division. It was pulled out from the market soon after realizing the existence of its more robust and less soluble form.^{31,57} Other examples of drug failures due to polymorphism are Rotigotine ((6S)-6-[propyl(2-thiophen-2-ylethyl)amino]-5,6,7,8-tetrahydronaphthalen-1-ol), a remedy for Parkinson disease, and Irbesartan ((2-butyl-3-[[4-[2-(2H-tetrazol-5-yl)phenyl]phenyl]methyl]-1,3-diazaspiro[4,4]non-1-en-4-one), a remedy for diabetes.⁵⁸ Some of these drug molecules are shown in Figure 1.7.

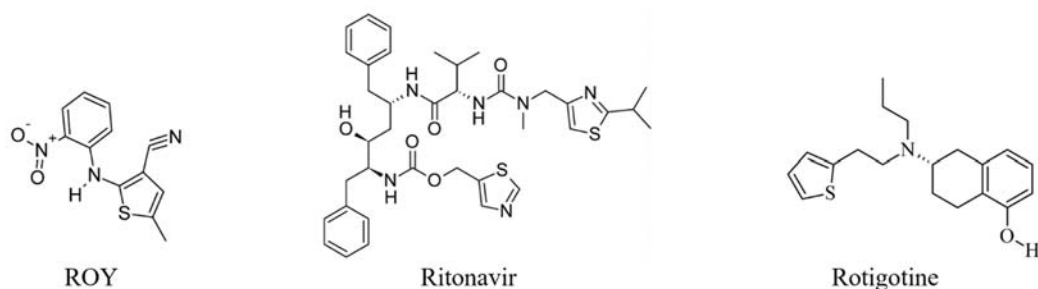


Figure 1.7 Pharmaceuticals that failed on the market due to polymorphic tendencies

1.8 Multicomponent systems

Multicomponent systems are a far-reaching group of pharmaceutical products within supramolecular chemistry.⁵⁹ As the name suggests, ‘multi’ means many, and component describes the pharmaceutical substance and a solvent or a co-former involved. Literature also calls it the pharmaceutical co-crystal⁶⁰ because the constituents involved are usually APIs of some kind. Alternatively, it may simply be another compound that is Generally Regarded as Safe (GRAS) by the Food and Drug Administration (FDA). GRAS compounds are solid at room temperature and implemented in the formation of new forms of therapy. It has become common in crystal design and solid-state chemistry to use numerous components for modifying the physical and chemical properties of an API without necessarily altering its molecular structure. For a long time now this has been a fairly easy and accessible method for achieving the right therapeutic qualities in drug substances.²⁸ As opposed to single component crystalline substances, multicomponent systems require careful calculation and regulation during screening and development.³² A much easier strategy for finding possibilities to build multicomponent systems is using supramolecular synthons. Crystal engineering focuses on these key structural units to predict intermolecular interactions within multicomponent systems.⁶¹ Each form shows distinctive physicochemical properties that can intensely impact the bioavailability, ability to be manufactured, purification, stability and other performance characteristics of the drug.⁶²

Probable results from a solvent based co-crystallisation experiment are polymorphs, hydrates, solvates, salts or co-crystals.³¹ Hydrates are interesting because of the presence of water in many drug formulations. However, their stoichiometry is not guaranteed and their thermal stability is so low that it becomes a hindrance to their pharmaco-action.⁶³ Multicomponent crystal formation has become a headline as far as the pharmaceutical industry is concerned.¹⁴

The possible different environments in which a co-crystallization reaction can occur, such as using different solvents or solvent mixtures, may create greater opportunities for discovering new crystals.¹⁵

Solvates and co-crystals differ in the physical state of the isolated pure parts.⁶⁴ When one part is a liquid at room temperature, the crystals are regarded as solvates but if both parts are solids at room temperature, the crystals are regarded as co-crystals.⁶⁵ Poor solubility is a major challenge to solvates such that the likelihood for them being a good candidate for a drug product is lessened.⁶³ Co-crystals are crystalline complexes of more than one solid component that are held together by non-covalent interactions, mostly hydrogen bonding.⁶³

The formation of a salt is the result of a neutralization reaction between a base and an acid.⁶⁶ It has been determined that more than half of medicines are taken in as salts.^{67,68} Salt formation is founded upon reputable principles for generating new solid-state drugs with desired properties. What may limit this multicomponent system is the fact that salt formation cannot happen without ionizable moieties.

The makeup of the molecule under investigation determines the outcome and authenticity of the solid form discovered. Generally, scientists go with the thermodynamically most stable crystalline form of the compound. It is important to note that the stability of a crystal does not guarantee excellent solubility properties. Poor dissolution rate means reduced oral absorption.⁶⁹

1.9 Pharmaceutical salts

One strategy that crystal engineers apply during multicomponent crystal formation is to deliberately choose drug substances that are susceptible to protonation. These drug substances typically have molecules containing electron-withdrawing atoms (e.g. fluorine, chlorine, nitrogen and oxygen) in a heteroatomic pair and/or delocalized benzene pi-electrons.⁷⁰ In such cases, ionic multicomponent systems are anticipated to form. An example of an ionic system is a salt.⁷¹ Shiraki says that if a compound can be ionized, salt formation is a characteristic proposition to tackle the problem of poor solubility.³² Cimetidine hydrochloride salt has been reported by Watts *et al.* It has been marketed in its base or salt form.⁷² Dennany also reports the hydrochloride salt of (S)-amphetamine ((2S)-1-phenylpropan-2-aminium chloride).⁷³ Moxifloxacin, Ciprofloxacin and Tetracycline possess characteristic proton-accepting

functional groups. Varanda *et al.* report solubility determination of their hydrochloride salt forms, namely, moxifloxacin hydrochloride, ciprofloxacin hydrochloride and tetracycline hydrochloride under different conditions.⁷⁰ Their results showed a higher dissolution rate of the salt form of the antibiotic drugs in water than other solvents. Some have reported that the downside of highly soluble crystal salts is their awful taste,⁷⁴ and some suggested the solution to the taste problem is to decrease the drug's solubility.⁷⁴

Most pharmaceutical salts have been prepared using organic acids.⁶⁷ Literature reports formation of ethionamide salts using carbon-based acids.⁷¹ Active salt ingredients are presented in Figure 1.8.

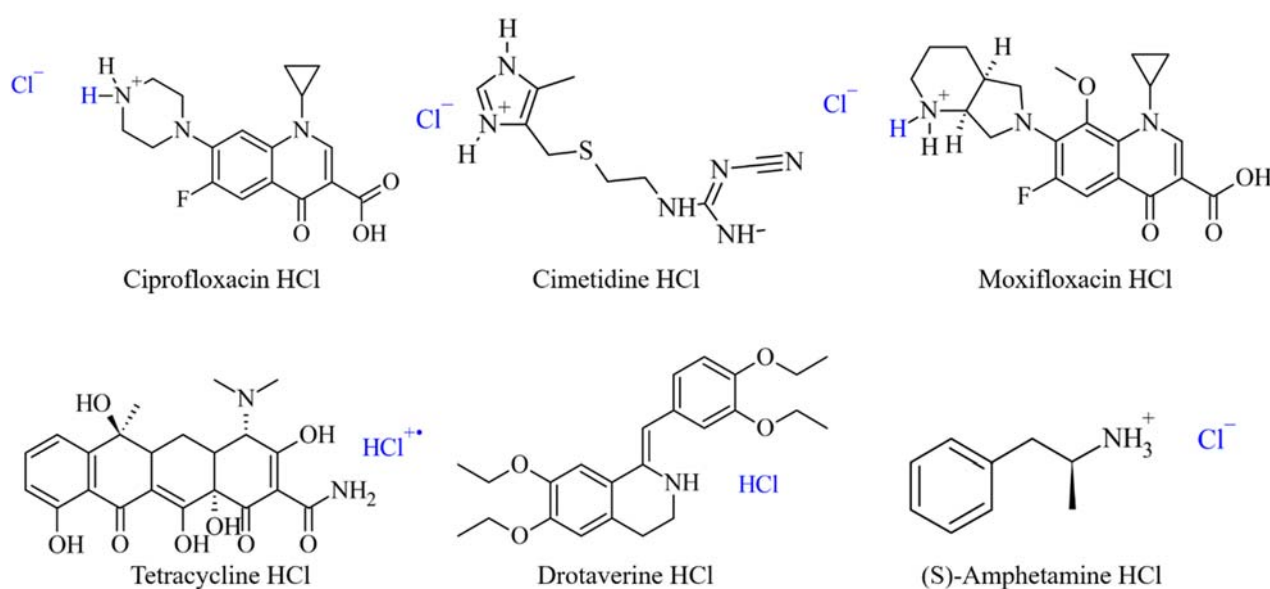


Figure 1.8 HCl pharmaceutical salts

It has been observed that sulfur compounds formed synthons with qualities of more than one multicomponent crystal. Caira *et al.* studied the 1:1 crystal of sulfamethoxazole (4-amino-N-(5-methyl-1,2-oxazol-3-yl) benzenesulfonamide) and trimethoprim (2,4-diamino-5-(3,4,5-trimethoxybenzyl pyrimidine)). The results showed that the crystal displayed qualities of both a salt and a co-crystal.⁷⁵

Salts are good solutions to the solubility problem. They are obtained from the co-crystallisation of the API with generally regarded as safe acids and bases.³ Like the API, crystalline salts may be found in several polymorphic, solvated and/or hydrated forms. Most drugs and their salts are purified and isolated by crystallisation from a suitable solvent during the last synthetic step.³

A large number of factors can influence crystal nucleation and growth during this process, including the composition of the crystallisation medium and the process used to generate supersaturation and stimulate crystallisation.²

In the general sense, salt formation results from a neutralization reaction between an acid and a base. In crystal engineering, salt formation involves calculated and monitored crystallization of an acid/base API with a suitable basic/acidic co-former. Salt formation is utilised as the key solution to the problem of solubility and dissolution rates of substances of ionic nature. Other functions of pharmaceutical salts include resolution to the problem of stability, toxicity and purity. Salt formation is therefore a major player in both drug development in the industry as well as metabolic processes in the body⁷⁶ because the degree of dissociation of hydrochloride salts in the alimentary canal is suppressed by common ion effect fluids.

1.10 Nitrofurazone (NFZ)

A high degree of focus is on the broad spectrum bactericide, nitrofurazone (NFZ), IUPAC name 5-nitro-2-furaldehydesemicarbazone; pale yellow compound, with melting point range 236°C -240°C.⁷⁷ It is very slightly soluble (1:420) in water at pH 6.0-6.5, soluble in alkaline solutions; slightly soluble in ethanol (1:590), propylene glycol (1:350), acetone (1:415), dimethylformamide (1:15) and polyethylene glycol (1:86); almost insoluble in chloroform (1:2700) and benzene (1:43500).⁷⁸ Olszak *et al.* also reports that the molecule is generally planar and that no conjugation is exhibited by the compound within the chain. NFZ degrades in the presence of sunlight and loses its therapeutic properties.⁷⁷ Samsonova *et al.* state, “*The nitrofurazone antibiotics are characterised by quick metabolism, half-life time in vivo is a few hours.*”⁷⁹

Silva *et al.* report, “...a nitroheterocyclic topicantiseptic, which is known to have antitrypanosomal activity by generating oxygen reactive species, which interferes with trypanothione reductase, a specific parasite detoxifying enzyme, and also an inhibition of cruzipain, the main parasite protease.”⁸⁰ NFZ is a broad-spectrum bactericidal with antiprotozoal and anti-parasitic activities. Popiolek *et al.* report the bactericidal action of NFZ against Gram (+) *Staphylococcus* and *Bacillus*.⁸¹ Therapeutic action has been observed on *salmonella* and *coli* bacteria. Rahi *et al.* also report its action against Gram (-) microbial organisms.⁸²

NFZ is used for the treatment of wounds, burns, ulcers and skin infections; it has also been applied to the ear, eye and bladder. NFZ is used as a coccidiostatic and antibacterial agent in domestic animals, administered in water or alcohol.⁷⁸ Although nitrofurazone is very slightly soluble in water, it has more flexibility in forming new solid forms without any covalent changes of its molecular structure. This means that nitrofurazone undergoes more bond rotation in the presence of a guest compound in a solvent medium and arranges itself or packs in a way different from the original conformation.¹² Under exposure to reflux heating, NFZ emits oxides of nitrogen which are hazardous to health. The use of Nitrofurazone as a pharmaceutical has dwindled of late, although it is still being used on a small scale as an antibiotic drug, mainly targeting mucosal organs.⁸³

1.11 Statement of research problem

According to literature, over 75% of the drugs in drug development have poor aqueous solubility.⁶³ The drug of interest, nitrofurazone (NFZ), poses a problem of solubility in water.⁶³ Its solubility is only 1 g in 4200 ml of water; therefore, one will require a bulk of nitrofurazone for its bioavailability in the body to suffice. Several approaches have been used to address the challenge of poor bioavailability of drugs. Production of multicomponent crystals, namely salts and co-crystals, have gained momentous interest because the physicochemical properties of pharmacological materials are improved via intermolecular interactions.

1.12 Objectives of the research

- To form multicomponent crystals of nitrofurazone with selected co-formers by applying crystal engineering principles
- To make multicomponent crystals of nitrofurazone using different liquid mineral and organic acids
- To subsequently understand their stability via their supramolecular structure
- To compare the physicochemical properties of the multicomponent crystals to the starting material NFZ

The main aim of this research is to produce a series of enhanced and modified crystals of nitrofurazone via systematically varying the co-former compounds and without changing the molecular structure of the API. The API and the co-formers adhere to each other via

intermolecular interactions. We have used strong acids so that we may transfer a proton onto the nitrogen of the hydrazone C=N bond (predicted pKa value on nitrogen is -1.97).⁸⁴ Figure 1.9 shows the molecular structure of the drug of interest, nitrofurazone (NFZ).

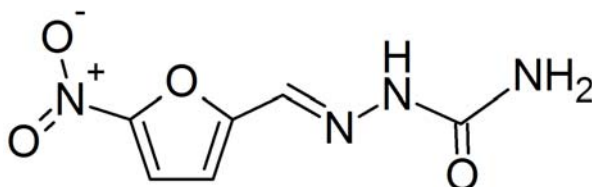


Figure 1.9 Nitrofurazone (5-nitro-2-furaldehydesemicarbazone, NFZ)

Table 1.3 Predicted properties of nitrofurazone

Property	Value
pKa strongest base	11.79
pKa strongest acid	-1.97
Hydrogen acceptor count	4
Hydrogen donor count	2

The two strategies we devised to achieve our objective were co-crystal formation via hydrogen bond synthons at the hydrazone and amide group on the semicarbazone chain and protonation of the hydrazone group, where we needed strong acids. This was achieved by thorough selection of co-formers and/or solvents for the impending crystallization experiments.

1.13 Research hypothesis

The proposed hypothesis is (1) that we can form co-crystals via the functional groups (mentioned previously) and (2) that we can protonate the hydrazone using strong acids.

References

- (1) Ebbell, B., *The Papyrus Ebers: the greatest Egyptian medical document*. ed.; Levin & Munksgaard: 1937.
- (2) Potter, P., *Short handbook of hippocratic medicine*. ed.; Les Editions Du Sphinx: 1988.
- (3) Leroux, H., Discovery of salicine. *Journal of Medicinal Chemistry* **1830**, 6, 340-432.
- (4) Jack, D. B., One hundred years of aspirin. *The Lancet* **1997**, 350, (9075), 437-439.
- (5) Tu, Y., Chapter 10 - Structure and Properties of Artemisinin. In *From Artemisia Annua L. to Artemisinins*, Academic Press: 2017; pp 213-220.
- (6) Tu, Y., The discovery of artemisinin (qinghaosu) and gifts from Chinese medicine. *Nature Medicine* **2011**, 17, 1217.
- (7) Tu, Y. Y.; Ni, M. Y.; Zhong, Y. R.; Li, L. N.; Cui, S. L.; Zhang, M. Q.; Wang, X. Z.; Liang, X. T., Studies on the constituents of *Artemisia annua* L. (author's transl). *Acta Pharmaceutica Sinica* **1981**, 16, (5), 366-370.
- (8) Dias, D. A.; Urban, S.; Roessner, U., A Historical Overview of Natural Products in Drug Discovery. *Metabolites* **2012**, 2, (2), 303-336.
- (9) Manglik, A.; Kruse, A. C.; Kobilka, T. S.; Thian, F. S.; Mathiesen, J. M.; Sunahara, R. K.; Pardo, L.; Weis, W. I.; Kobilka, B. K.; Granier, S., Crystal structure of the micro-opioid receptor bound to a morphinan antagonist. *Nature* **2012**, 485, (7398), 321-6.
- (10) Aronson, J. K., Chapter 8 - Opioid analgesics and narcotic antagonists. In *Side Effects of Drugs Annual*, Aronson, J. K., Ed. Elsevier: **2014**; Vol. 35, pp 171-195.
- (11) Bentley, K. W., CHAPTER 7 - The Morphine Alkaloids. In *The Isoquinoline Alkaloids*, Pergamon: **1965**; pp 79-154.
- (12) Fleming, A., On the Antibacterial Action of Cultures of a *Penicillium*, with Special Reference to their Use in the Isolation of *B. influenzae*. *British Journal of Experimental Pathology* **1929**, 10, (3), 226-236.
- (13) Hahn, F. E., Penicillin Until 1957. In *Progress in Molecular and Subcellular Biology*, Hahn, F. E.; Kopecko, D. J.; Müller, W. E. G., Eds. Springer Berlin Heidelberg: Berlin, Heidelberg, **1983**; pp 1-21.
- (14) Crellin, J. K., A social history of medicines in the twentieth century : to be taken three times a day / John K. Crellin. In ed.; Pharmaceutical Products Press: London :, **2004**.

- (15) Cragg, G. M.; Newman, D. J., Natural products: A continuing source of novel drug leads. *Biochimica et Biophysica Acta (BBA) - General Subjects* **2013**, 1830, (6), 3670-3695.
- (16) Desiraju, G. R., Crystal engineering. From molecules to materials. *Journal of Molecular Structure* **2003**, 656, (1), 5-15.
- (17) Braga, D.; Grepioni, F., Intermolecular Interactions in Nonorganic Crystal Engineering. *Accounts of Chemical Research* **2000**, 33, (9), 601-608.
- (18) Nanjwade, V. K.; Manvi, F.; Ali, M. S.; Nanjwade, B. K.; Maste, M. M., New trends in the co-crystallization of active pharmaceutical ingredients. **2011**.
- (19) Drozd, K. V.; Manin, A. N.; Churakov, A. V.; Perlovich, G. L., Drug-drug cocrystals of antituberculous 4-aminosalicylic acid: Screening, crystal structures, thermochemical and solubility studies. *European Journal of Pharmaceutical Sciences* **2017**, 99, 228-239.
- (20) Hickey, M. B.; Peterson, M. L.; Scoppettuolo, L. A.; Morrisette, S. L.; Vetter, A.; Guzmán, H.; Remenar, J. F.; Zhang, Z.; Tawa, M. D.; Haley, S.; Zaworotko, M. J.; Almarsson, Ö., Performance comparison of a co-crystal of carbamazepine with marketed product. *European Journal of Pharmaceutics and Biopharmaceutics* **2007**, 67, (1), 112-119.
- (21) Anthony, A.; Desiraju, G. R.; Jetti, R. K. R.; Kuduva, S. S.; Madhavi, N. N. L.; Nangia, A.; Thaimattam, R.; Thalladi, V. R., Crystal Engineering: Some Further Strategies. *Crystal Engineering* **1998**, 1, (1), 1-18.
- (22) Bavishi, D. D.; Borkhataria, C. H., Spring and parachute: How cocrystals enhance solubility. *Progress in Crystal Growth and Characterization of Materials* **2016**, 62, (3), 1-8.
- (23) Zhang, M.; Liang, Z.; Wu, F.; Chen, J.-F.; Xue, C.; Zhao, H., Crystal engineering of ibuprofen compounds: From molecule to crystal structure to morphology prediction by computational simulation and experimental study. *Journal of Crystal Growth* **2017**, 467, 47-53.
- (24) Desiraju, G. R., The supramolecular concept as a bridge between organic, inorganic and organometallic crystal chemistry. *Journal of Molecular Structure* **1996**, 374, (1), 191-198.
- (25) Desiraju, G. R.; Hulliger, J., Molecular crystals. *Current Opinion in Solid State and Materials Science* **2002**, 6, (2), 107-108.
- (26) Mishra, M. K.; Ramamurty, U.; Desiraju, G. R., Mechanical property design of molecular solids. *Current Opinion in Solid State and Materials Science* **2016**, 20, (6), 361-370.

- (27) Zhang, G. G. Z.; Zhou, D., Chapter 2 - Crystalline and Amorphous Solids. In *Developing Solid Oral Dosage Forms (Second Edition)*, Academic Press: Boston, **2017**; pp 23-57.
- (28) Berry, D. J.; Steed, J. W., Pharmaceutical cocrystals, salts and multicomponent systems; intermolecular interactions and property based design. *Advanced Drug Delivery Reviews* **2017**.
- (29) Kasten, G.; Nouri, K.; Grohgan, H.; Rades, T.; Löbmann, K., Performance comparison between crystalline and co-amorphous salts of indomethacin-lysine. *International Journal of Pharmaceutics* **2017**, 533, (1), 138-144.
- (30) Gupta, P. K., Non-crystalline solids: glasses and amorphous solids. *Journal of Non-Crystalline Solids* **1996**, 195, (1), 158-164.
- (31) Duggirala, N. K.; Perry, M. L.; Almarsson, O.; Zaworotko, M. J., Pharmaceutical cocrystals: along the path to improved medicines. *Chem Commun (Camb)* **2016**, 52, (4), 640-55.
- (32) Shiraki, K.; Takata, N.; Takano, R.; Hayashi, Y.; Terada, K., Dissolution Improvement and the Mechanism of the Improvement from Cocrystallization of Poorly Water-soluble Compounds. *Pharmaceutical Research* **2008**, 25, (11), 2581-2592.
- (33) Steed, J. W.; Atwood, J. L., *Supramolecular chemistry*. ed.; John Wiley & Sons: 2013.
- (34) Steed, J. W., The role of co-crystals in pharmaceutical design. *Trends in Pharmacological Sciences* **2013**, 34, (3), 185-193.
- (35) Warnken, Z. N.; Smyth, H. D. C.; Watts, A. B.; Weitman, S.; Kuhn, J. G.; Williams, R. O., Formulation and device design to increase nose to brain drug delivery. *Journal of Drug Delivery Science and Technology* **2016**, 35, 213-222.
- (36) Desiraju, G. R., Crystal engineering: Structure, design and function. *Current Opinion in Solid State and Materials Science* **2009**, 13, (3), 35.
- (37) Golob, S.; Perry, M.; Lusi, M.; Chierotti, M. R.; Grabnar, I.; Lassiani, L.; Voinovich, D.; Zaworotko, M. J., Improving Biopharmaceutical Properties of Vinpocetine Through Cocrystallization. *Journal of Pharmaceutical Sciences* **2016**, 105, (12), 3626-3633.
- (38) Allen, M. T.; Burrows, A. D.; Mahon, M. F., Hydrogen bond directed crystal engineering of nickel complexes: the effect of ligand methyl substituents on supramolecular structure. *Journal of the Chemical Society, Dalton Transactions* **1999**, (2), 215-222.

- (39) Wang, Y.; Zhang, Y.; Xu, Z.; Tong, J.; Teng, W.; Lu, Y., Intramolecular CS...OS(C) chalcogen bonds: A theoretical study of the effects of substituents and intermolecular hydrogen bonds. *Computational and Theoretical Chemistry* **2017**, 1115, 190-196.
- (40) Zhao, Y.; Li, Z.; Liu, J.; Hu, C.; Zhang, H.; Qin, B.; Wu, Y., Intermolecular vibrational modes and H-bond interactions in crystalline urea investigated by terahertz spectroscopy and theoretical calculation. *Spectrochimica Acta Part A: Molecular and Biomolecular Spectroscopy*.
- (41) Bernstein, J.; Davis, R. E.; Shimoni, L.; Chang, N.-L., Patterns in Hydrogen Bonding: Functionality and Graph Set Analysis in Crystals. *Angewandte Chemie International Edition in English* **1995**, 34, (15), 1555-1573.
- (42) Etter, M. C.; MacDonald, J. C.; Bernstein, J., Graph-set analysis of hydrogen-bond patterns in organic crystals. *Acta Crystallographica Section B* **1990**, 46, (2), 256-262.
- (43) Desiraju, G. R., Carrying out organic chemistry within crystalline solids. *Endeavour* **1984**, 8, (4), 201-206.
- (44) Seth, S. K.; Das, N. K.; Aich, K.; Sen, D.; Fun, H.-K.; Goswami, S., Exploring contribution of intermolecular interactions in supramolecular layered assembly of naphthyridine co-crystals: Insights from Hirshfeld surface analysis of their crystalline states. *Journal of Molecular Structure* **2013**, 1048, 157-165.
- (45) Seth, S. K.; Maity, G. C.; Kar, T., Quantifying intermolecular interaction of anthrylidene methyl arjunolate: Insights from Hirshfeld surface analysis. *Journal of Molecular Structure* **2012**, 1021, 89-94.
- (46) Chen, P.-Y.; Zhang, L.; Zhu, S.-G.; Cheng, G.-B., Role of intermolecular interaction in crystal packing: A competition between halogen bond and electrostatic interaction. *Journal of Molecular Structure* **2017**, 1131, 250-257.
- (47) Mitscherlich, E. A., *Ueber die Krystallisation der Salze, in denen das Metall der Basis mit zwei Proportionen Sauerstoff verbunden ist.* ed.; **1820**.
- (48) Bernstein, J., Polymorphism. In *Strength from Weakness: Structural Consequences of Weak Interactions in Molecules, Supramolecules, and Crystals*, Domenicano, A.; Hargittai, I., Eds. Springer Netherlands: Dordrecht, **2002**; pp 247-260.
- (49) Higashi, K.; Ueda, K.; Moribe, K., Recent progress of structural study of polymorphic pharmaceutical drugs. *Advanced Drug Delivery Reviews* **2017**, 117, (Supplement C), 71-85.


- (50) Iida, Y.; Kataoka, M.; Okuno, T., Conformational polymorphs of a novel TCNQ derivative carrying an acetylene group. *Journal of Molecular Structure* **2018**, 1152, (Supplement C), 261-265.
- (51) Susano, M. A.; Martín-Ramos, P.; Maria, T. M. R.; Folkersma, S.; Pereira, L. C. J.; Silva, M. R., Co-crystal of suberic acid and 1,2-bis(4-pyridyl)ethane: A new case of packing polymorphism. *Journal of Molecular Structure* **2017**, 1147, (Supplement C), 76-83.
- (52) Aitipamula, S.; Chow, P. S.; Tan, R. B. H., Polymorphism in cocrystals: a review and assessment of its significance. *CrystEngComm* **2014**, 16, (17), 3451-3465.
- (53) Chan, K.-L.; Yuen, K.-H.; Takayanagi, H.; Janadasa, S.; Peh, K.-K., Polymorphism of artemisinin from *Artemisia annua*. *Phytochemistry* **1997**, 46, (7), 1209-1214.
- (54) Lemmerer, A.; Báthori, N. B.; Esterhuysen, C.; Bourne, S. A.; Caira, M. R., Concomitant Polymorphs of the Antihyperlipoproteinemic Bezafibrate. *Crystal Growth & Design* **2009**, 9, (6), 2646-2655.
- (55) Chen, S.; Guzei, I. A.; Yu, L., New Polymorphs of ROY and New Record for Coexisting Polymorphs of Solved Structures. *Journal of the American Chemical Society* **2005**, 127, (27), 9881-9885.
- (56) Zhang, W.-P.; Chen, D.-Y., Crystal structures and physicochemical properties of amisulpride polymorphs. *Journal of Pharmaceutical and Biomedical Analysis* **2017**, 140, (Supplement C), 252-257.
- (57) Vasileiadis, M.; Pantelides, C. C.; Adjiman, C. S., Prediction of the crystal structures of axitinib, a polymorphic pharmaceutical molecule. *Chemical Engineering Science* **2015**, 121, (Supplement C), 60-76.
- (58) Quiñones, R.; Brown, R. T.; Searls, N.; Richards-Waugh, L., Study of polymorphism using patterned self-assembled monolayers approach on metal substrates. *Applied Surface Science* **2018**, 427, (Part B), 97-105.
- (59) MacGillivray, L. R.; Papaefstathiou, G. S.; Friscic, T.; Hamilton, T. D.; Bucar, D. K.; Chu, Q.; Varshney, D. B.; Georgiev, I. G., Supramolecular control of reactivity in the solid state: from templates to ladderanes to metal-organic frameworks. *Acc Chem Res* **2008**, 41, (2), 280-91.
- (60) Thipparaboina, R.; Kumar, D.; Chavan, R. B.; Shastri, N. R., Multidrug co-crystals: towards the development of effective therapeutic hybrids. *Drug Discovery Today* **2016**, 21, (3), 481-490.

- (61) Douroumis, D.; Ross, S. A.; Nokhodchi, A., Advanced methodologies for cocrystal synthesis. *Advanced Drug Delivery Reviews* **2017**.
- (62) Pereira, D. C.; Faria, D. L. A. d.; Constantino, V. R. L., CuII hydroxy salts: characterization of layered compounds by vibrational spectroscopy. *Journal of the Brazilian Chemical Society* **2006**, 17, 1651-1657.
- (63) Clarke, H. D.; Arora, K. K.; Bass, H.; Kavuru, P.; Ong, T. T.; Pujari, T.; Wojtas, L.; Zaworotko, M. J., Structure–Stability Relationships in Cocrystal Hydrates: Does the Promiscuity of Water Make Crystalline Hydrates the Nemesis of Crystal Engineering? *Crystal Growth & Design* **2010**, 10, (5), 2152-2167.
- (64) Tilborg, A.; Norberg, B.; Wouters, J., *Pharmaceutical Salts and Cocrystals Involving Amino Acids: A Brief Structural Overview of the State-of-Art.* ed.; **2014**; Vol. 74C, p 411-426.
- (65) Trask, A. V.; Motherwell, W. D. S.; Jones, W., Physical stability enhancement of theophylline via cocrystallization. *International Journal of Pharmaceutics* **2006**, 320, (1–2), 114-123.
- (66) The A to Z of pharmaceutical cocrystals: a decade of fast-moving new science and patents. *Pharmaceutical Patent Analyst* **2012**, 1, (3), 313-327.
- (67) Surov, A. O.; Manin, A. N.; Voronin, A. P.; Drozd, K. V.; Simagina, A. A.; Churakov, A. V.; Perlovich, G. L., Pharmaceutical salts of ciprofloxacin with dicarboxylic acids. *European Journal of Pharmaceutical Sciences* **2015**, 77, 112-121.
- (68) Saal, C.; Becker, A., Pharmaceutical salts: A summary on doses of salt formers from the Orange Book. *European Journal of Pharmaceutical Sciences* **2013**, 49, (4), 614-623.
- (69) Dahan, A.; Beig, A.; Lindley, D.; Miller, J. M., The solubility–permeability interplay and oral drug formulation design: Two heads are better than one. *Advanced Drug Delivery Reviews* **2016**, 101, 99-107.
- (70) Varanda, F.; Pratas de Melo, M. J.; Caço, A. I.; Dohrn, R.; Makrydaki, F. A.; Voutsas, E.; Tassios, D.; Marrucho, I. M., Solubility of Antibiotics in Different Solvents. 1. Hydrochloride Forms of Tetracycline, Moxifloxacin, and Ciprofloxacin. *Industrial & Engineering Chemistry Research* **2006**, 45, (18), 6368-6374.
- (71) Nechipadappu, S. K.; R. Trivedi, D., Pharmaceutical salts of ethionamide with GRAS counter ion donors to enhance the solubility. *European Journal of Pharmaceutical Sciences* **2017**, 96, 578-589.

- (72) Watts, A. E.; Maruyoshi, K.; Hughes, C. E.; Brown, S. P.; Harris, K. D. M., Combining the Advantages of Powder X-ray Diffraction and NMR Crystallography in Structure Determination of the Pharmaceutical Material Cimetidine Hydrochloride. *Crystal Growth & Design* **2016**, 16, (4), 1798-1804.
- (73) Dennany, L.; Kennedy, A. R.; Walker, B., The hydrochloride and hydrobromide salt forms of (S)-amphetamine. *Acta Crystallographica Section C* **2015**, 71, (10), 844-849.
- (74) He, Y.; Ho, C.; Yang, D.; Chen, J.; Orton, E., Measurement and Accurate Interpretation of the Solubility of Pharmaceutical Salts. *Journal of Pharmaceutical Sciences* **2017**, 106, (5), 1190-1196.
- (75) Caira, M. R., Sulfa Drugs as Model Cocrystal Formers. *Molecular Pharmaceutics* **2007**, 4, (3), 310-316.
- (76) Pindelska, E.; Sokal, A.; Kolodziejski, W., Pharmaceutical cocrystals, salts and polymorphs: Advanced characterization techniques. *Advanced Drug Delivery Reviews* **2017**.
- (77) De Luca, M.; Mas, S.; Ioele, G.; Oliverio, F.; Ragno, G.; Tauler, R., Kinetic studies of nitrofurazone photodegradation by multivariate curve resolution applied to UV-spectral data. *International Journal of Pharmaceutics* **2010**, 386, (1), 99-107.
- (78) *Remington's pharmaceutical sciences*. ed.; Mack: Estados Unidos, **1980**.
- (79) Samsonova, J. V.; Douglas, A. J.; Cooper, K. M.; Kennedy, D. G.; Elliott, C. T., The identification of potential alternative biomarkers of nitrofurazone abuse in animal derived food products. *Food and Chemical Toxicology* **2008**, 46, (5), 1548-1554.
- (80) Silva, F. T.; Franco, C. H.; Favaro, D. C.; Freitas-Junior, L. H.; Moraes, C. B.; Ferreira, E. I., Design, synthesis and antitrypanosomal activity of some nitrofurazone 1,2,4-triazolic bioisosteric analogues. *European Journal of Medicinal Chemistry* **2016**, 121, 553-560.
- (81) Popiołek, Ł.; Biernasiuk, A., Synthesis and investigation of antimicrobial activities of nitrofurazone analogues containing hydrazide-hydrazone moiety. *Saudi Pharmaceutical Journal* **2017**.
- (82) Rahi, A.; Sattarahmady, N.; Dehdari Vais, R.; Heli, H., Sonoelectrodeposition of gold nanorods at a gold surface – Application for electrocatalytic reduction and determination of nitrofurazone. *Sensors and Actuators B: Chemical* **2015**, 210, 96-102.
- (83) Robertson, D., *AMA drug evaluations, 4th edn.* ed.; **1982**; Vol. 3, p 84-84.
- (84) *Calculator Plugins were used for structure property prediction and calculation, Marvin 16.4.25.*, **2016**, ChemAxon (<http://www.chemaxon.com>). # The pKa prediction is done on the

basis of the partial charge distribution calculated for the atoms in the molecule and this method provides an efficient and robust way to locate the most acidic and basic sites.

CHAPTER 2

A blue decorative graphic consisting of a solid blue triangle on the left that tapers to a point on the right, with a lighter blue gradient overlaying it.

Crystal formation procedures as well as techniques used to analyse and collect crystal data are introduced in this section

2 Materials and methods

2.1 Materials

All materials were purchased from Sigma-Aldrich and were used without further purifications.

2.2 Engineering multicomponent crystals

As the first step in multicomponent crystal formation, the functional groups of the NFZ molecule were investigated and synthon engineering principles were used to select a series of possible co-formers with complementary functional groups. Primarily, the (i) amide-amide homosynthon and the (ii) amide-carboxylic acid heterosynthon were aimed to be formed. Therefore, in the first run of the crystallization experiments, a series of carboxylic acids and substituted amides were used. All these crystallisations resulted in the formation of polymorphs α -, β - or γ -form of NFZ; i.e. no crystallization had happened between the API and the cofomers. Parallel to these experiments, NFZ was exposed to a large variety of typical organic solvents with hydrogen bond donor or hydrogen bond acceptor functionalities.

The aim of these crystallisations was to test if hydrogen bonds could be formed with the API via the semicarbazone functional group. The latter mentioned experiments also led to polymorph formation only. It was noted that in the α - and β -polymorphs of NFZ the amide-amide homosynthon was formed between two API molecules and it was concluded that the formation of this synthon is favoured. It became obvious that the applied co-former should have the ability to compete for the formation of the favoured synthon and thus our attention was turned towards the application of short chain aliphatic carboxylic acids and strong mineral acids. Eventually crystallisation of NFZ with perchloric acid (chloric (VII) acid, HClO_4), phosphoric acid (phosphoric (V) acid, H_3PO_4), and propionic acid (propanoic acid, $\text{C}_2\text{H}_5\text{COOH}$) resulted in multicomponent crystals. (Figure 2.1 and Table 2.1).

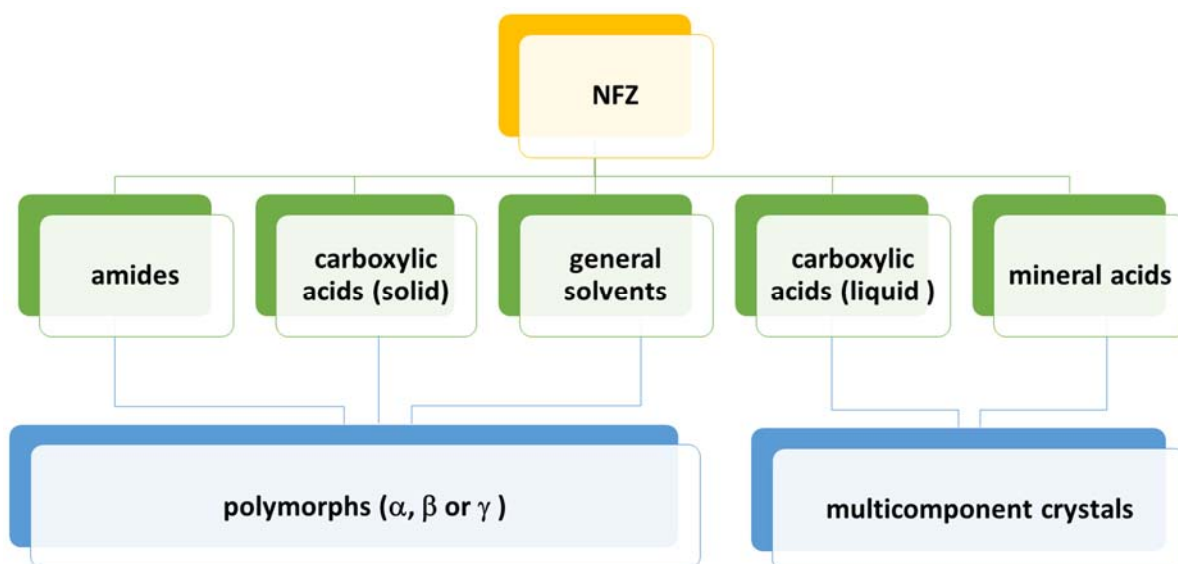


Figure 2.1 Flow chart of crystallisation work

Table 2.1 List of solvents/co-formers applied in cocrystallization experiments

Solvent/Co-former	Molecular formula	Polarity index	Dielectric constant (ϵ)	Outcome
acetamide:acetonitrile	$C_2H_5NO:C_2H_3N$	-	$\epsilon_{\text{vacuum}}=1$	β -polymorph
acetonitrile	C_2H_3N	5.8	37.5	β -polymorph
acetone	C_3H_6O	5.1	21.5	α -polymorph
aspirin- isopropanol:H ₂ O (2:1)	$C_9H_8O_4:C_3H_8O:H_2O$	-	-	β -polymorph
1,4-dioxane	$C_4H_8O_2$	4.8	2.0	β -polymorph
2-aminopyridine:isopropanol	$C_5H_6N_2:C_3H_8O$	-, 3.9	-, 18.0	γ -polymorph
2-aminopyridine:ethanol	$C_5H_6N_2:C_2H_6O$	-, 5.2	-, 16.2	β -polymorph
2,3-lutidine	C_7H_9N	-	-	β -polymorph
2-picoline	C_6H_7N	9.8	-	γ -polymorph
3,4-lutidine	C_7H_9N	-	-	β -polymorph
4-picoline	C_6H_7N	-	-	β -polymorph
dimethylacetamide	C_3H_6O	6.5	-	β -polymorph
dimethylformaldehyde	C_3H_7NO	6.4	-	β -polymorph
HNO ₃	HNO ₃	-	19.0	α -polymorph
H ₂ SO ₃	H ₂ SO ₃	-	-	β -polymorph
isopropanol	C_3H_8O	3.9	18.0	γ -polymorph
methylethylketone	C_3H_6O	4.7	-	β -polymorph
methanol	CH ₄ O	5.1	33.0	α -polymorph
perchloric acid	HClO ₄	-	-	co-crystal salt
phosphoric acid	H ₃ PO ₄	-	-	solvate
propionic acid	$C_3H_6O_2$	-	-	solvate
pyridine	C_5H_5N	5.3	13.2	solvate
tetrahydrofuran	C_4H_8O	4.0	-	β -polymorph

2.3 Methods of crystal growth

Crystals can be acquired using different techniques in solid, liquid or gaseous phase. Possible methods include liquid-assisted grinding (LAG), solution crystallization and spray drying.¹ Each takes advantage of one or more of the following: vaporization, melting, slurry sonication and sublimation.² The most cost-effective method is liquid-assisted grinding, since it uses less solvent than solution crystallization.¹ This work focused on crystallization in solution and liquid-assisted grinding.

2.3.1 Crystallization in solution

Solution crystallization has been useful in making therapeutic solids.³ It is important to know that obtaining different multi-component systems in a co-crystallization experiment is a strong possibility.² Probably the most important advantage of this technique is that it retains the molecular structure of the original API. In other words, change or creation of bonds is only applied within molecules interacting with each other. Solution crystallization allows for modification of the overall behaviour of the crystalline system when it captures another organic compound in solution.⁴ Co-crystallization is specific in terms of stoichiometry. The mole ratios need to be measured and taken into consideration for formation to be predictable. That makes it a very specific method which limits the chances of crystallization to a fine line of relative measurements.⁵ Despite how economically friendly this technique is, there are a few drawbacks too. Impurities can alter the pathway of nucleation and crystal growth. Contamination can affect the process to the point of suppressing crystal growth itself.⁶ That is the reason why solutions are normally filtered using micro-filters or filter papers to reduce the negative effects. It is apparent from crystallization that various crystal shapes have an impact on pharmacological properties, hence the need to enhance and achieve desired crystal shapes.³

Varying the solvent can easily change the outcome of the crystalline solid obtained. Solvent effects can be predicted by the capacity of the solvent to form hydrogen bonds. Solvent variation also has a notable influence on crystal growth as well as crystal outcomes. The variance in solvent also implies that different intermolecular interactions will be formed, hence, different crystal products. The goal here is not to simply get different crystal products but to obtain better drug properties in the end.⁷ Mixing of solvents is normally applicable to similar solvents or those of the same 'family' (i.e. polar solvents): for example, alcohols, amines or

ketones. Sometimes concentration can be varied especially when working with strong mineral acids which are very corrosive. In this research, strong inorganic acids were diluted before being used for crystallization. Another factor that was considered is the boiling point of solvent. Crystallization is improbable with solvents that have very high boiling points. Volatile solvents like primary alcohols, primary ketones or aromatic amines were used in these experiments. Crystal formation depends on many environmental factors like the evaporation rate. Sometimes only a small increase in temperature will dramatically change the solubility of the compound and crystallisation will occur faster. The main groupings of solvent variation with respect to crystal formation are shown in Table 2.2.

Table 2.2 Typical crystallisation methods

Solvent based crystallisation	Non-solvent based crystallisation
Mixing solvents	Thermal activation
Order of addition (ratios)	Sublimation
Rate of addition	Melt crystallization
Concentration	Solvate dehydration
Solvent temperature	Mechanical activation

Another critical factor in crystallization setup is super-saturation. Super-saturation is when a fluid contains more of the dissolved material than could be dissolved by the solvent under given conditions. This solution state is fundamental in the production of crystals.⁸ Super-saturation influences the kinetic reactions within the solution and is subsequently responsible for the size of crystals and crystal faces, as well as their shape.^{3,9} Seeding is also a useful practice in crystallisation. In this practice, an already formed crystal is deposited into a solution to induce nucleation and crystal growth.^{10, 11}

2.3.2 Liquid-assisted grinding

In mechanochemistry, a sub-category of solid-state chemistry, scientists utilize mechanical energy to obtain the desired substances. Crystal engineering has also adopted these techniques in formation of co-crystals. They apply mechano-chemical procedures such as Liquid-Assisted Grinding (LAG).⁷ LAG is among the popular ways of making co-crystals. LAG is a kinetic method of crystal formation and can help to obtain the metastable crystalline systems in relation to Gibbs free energy. One advantage of using LAG is that results are obtained in a matter of

minutes, and in some cases, seconds. Other kinetic methods include slurry sonication or spray-drying.¹² Although LAG produces immediate results relevant to kinetic studies, there is less likelihood of this process producing crystalline materials.¹² Grinding is more likely to produce compounds with smaller grain size as it involves mechanical procedures, and thus their structural analysis with single crystal X-ray diffraction is often impossible. Obtaining the structural information of the formed microcrystalline material is possible with solving the structure from the powder X-ray diffraction patterns, but this is still not a straightforward process. The powder patterns are mainly used for fingerprinting of the compounds, i.e. follow up structural changes when the chemical reaction happens. That is why most crystal engineers resort to the more long-term solution crystallization. When you apply grinding to carry out a chemical reaction between selected starting materials it is very likely that the conversion rate will stay below 100%. Some starting material will always remain in the pestle or pan. When a compound fails to produce any crystal forms using crystallization, then grinding would be an option. In a typical grinding experiment the process is stopped at time intervals and a portion of the reaction mixture is analysed using PXRD, DSC or TG to see the progression of the reaction.⁷

2.4 Crystal growth

Crystallisations were set up in the laboratory and the obtained crystals were analysed. Crystal samples were characterized by various analytical techniques, such as single crystal and powder X-ray diffraction (SCXRD and PXRD), differential scanning calorimetry (DSC), thermogravimetric analysis (TGA), hot-stage microscopy (HSM) and Fourier Transform Infra-Red Spectroscopy (FTIR). Mineral acids, amides, amines, alcohols, nitriles, aromatic amines and some carboxylic acids were used as co-formers. NFZ was crystallized with selected amides and carboxylic acids in a 1:1 ratio (Table 2.1) in all cases.

Preparation of Polymorphs of NFZ

Generally, about 2 ml of each solvent was measured using a syringe and added into the vial with 0.01 g NFZ. The solutions were heated at 60°C and stirred for at least 20 minutes to allow the solid to dissolve. Each vial was left to cool to room temperature and the solutions were filtered. The vials were sealed using parafilm and holes were made in the film to allow the slow evaporation of the solvent. All vials were left in a sunlight-free room and kept away from any

possible disturbances of crystal growth such as frequent agitations and movements. Some crystals were harvested after a week while others were only collected a month later.

Preparation of $4\text{NFZ} \cdot [\text{H}_3\text{O}^+][\text{ClO}_4^-]$ co-crystal salt

Ca. 0.01 g of NFZ was transferred into a vial. 3 ml of 60% HClO_4 (aq) was added into the vial using a glass pipette. The vial was heated and stirred for ca. 60 minutes at 60°C until it completely dissolved. The yellow solution slowly turned into a deeper colour with time. The vial was left on the bench to cool to room temperature. The solution was filtered after cooling and sealed using parafilm. Holes were made on the film to allow the slow evaporation of the solvent. Reddish brown crystals were harvested after 3 months.

Preparation of $\text{NFZ} \cdot \text{H}_3\text{PO}_4$ solvate

Ca. 0.01 g of NFZ was transferred into a vial. 3 ml of 3.4% H_3PO_4 (aq) was added into the vial using a syringe. The vial was heated and stirred for ca. 60 minutes at 60°C to allow maximum dissolution. The solution was left on the bench to cool and filtered afterwards. The vial was sealed using parafilm. Holes were made on the film to allow the slow evaporation of the solvent. Dark brown crystals were harvested after ca. 4 months.

Preparation of $\text{NFZ} \cdot \text{PA}$

Ca. 0.01 g of NFZ was transferred into a vial. About 3 ml of propionic acid was added into the vial using a syringe. The vial was heated and stirred for ca. 60 minutes at 60°C to allow maximum dissolution. The solution was left to cool and filtered afterwards. The vials were sealed using parafilm. Holes were made on the film to allow the slow evaporation of the solvent. All vials were left in a sunlight-free room. Crystals were harvested after about 5 months.

2.5 Analytical tools

2.5.1 Single crystal X-ray diffraction (SCXRD)

Single-crystal X-ray Diffraction is a non-damaging systematic method which offers comprehensive statistics regarding the inside structure of crystals. Analysis by X-rays employs Bragg's Law.¹⁴ William Henry and William Lawrence Bragg simplified Laue's understanding by looking at crystals as mirrors that reflect X-ray radiation on each crystal plane.¹⁴ The law is stated as follows:

$$n\lambda = 2d\sin\theta$$

where:

n= number of slits

λ = wavelength of radiation (Å)

d= distance from one plane to the next (Å)

θ = diffraction angle between incident radiation and crystal (°)

Scattering intensity of diffraction peaks is given by the expression:

$$\frac{1}{2}(1 + \cos^2 2\theta).$$
¹⁴

The larger the 2θ angle, the lower the peak intensity will be. Decent 2θ angle measurements range from 10-70 degrees, depending on type of substance.

A Bruker KAPPA APEX II DUO X-ray diffractometer using 1200 W graphite monochromated Mo K α ($\lambda = 0.71073$ Å) radiation was used for data collections. The selected crystal was cooled using an Oxford Cryostream-700 with liquid nitrogen at a flow rate of 20 ml min⁻¹. The X-rays were produced at 50 kV and 30 mA using a Bruker K780 generator.

Single crystals were analysed as follows: the single crystals were selected with respect to size and any bigger crystals than necessary were cut to get the right size of between 100-500 μm . The selected monocrystalline piece was mounted on a cryoloop and covered with Paratone N oil to retain crystallinity. The stream of nitrogen gas was set at 20 ml min⁻¹. Cell refinement and data reduction were carried out using SAINT-Plus. The X-ray diffraction data were scaled for absorption effects by using SADABS.¹⁵ Crystal assemblies, information and other figures were generated using Mercury 3.9 software.¹⁶ The systematic absences found in the X-ray data

were studied and used to determine the point group through contrast with known space groups. The value of $|E^2 - 1|$ was also inspected specifically for characteristic centrosymmetric and non-centrosymmetric point groups. The space groups were confirmed using XPREP¹⁷. XPREP¹⁷ was also used to prepare SHELXS-97¹⁸ data input files which were subsequently used in structure determination using X-Seed.¹⁹ SHELXS-97²⁰ was used to directly solve and refine all structures by using full-matrix least squares against F^2 for unique reflections, where F is the structure factor.

The structure factor is given by the following expression:

$$\mathbf{F} = \sum_{n=1}^N f_n e^{2\pi i (hu_n + kv_n + lw_n)}, \quad \text{where } f \text{ is the scattering factor}$$

Structure refinement is done via minimizing the function:

$$\sum W^2 (F_o^2 - F_c^2)^2$$

where F_o = observed structure factor and F_c = calculated structure factor.

The R value is assessed to validate the agreement between F_c and F_o . R_1 describes the agreement between F values while wR_2 describes the agreement between intensities for the refinement against F^2 values. The relationship between R and F can be summarized in the following equations:

$$R_1 = \frac{\sum | |F_o| - |F_c| |}{\sum |F_o|}$$

$$R_2 = \left[\frac{\sum w (F_o^2 - F_c^2)^2}{\sum w (F_o^2)^2} \right]^{1/2}$$

W is the default weighing scheme and it is described by the parameters a and b in the following equation:

$$w = \frac{1}{\sigma^2(F_o^2) + (aP)^2 + bP}$$

P is defined by:

$$P = \frac{\max(0, F_o^2) + 2F_c^2}{3}$$

The Goodness of fit (S) is described as follows:

$$S = \left[\frac{\sum w(|F_o|^2 - |F_c|^2)^2}{(N - n_p)} \right]^{1/2}$$

where,

N= number of reflections

n_p= total number of refinement parameters

Other programs used:

ChemSketch²¹ was used to draw line diagrams.

Conquest 1.19²² was used to browse crystal structural data and other geometric parameters.

Platon²³ was used to determine molecular geometric parameters and non-bonded interactions.

2.5.2 Powder X-ray diffraction (PXRD)

PXRD monitors phase changes and identifies forms of crystalline compounds. Samples were finely ground and mounted onto a zero-background sample holder. A diffractogram was acquired under ambient conditions at a power setting of 40 kV and 20 mA in reflection mode while the sample oscillated perpendicular to the beam. X-ray powder diffraction data was collected for all crystals obtained. The Bruker AXS D2 Phaser X-ray Diffractometer was used for analyses.

2.5.3 Differential Scanning Calorimetry (DSC)

DSC is a direct technique used to determine thermal profiles of solid materials. DSC measurements are based on enthalpy changes that are measured for the reference and the sample. The thermal behaviour of the obtained crystals was recorded with a Perkin Elmer DSC 6000. Crystals taken from the mother liquor were dried with filter paper and manually crushed.

They were placed into a vented aluminium sample pan. The sample sizes were between 2–5 mg and the temperature range typically 25–350°C at a heating rate of 10–30°C min⁻¹ depending on sample being analysed. The samples were purged with a stream of nitrogen flowing at 20 ml min⁻¹. Calibration was done using Indium as the reference material. A supplementary DTA instrument was used to run one of the crystal samples from an external laboratory. The sample size was between 2–5mg and the temperature was from 30–300°C

2.5.4 Thermogravimetric analysis (TGA)

TGA is a thermal analysis technique used to determine decomposition profiles of drug substances as a function of temperature. TGA graphs reflect reliably if there are any included solvent in the analysed material. It also gives information like estimated melting points, and indirectly implies crystal robustness. TGA was performed on a Pyris 6 thermogravimetric analyzer. Approximately 3 mg samples were added to an alumina crucible per sample analysed. The samples were heated over a typical temperature range of 30 to 400°C at a heating rate of 10°C min⁻¹. The samples were purged with a stream of flowing nitrogen throughout the experiment at 20 ml min⁻¹.

2.5.5 Fourier Transform Infra-Red Spectroscopy (FT-IR)

Fourier transform Infra-Red spectroscopy is a very useful, direct, fast and reliable technique that gives structural information through measuring peculiar vibrational modes within bonds of molecules. Infra-red radiation interacts with molecules based on molecular dipoles which are influenced by bond rotations and vibrations. FT-IR spectra were collected from pure samples of the crystals using a Perkin Elmer FT-IR spectrometer UATR TWO equipped with a diamond crystal, operating in the range 350 - 4000 cm⁻¹ with a resolution of 4 cm⁻¹ and four scans.

2.5.6 Optical microscopy


Optical microscopy analyses were carried out using a Carl Zeiss Discovery V8 Stereo Light Microscope coupled with a digital camera. This enabled the size of the crystals to be determined and recorded.

References

- (1) Gagniere, E.; Mangin, D.; Puel, F.; Valour, J.-P.; Klein, J.-P.; Monnier, O., Cocystal formation in solution: Inducing phase transition by manipulating the amount of cocrystallizing agent. *Journal of Crystal Growth* **2011**, 316, (1), 118-125.
- (2) Korotkova, E. I.; Kratochvíl, B., Pharmaceutical Cocystals. *Procedia Chemistry* **2014**, 10, 473-476.
- (3) Liang, Z.; Zhang, M.; Wu, F.; Chen, J.-F.; Xue, C.; Zhao, H., Supersaturation controlled morphology and aspect ratio changes of benzoic acid crystals. *Computers & Chemical Engineering* **2017**, 99, 296-303.
- (4) de Maere d'Aertrycke, J. B.; Robeyns, K.; Willocq, J.; Leyssens, T., Cocrystallization as a tool to solve deliquescence issues: The case of l-lactic acid. *Journal of Crystal Growth* **2017**, 472, 3-10.
- (5) Du, S.; Wang, Y.; Wu, S.; Yu, B.; Shi, P.; Bian, L.; Zhang, D.; Hou, J.; Wang, J.; Gong, J., Two novel cocrystals of lamotrigine with isomeric bipyridines and in situ monitoring of the cocrystallization. *European Journal of Pharmaceutical Sciences* **2017**.
- (6) Kubota, N.; Yokota, M.; Mullin, J. W., The combined influence of supersaturation and impurity concentration on crystal growth. *Journal of Crystal Growth* **2000**, 212, (3), 480-488.
- (7) Shimono, K.; Kadota, K.; Tozuka, Y.; Shimosaka, A.; Shirakawa, Y.; Hidaka, J., Kinetics of co-crystal formation with caffeine and citric acid via liquid-assisted grinding analyzed using the distinct element method. *European Journal of Pharmaceutical Sciences* **2015**, 76, 217-224.
- (8) He, G.; Wong, A. B. H.; Chow, P. S.; Tan, R. B. H., Effects of the rate of supersaturation generation on polymorphic crystallization of m-hydroxybenzoic acid and o-aminobenzoic acid. *Journal of Crystal Growth* **2011**, 314, (1), 220-226.
- (9) Prywer, J., Effect of supersaturation on evolution of crystal faces—theoretical analysis. *Journal of Crystal Growth* **2006**, 289, (2), 630-638.
- (10) Karunanithi, A. T.; Acquah, C.; Achenie, L. E. K.; Sithambaram, S.; Suib, S. L., Solvent design for crystallization of carboxylic acids. *Computers & Chemical Engineering* **2009**, 33, (5), 1014-1021.
- (11) Shiraki, K.; Takata, N.; Takano, R.; Hayashi, Y.; Terada, K., Dissolution Improvement and the Mechanism of the Improvement from Cocrystallization of Poorly Water-soluble Compounds. *Pharmaceutical Research* **2008**, 25, (11), 2581-2592.

- (12) Manin, A. N.; Voronin, A. P.; Drozd, K. V.; Manin, N. G.; Bauer-Brandl, A.; Perlovich, G. L., Cocystal screening of hydroxybenzamides with benzoic acid derivatives: A comparative study of thermal and solution-based methods. *European Journal of Pharmaceutical Sciences* **2014**, *65*, 56-64.
- (13) Jonathan W. Steed, J. L. A., *Supramolecular Chemistry, 2nd Edition*. ed.; **2009**; p 1002.
- (14) Bragg, W. H. B., W. L., The reflection of X-rays by crystals. *Proceedings of the Royal Society of London. Series A* **1913**, *88*, (605), 428.
- (15) Sheldrick, G. M., Sadabs. *University of Göttingen, Germany* **1996**.
- (16) Macrae, C. F.; Edgington, P. R.; McCabe, P.; Pidcock, E.; Shields, G. P.; Taylor, R.; Towler, M.; van de Streek, J., Mercury: visualization and analysis of crystal structures. *Journal of Applied Crystallography* **2006**, *39*, (3), 453-457.
- (17) XPREP, X-ray data preparation and reciprocal space exploration program. *Bruker AXS Inc., Madison, Wisconsin, USA* **1997**.
- (18) Sheldrick, G., A short history of SHELX. *Acta Crystallographica Section A* **2008**, *64*, (1), 112-122.
- (19) Barbour, L. J., X-Seed — A Software Tool for Supramolecular Crystallography. *Journal of Supramolecular Chemistry* **2001**, *1*, (4), 189-191.
- (20) Sheldrick, G. M.; Schneider, T. R., [16] SHELXL: High-resolution refinement. In *Methods in Enzymology*, Academic Press: **1997**; Vol. 277, pp 319-343.
- (21) Advanced Chemistry Development, I. A. L. ACD/Chemsketch. **2015**.
- (22) Allen, F. H.; Motherwell, W. D. S.; Iucr, Applications of the Cambridge Structural Database in organic chemistry and crystal chemistry. *Acta Crystallographica Section B: Structural Science* **2002**, *58*, (ARRAY(0xa9a5c54)), 407-422.
- (23) Bruno, I. J.; Cole, J. C.; Kessler, M.; Luo, J.; Motherwell, W. D. S.; Purkis, L. H.; Smith, B. R.; Taylor, R.; Cooper, R. I.; Harris, S. E.; Orpen, A. G., Retrieval of Crystallographically-Derived Molecular Geometry Information. *Journal of Chemical Information and Computer Sciences* **2004**, *44*, (6), 2133-2144.
- (24) Macrae, C. F.; Bruno, I. J.; Chisholm, J. A.; Edgington, P. R.; McCabe, P.; Pidcock, E.; Rodriguez-Monge, L.; Taylor, R.; van de Streek, J.; Wood, P. A., Mercury CSD 2.0 - new features for the visualization and investigation of crystal structures. *Journal of Applied Crystallography* **2008**, *41*, (2), 466-470.

CHAPTER 3

A blue decorative graphic consisting of a solid blue triangle on the left that tapers to a point on the right, with a lighter blue gradient overlaying it.

The following chapter is the presentation and discussion of the obtained NFZ polymorphic crystals.

3 Polymorphs of NFZ

In this section the polymorphic forms of nitrofurazone (NFZ) will be discussed. Several crystallizations were carried out from solvents with a wide range of polarities, namely: primary and secondary alcohols, ketones, amines, amides, aromatic amines and carboxylic acids, with the hope of forming multicomponent crystals with NFZ. 95% of the crystallizations resulted in crystals of a single polymorph of NFZ. Thus, it may be concluded that the majority of the co-crystallization experiments failed to produce multicomponent crystals. Three different polymorphs were found: initially the only known polymorphic form of NFZ was the α -polymorph, which was reported under the code WERVEU in the Cambridge Structural Database. This structure was published by Olszak *et al.* in 1994.¹ It is interesting to note that when the project was initiated in December 2015, the powder X-ray analysis of the starting material (i.e. the form of NFZ used for crystallisations), did not agree with the generated powder pattern of the known α -polymorph. This gave early indications of the existence of possible new polymorphs. The first new form was identified as the β -polymorph. In the following few weeks of January and February of 2016, another new polymorph, the γ -polymorph, was obtained. At this time, parallel to our research, Pogoda *et al.* reported the two new polymorphs of NFZ independently from our research group (WERVEU01 and WERVEU02, as the β - and γ -polymorph, respectively).² Pogoda and co-workers have obtained the crystals of the β -polymorph by dissolving 0.0198 g of NFZ into a solution mixture of 2.5 ml acetonitrile and 8.5 ml methanol. They have obtained the γ -polymorph from dissolving 0.0198 g NFZ in a solution mixture of 3.5 ml deionized water and 7.5 ml acetone, and separately from methanol, ethanol, propan-1-ol, isopropanol, butan-2-ol and acetonitrile.² They reported that the β - and γ -polymorphs were grown concomitantly in a vial containing a 1:1:1 mixture of methanol, n-propanol and acetonitrile.² When our results were compared to the published crystal structures, it was noted that the temperatures of the data collections for the two sets of investigations were different. WERVEU, WERVEU01 and WERVEU02 datasets representing room temperature crystal structures (i.e. their data were collected at 295 K), while our data were collected at low temperature (i.e. at 173 K). The room temperature and the low temperature crystal structures of the polymorphs are basically the same with the obvious difference being their atomic thermal ellipsoids. In Table 3.1, the crystal data for the three published structures are compared with the low temperature crystal data and are labelled as room temperature (RT) and low temperature (LT), respectively.

Table 3.1 Crystallographic data of the three polymorphic forms collected at low (LT) or room temperature (RT).

	α -RT	β -RT	β -LT	γ -RT	γ -LT
Refcode	WERVEU	WERVEU01	-	WERVEU02	-
Formula	C ₆ H ₆ N ₄ O ₄	C ₆ H ₆ N ₄ O ₄	C ₆ H ₆ N ₄ O ₄	C ₆ H ₆ N ₄ O ₄	C ₆ H ₆ N ₄ O ₄
Mr	198.15	198.15	198.15	198.15	198.14
Temp (K)	295	295	173	295	173
System	Monoclinic	Monoclinic	Monoclinic	Monoclinic	Monoclinic
Group	<i>P</i> 2 ₁ / <i>a</i>	<i>P</i> 2 ₁	<i>P</i> 2 ₁	<i>P</i> 2 ₁ / <i>c</i>	<i>P</i> 2 ₁ / <i>c</i>
a/Å	9.943(1)	4.1964(3)	4.2098(5)	13.5703(6)	13.4449(14)
b/Å	8.402(1)	7.0129(5)	6.9632(9)	7.8254(3)	7.8221(9)
c/Å	10.220(1)	14.4528(10)	14.2021(18)	7.9677(4)	7.8587(9)
α/°	90	90	90	90	90
β/°	101.18(1)	90.924(7)	92.360(3)	102.260(4)	103.134(3)
γ/°	90	90	90	90	90
Vol. /Å³	837.587	425.28(5)	415.96(9)	804.859	804.86(16)
Z	4	2	2	4	4
ρ (gcm⁻³)	1.571	1.547	1.582	1.592	1.635
μ (mm⁻¹)	0.126	0.13	0.135	0.14	0.140
Dataset (<i>hkl</i>)	-13,13;-11,11:0,13	-5,5;-7,9;-19,19	-5,5;-9,9;-18,18	-18,17;-10,10;-10,10	-16,17;-10,10;-10,10
F(000)	408	204	204	408	408
Crystal size (mm)	-	0.24 x 0.22 x 0.16	0.08 x 0.17 x 0.41	0.31 x 0.27 x 0.22	0.25 x 0.25 x 0.1
Radiation [Å]	MoK α , 0.7107	MoK α , 0.71073	MoK α , 0.71073	MoK α , 0.71073	MoK α , 0.71073
Theta min-max [°]	2.03, 27.50	2.8, 29.4	1.435, 28.033	3.0, 29.4	3.034, 28.423
Final R indices [I>2.0 (I)]		R ₁ = 0.032 wR ₂ = 0.059	R ₁ = 0.0331 wR ₂ = 0.0806	R ₁ = 0.029 wR ₂ = 0.081	R ₁ = 0.0333 wR ₂ = 0.0892
Tot.,uniqu.data, R(int)	1927, 948, -	5895, 1893, 0.020	5583, 1996, 0.022	11 142, 2127, 0.015	19287, 2029, 0.310
N_{ref}, N_{par}	-	1893, 136	1996, 151	2127, 133	2029, 139
S	-	1.00	1.038	1.00	1.047
Max. and av. Shift/error	-	-	0.000, 0.000	-	0.000, 0.000
Min. and max. resd. dens	-	-0.10, 0.10	-0.198, 0.123	-0.17, 0.13	-0.269, 0.249

Table 3.2 shows the solvents used in crystallizations with NFZ. The outcome of the crystallisations listed in Table 3.2 are based on the PXRD and DSC results (DSC Figures A16-31 in Appendix). We observed that when NFZ was exposed to pyridine, the TG curve suggested that an inclusion compound had been formed. (Figure A25) However, we could not get crystals that were good enough quality for single crystal analysis. We have also included the crystallizations that were done by Pogoda and co-workers in Table 3.2 for completeness.

Table 3.2 List of general solvents used and their respective crystallizations

Solvents and co-formers used	Result
acetamide:acetonitrile	α -polymorph
acetone	α -polymorph
acetonitrile	β -polymorph
acetonitrile:methanol (2.5:8.5)	β -polymorph ²
acetone:H ₂ O (3.5:7.5)	γ -polymorph ²
aspirin:isopropanol-H ₂ O (2:1)	α -polymorph
1,4-dioxane	β -polymorph
2-aminopyridine:ethanol	β -polymorph
2-aminopyridine:isopropanol	γ -polymorph
2,3-lutidine	β -polymorph
2-picoline	γ -polymorph
3,4-lutidine	β -polymorph
4-picoline	β -polymorph
dimethylacetamide	β -polymorph
dimethylformamide	β -polymorph
ethanol	γ -polymorph ²
HNO ₃	α -polymorph
H ₂ SO ₃	β -polymorph
isopropanol	γ -polymorph
methyl:ethylketone	β -polymorph
methanol	α -polymorph
methanol:propanol:acetonitrile (1:1:1)	β and γ (concomitant) ²
pyridine	inclusion compound
tetrahydrofurane	β -polymorph

Micrographs of the three polymorphs were taken to demonstrate the differences in the crystal morphology between them (Figure 3.1). Crystals of α and γ -polymorphs are thin plates, while β -polymorph crystals are prism-shaped. The plate-shaped crystals are bright yellow while the β -polymorph prisms have a darker yellow colouration. All polymorphs were grown separately from at least one kind of solution during the crystallisation experiments, but similar to Pogoda and co-workers' observation, concomitant appearance of α and γ -polymorphs was noticed.

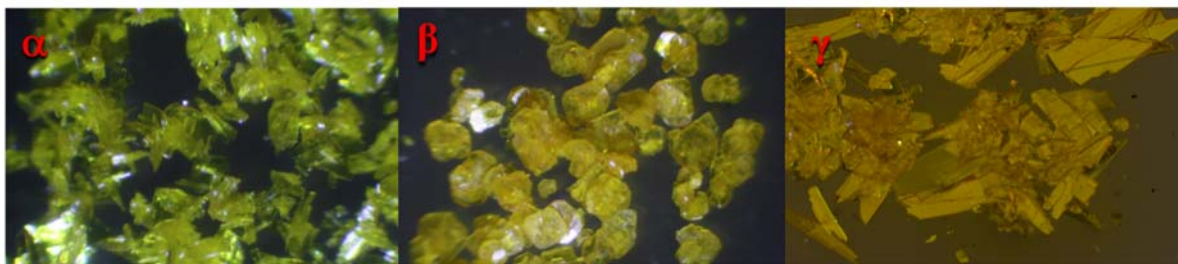


Figure 3.1 Differences in morphology and colour for the three polymorphs

3.1 Crystal structures of NFZ polymorphs

The β -polymorph crystallized in the monoclinic chiral space group $P2_1$ with a single molecule of NFZ ($C_6H_6N_4O_4$) in the asymmetric unit (ASU), and the γ -polymorph crystallized in the monoclinic achiral space group $P2_1/c$ also with one molecule of NFZ in the ASU. In both cases, no solvent nor co-former was able to sufficiently compete with the formation of the amide-amide synthon between the NFZ molecules.

Pogoda *et al.*² designated the NFZ molecule as E and Z with respect to the C=N hydrazone double bond. They went on to find the possible NFZ conformers by classifying the position of hydrogens in the semicarbazone chain as *syn/anti* with respect to the rigid carbonyl group.² According to their classification, they derived four possible different conformers. We found this system for designating molecules to be somewhat confusing, so we applied a simpler classification.

G.P Moss³ published a paper for IUPAC basic terminology and stereochemistry in which he classified torsion angles as follows: given a chain of W-X-Y-Z, the torsion (τ_x) is determined from the W-X-Y and the X-Y-Z plane. The angle is assigned a positive value if the W-X covalent bond has revolved in a clockwise direction.³ It is assigned a negative value if it has rotated otherwise. A torsion is referred to as synperiplanar (*sp*) if the angle is between $0^\circ - \pm 30^\circ$; synclinal (*sc*) if the angle is between $30^\circ - 90^\circ$ or $-30^\circ - -90^\circ$; anticlinal (*ac*) if the angle is between $90^\circ - 150^\circ$ or $-90^\circ - -150^\circ$ and antiperiplanar (*ap*) if the angle is between $\pm 150^\circ - 180^\circ$.³ Because of the planar nature of the NFZ, the most prominent descriptors used in the future descriptions are the *sp* and the *ap*. A summary of the type of torsion angles is shown in Table 3.3.

Table 3.3 Torsion angle classes

Arrangement	Symbol	τ_x (W-X-Y-Z) (°)
synperiplanar	<i>sp</i>	$0^\circ - \pm 30^\circ$
synclinal	<i>sc</i>	$90^\circ - 150^\circ$ or $-90^\circ - -150^\circ$
anticlinal	<i>ac</i>	$30^\circ - 90^\circ$ or $-30^\circ - -90^\circ$
antiperiplanar	<i>ap</i>	$\pm 150^\circ - 180^\circ$

It is important to note that anticlinal (*ac*) and synclinal (*sc*) arrangements were not considered in NFZ due to its typical planar geometry. Having independently applied the synperiplanar (*sp*) and antiperiplanar (*ap*) arrangements to the chain (shown in Figure 3.3), we came up with torsion combinations resulting in 8 different *sp* and *ap* conformers. The arrangements are summarized in Figure 3.3.

The three torsion angles measured in the NFZ molecule are (1) τ_1 (O5-C6-C9-H9), which describes the revolution of either the furan ring or semicarbazone group about the C-C bond; (2) τ_2 (H9-C9•••N11-H11) which describes the revolution of the N-N single bond of the hydrazone group, and (3) τ_3 (H11-N11•••N14-H14), which describes the rotation of the N-C single bond on the NFZ chain. The measured torsion angles are summarized in Table 3.4.

Based on the IUPAC torsion angle classes, we can conclude that α -polymorph is the *ap-sp-sp* conformer while the γ and β -polymorphs are the *sp-sp-ap* conformer. (Figure 3.4) Conformations exhibited in these polymorphs take the expected molecular orientation of semicarbazones as inferred in a CSD analysis done by Pogoda *et al.*²

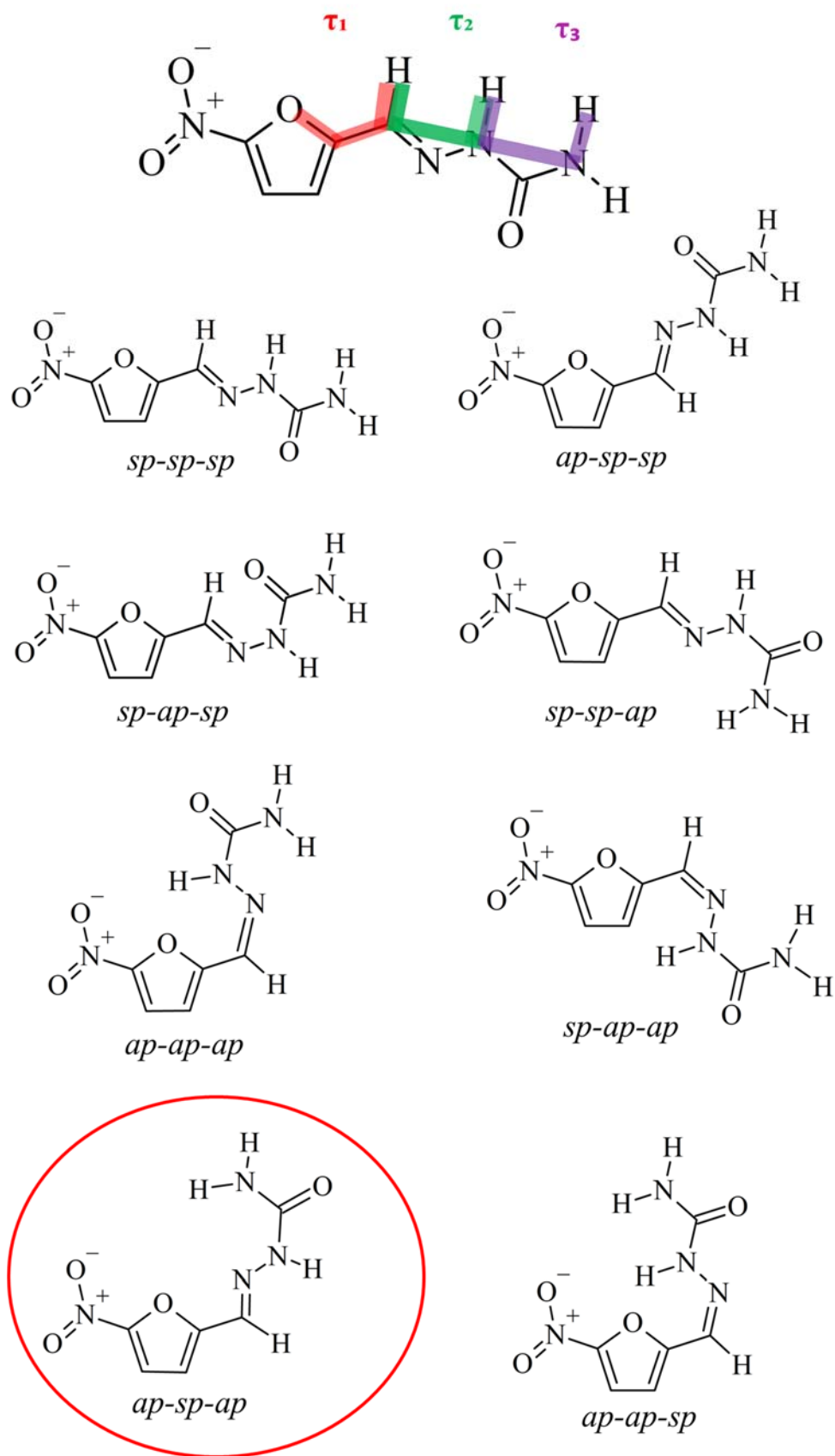


Figure 3.2 Eight possible conformers arising from the *sp* and *ap* torsion combinations. Newly found conformer of NFZ in NFZ·H₃PO₄ crystal is circled in red

Table 3.4 Torsion angles of polymorphs α -, β - and γ -polymorphs

Polymorph	τ_1 (O5-C6-C9-H9) ($^\circ$)	τ_2 (H9-C9...N11-H11) ($^\circ$)	τ_3 (H11-N11...N14-H14) ($^\circ$)
α -polymorph*	177.46	-10.14	-1.32
β -polymorph	-3.07	-8.54	-162.67
γ -polymorph	-0.71	3.29	174.22

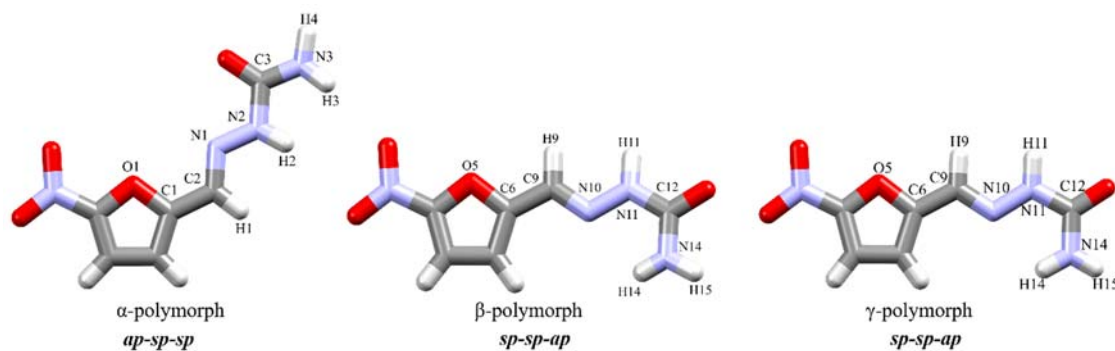


Figure 3.3 Conformers observed in the known polymorphs of NFZ

In all three polymorphs the NFZ molecules are arranged into hydrogen-bonded tapes via their carbamide (α - and β -polymorphs) or semicarbazone (γ -polymorph) functionalities. (Figure 3.4) The major difference between the crystal structures lies in the intricate details of the hydrogen bonding synthons. In the α -polymorph, the NFZ molecules are connected via two hydrogen bonds, namely N2—H2...O2 and N3—H3...O2, that are described with $R_2^1(6)$ graph set notation.⁴ In the β -polymorph, the NFZ molecules form dimers via N11—H11...O13 and N14—H15...O13 hydrogen bonds, and are described with the graph set $R_2^2(8)$. In the γ -polymorph, the NFZ molecules are connected via three sets of hydrogen bonds. A ring motif is formed with N11—H11...O13 and C9—H9...O13 that are described with the graph set $R_2^1(6)$, and two individual hydrogen bonds are noted between the neighbouring NFZ molecules (N14—H14...O2 and C7—H7...O2). The geometrical details of the hydrogen bonds are listed in Table 3.5. To summarize, the most robust hydrogen bonding is observed in the β -polymorph, where non-centrosymmetric amide dimers are formed. The hydrogen-bonded tapes in the α - and the γ -polymorphs are formed via bifurcated hydrogen bonds.⁵ Also, no additional interactions can be noted between the layers of molecules in these two structures. It is interesting to note that although the NFZ molecules of β - and γ -polymorphs are the same conformers based on the selected torsion angles, there is a minor difference between the

* structural data of α was retrieved from Mercury, hence the different atomic numbering in Figure 3.3.

molecular structures. This was represented by inserting planes to the furan ring and subsequently to the semicarbazone moiety (atoms included N4, C6, O4 and N3) and measuring the plane angle (Figure 3.5). The plane angle in the β and γ -polymorphs are 7.32° and 1.96° , respectively. This larger tilt of the semicarbazone moiety aids the formation of the N14—H14 \cdots O2 interlayer hydrogen bond in the β -polymorph and adds extra robustness to the structure (Figure 3.6).

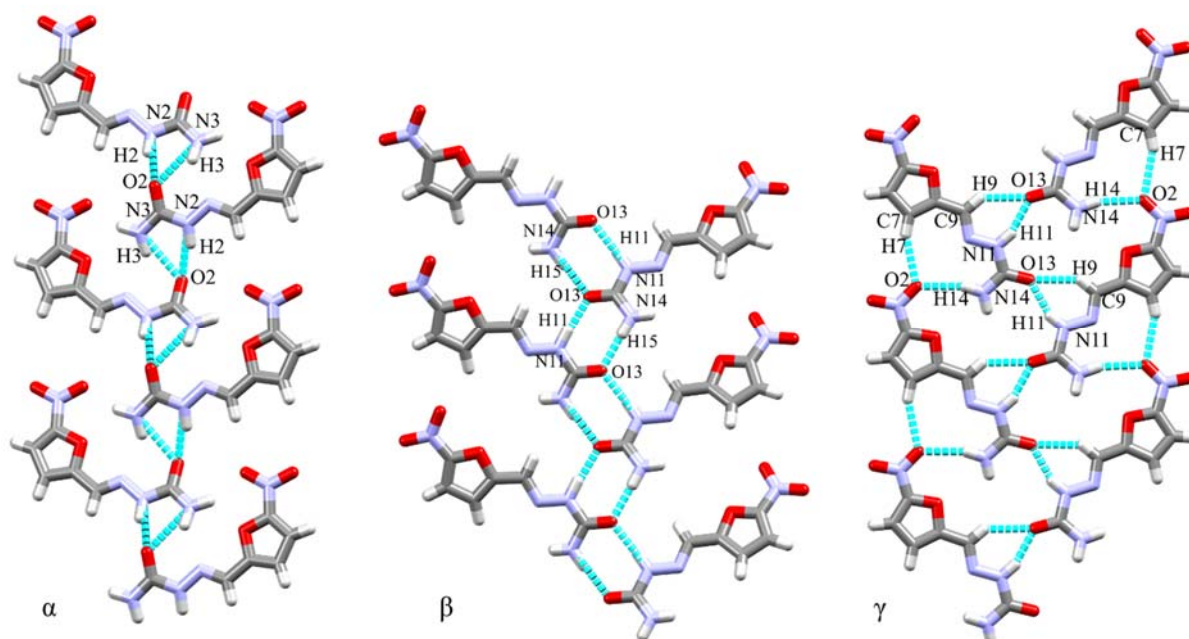


Figure 3.4 Hydrogen bonding interactions forming the NFZ tapes

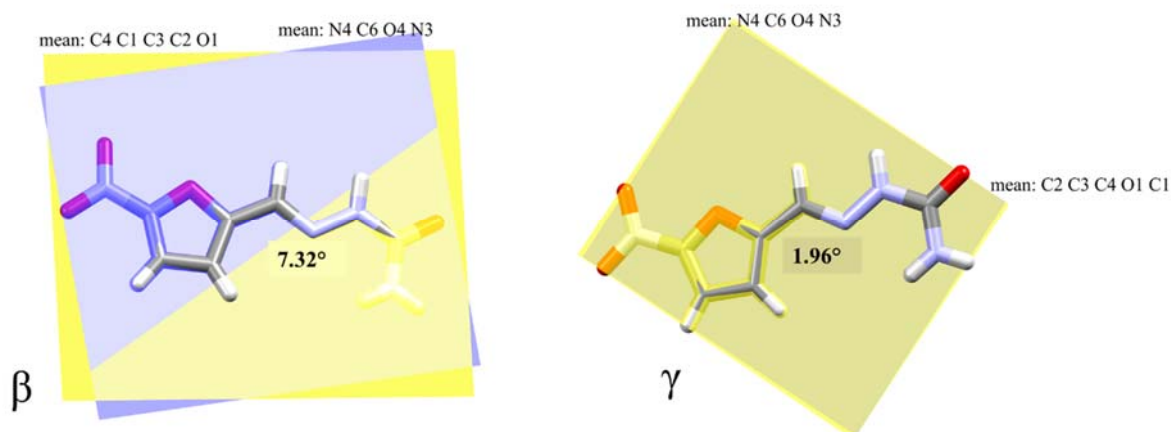


Figure 3.5 Representation of the slight difference in the NFZ conformers in the β - and γ -polymorphs

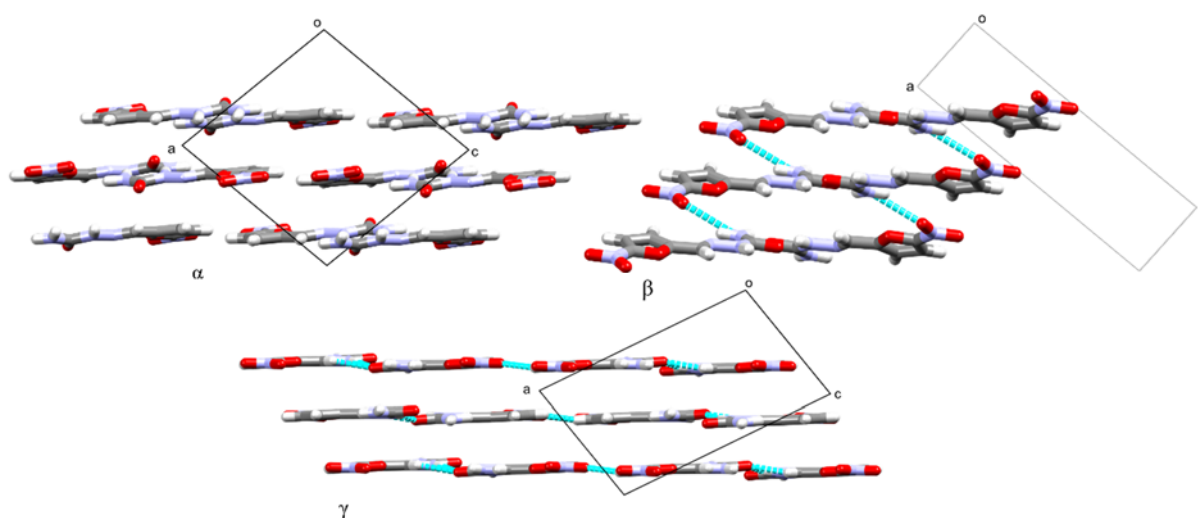


Figure 3.6 Packing of the parallel sheets in the NFZ polymorphs

Table 3.5 Geometric parameters for the intermolecular interactions in the three NFZ polymorphs

D-H...A	d(D-H) (Å)	d(H...A) (Å)	d(D...A) (Å)	D-A...A (°)	Symmetry operators
α-polymorph					
N2-H2...O2	0.916	1.867	2.743	159.48	$\frac{1}{2}-x, \frac{1}{2}+y, 2-z$
N3-H3...O2	0.909	2.133	2.918	144.03	$\frac{1}{2}-x, \frac{1}{2}+y, 2-z$
N3-H3...N1	0.909	2.318	3.088	142.38	$\frac{1}{2}-x, \frac{1}{2}+y, 2-z$
β-polymorph					
N11-H11...O13	0.930	1.899	2.804	163.61	$-x+3, -\frac{1}{2}+y, -z$
N14-H15...O13	0.915	2.009	2.80	163.35	$-x+3, \frac{1}{2}+y, -z$
N14-H14...O2	0.833	2.444	3.197	150.70	$x+1, y+1, z$
C8-H8...O3	0.953	2.390	3.325	166.93	$-x, \frac{1}{2}+y, -z+1$
C9-H9...O13	0.955	2.638	3.171	115.67	$-x+2, -\frac{1}{2}+y, -z$
γ-polymorph					
N11-H11...O13	0.882	1.976	2.812	157.82	$-x+1, -\frac{1}{2}+y, \frac{1}{2}-z$
N14-H14...O2	0.906	2.297	3.175	162.95	$x, 1+y, z$
C7-H7...O2	0.950	2.523	3.421	157.74	$x, 1+y, z$
C8-H8...O3	0.950	2.343	3.223	153.80	$-x, \frac{1}{2}+y, \frac{3}{2}-z$
C9-H9...O13	0.950	2.419	3.203	139.69	$1-x, -\frac{1}{2}+y, \frac{1}{2}-z$

3.2 Bulk property analysis of NFZ polymorphs

Bulk properties of the polymorphs were analysed using powder X-ray diffraction, thermal analytical methods (TGA and DSC) and FTIR spectroscopy.

3.2.1 Powder X-ray diffraction of NFZ polymorphs

The PXRD analysis played a significant role in the initial stages of this project. Initially, the PXRD pattern of the starting NFZ material was compared to the PXRD patterns of the then only known α -polymorph, which revealed significant differences in the positions of their characteristic peaks. Once the crystal structures of the β - and γ -polymorphs were obtained, it was concluded that the starting material was the β -form. Figure 3.6 summarizes the PXRD patterns of all three polymorphs and shows the experimental pattern of the starting material (α , β and γ represented as green, blue and red, respectively) (Figure 3.7). The purple pattern represents the starting material and shows good agreement with the blue; hence it is concluded that the starting material was the β -polymorph. The differences between the three patterns are obvious and thus PXRD could be successfully used to distinguish between the solid forms obtained from crystallisations.

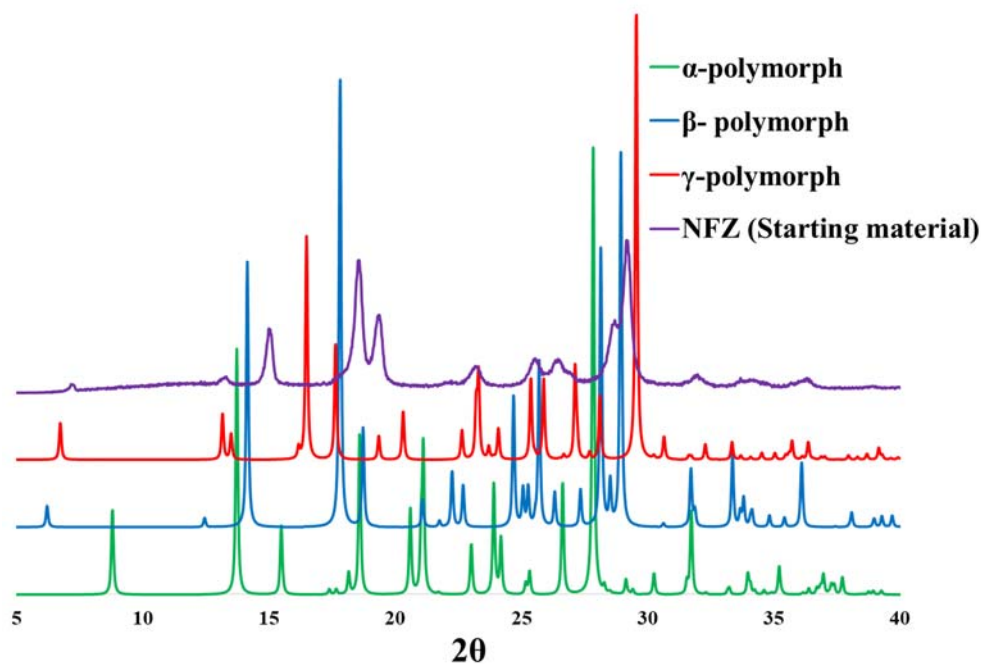


Figure 3.7 Generated SCXRD patterns of α -, β - and γ -polymorphs versus PXRD pattern of NFZ starting material

In all crystallisations, the experimental PXRD pattern was compared to the patterns of the three polymorphs, taking into account possible peak shifts of PXRD patterns since they are obtained at different temperatures. All relevant experimental and generated patterns are represented in Figures A1-A15 in the Appendix and the outcomes of the crystallisations are listed in Table 3.2.

3.2.2 Thermal analysis of NFZ polymorphs

The melting temperatures for the three NFZ polymorphs were published as 238-241 °C for α^1 , 236.39 - 238.21 °C for β^2 and 239.70 – 241.20 °C for the γ -polymorph² (Table 3.6). These published thermal data would suggest that the β -polymorph is the least thermally stable form. The thermal stability of the α and the γ -polymorphs are better than the β -polymorph. When the three polymorphs were analysed in our laboratory, we have obtained strikingly different results for their thermal behaviour. The literature data were collected with a 5 K min⁻¹ heating rate while our system was run at 10-30 K min⁻¹, depending on the sample being analysed. During the polymorph screening the applied heating rate was typically 30 K min⁻¹ to prevent possible polymorphic transformation and thus enable us to observe the polymorphic purity.

The significant difference measured in the melting endotherms is mainly the result of the applied heating rate. However, it is interesting to note that the order of thermal stability for the three polymorphs were observed to be different. The γ form was found to be the least stable; this was followed by the α form; and the most stable form was found to be the β form. Figures 3.8-3.9 show the measured DSC curves of the three polymorphs. This order of stability shows good agreement with the crystal structure analysis where the extra interlayer hydrogen bonds in the β form were emphasized. It is also interesting to note that the NFZ sample used for the project was many years old and was stored without any precautions. This also supports the conclusion that the β -polymorph is likely to be the most stable form.

DSC results of the obtained crystals and the starting material are represented in Figures A16-31 in the Appendix (only relevant DSCs are inserted) and the results are summarized in Table 3.6. Polymorphic phases were identified based on the peak temperatures, because the onset temperatures were found to be very sensitive to the particle size of the sample; the phases were

subsequently confirmed by matching the PXRD patterns. It was concluded that co-crystallization of NFZ with aspirin and nicotinic acid in diluted iso-propanol solvent and crystallisation of NFZ from tert-butanol, methanol and acetone produced the α -polymorph, while crystals obtained from dimethylformamide, dimethylacetamide, 4-picoline and dioxane produced the β -polymorph. The DSC results from iso-propanol solvent and 2-picoline show the formation of the γ -polymorph. TGA was used to note if there was any inclusion compound formation during the crystallisations. Relevant curves are inserted in the Appendix (Figures A32-35).

Table 3.6 DSC data for NFZ crystals obtained from crystallizations

Known forms of NFZ	T _{onset} (°C)	T _{peak} (°C)
α -polymorph ¹	238	241
β -polymorph ²	236.39	238.21
γ -polymorph ²	239.70	241.20
α-polymorph	249.14	253.45
acetone	249.59	254.24
aspirin:isopropanol-H ₂ O	249.22	253.45
acetamide:acetonitrile	248.03	255.22
nicotinamide:acetonitrile	247.39	252.92
2-aminopyridine:ethanol	246.46	250.27
β-polymorph	252.30	259.34
dioxane	252.1	257.1
tetrahydrofuran	252.18	260.33
dimethylformamide	252.37	259.34
dimethylacetamide	250.59	258.88
4-picoline	253.60	258.77
γ-polymorph	241.06	248.95
isopropanol	241.06	248.95
2-picoline	242.17	248.00
3,4-lutidine	235.20	247.84
2,3-lutidine	239.40	244.78
2-aminopyridine-isopropanol	245.35	248.82

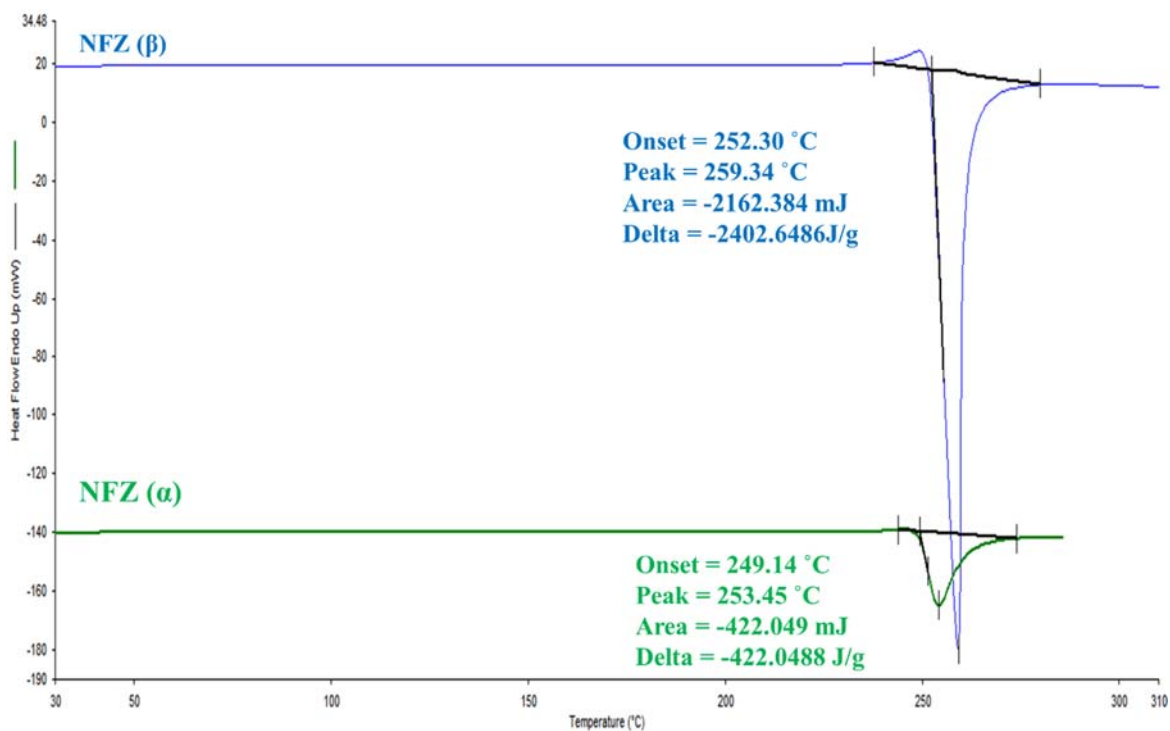


Figure 3.8 DSC curves of α form against the starting material (β form)

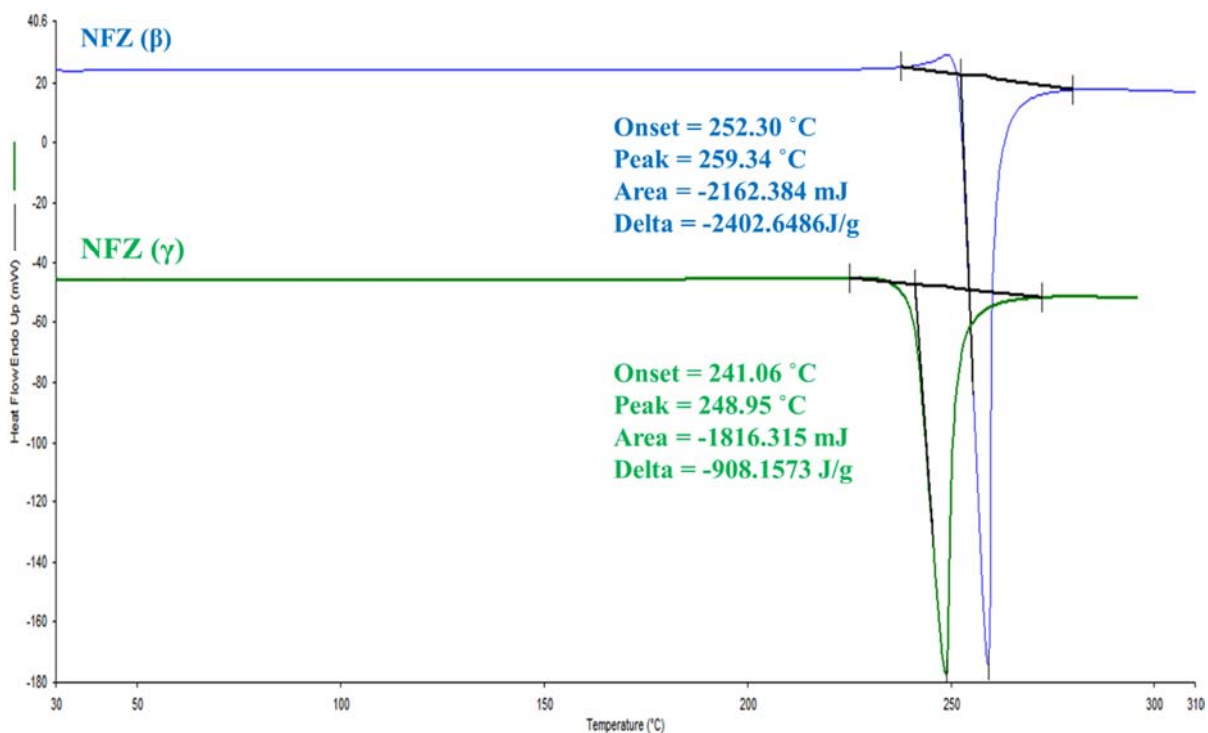


Figure 3.9 DSC curves of γ form against starting material (β form)

3.2.3 FTIR spectroscopy of NFZ polymorphs

FTIR spectroscopy was conducted on the NFZ crystals to determine the vibrational modes of each polymorphic form. Since the conformations of the molecules in the three polymorphs are similar, the three polymorphs were expected to have similar spectra. The typical IR peaks of the NFZ functional groups are expected to be the same for all three forms and only slight differences are likely to appear corresponding to the different intermolecular interactions noted in the three structures. We also expected the intermolecular interactions to influence the vibrational modes of the three forms differently. Spectral shift can occur due to hydrogen bond interactions and/or conjugation. However, the consequence of conjugation via the (C=O) is less in amides as compared to molecules containing aldehyde and carbonyl groups.⁶

Firstly, weak peaks were observed in the α -polymorph as compared to peaks of β and γ . (Figure 3.10) The diminishing of this spectrum is possibly due the amount of sample being too small. Both β and γ have visually similar spectra. The major peak at 1677 cm^{-1} is observed for α carbonyl (green spectra) with a diminished side peak observed at 1708 cm^{-1} . β - has one major peak projecting as well as a diminished peak. The major peak for β has shifted to a lower frequency of 1670 cm^{-1} while the diminished peak was observed at 1708 cm^{-1} . γ retains a 1705 cm^{-1} sharp peak and a diminished peak at 1680 cm^{-1} . The differences in the carbonyl characteristic peak (frequency range $1720\text{-}1640\text{ cm}^{-1}$) may be explained by the intermolecular interactions. It is important to note that hydrogen bonding affects the absorption of the carbonyl, but not as significantly as it would an O-H or C-H sigma vibrational mode. This explains why the spectral shift deviates less compared to the shift for O-H or C-H absorptions.⁶

Medium intensity asymmetric vibrations were experienced within NH_2 bonds. A characteristic peak is seen at 3459 cm^{-1} for all three polymorphs. This is probably due to the NH_2 symmetric stretching. It is worth mentioning that the occurrence of a carbonyl is sometimes confirmed by an overtone peak at ca. 3400 cm^{-1} . Either way, these frequencies support the presence of the amide functional group. The intensity, however, is expected to change whenever intermolecular interactions come into play. NH_2 symmetric vibrational mode peaks show at 3136 and 3120 cm^{-1} , observed as a characteristic double peak. The peaks however have slightly shifted to lower frequency because of hydrogen bonding. NH_2 in-plane bend were observed at ca. 1580 cm^{-1} with a sharp peak. The out-of-plane vibrational modes for NH_2 bonds were observed around 1300 cm^{-1} .

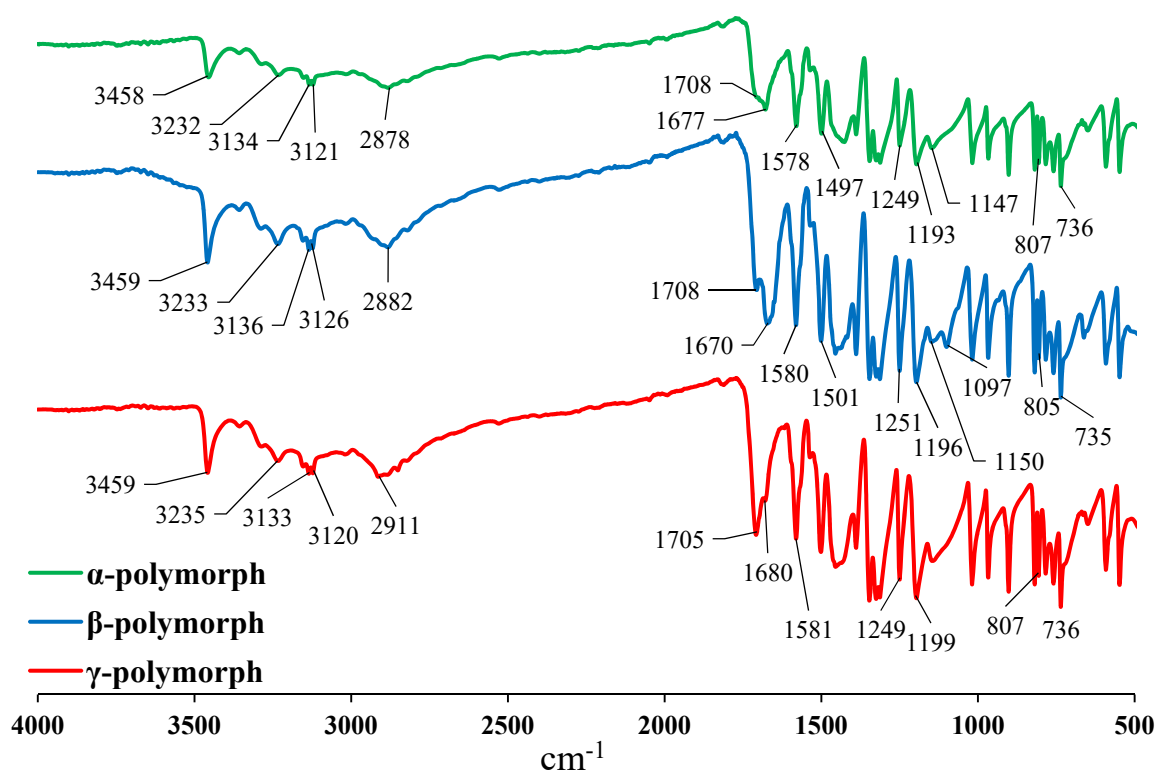


Figure 3.10 IR spectra of the three polymorphic forms

Medium to low intensity CH vibrational modes were observed between $3100\text{-}2900\text{ cm}^{-1}$, although they are not well-defined. This is due to the deficiency of alkyl bonds, hence active IR alkyl vibrations. Very strong and narrow carbonyl double bond vibrations were observed at peak $1710\text{-}1700\text{ cm}^{-1}$. The carbonyl peak frequency is not lowered because there is no conjugation within the carbonyl functional group. A furan ring carbon-carbon double bond peak was observed with very sharp descent at $1650\text{-}1600\text{ cm}^{-1}$. The nitro symmetric stretch was observed at ca. 1310 cm^{-1} , and almost overlaps with the out of plane bend peak for NH_2 (relevant Figures A36-A39 are presented in the Appendix). Vibrational modes observed in the conformers are summarized in Table 3.7.


Table 3.7 Molecular vibrations observed in the FTIR spectra of the polymorphic forms

Functional group	Assignment	Expected	Observed
IR peaks in cm⁻¹			
Amide	NH ₂ symmetric stretching	3360-3340	3458(α), 3459(β), 3459(γ)
	NH ₂ asymmetric stretching	3190-3170	3232(α), 3233(β), 3235(γ)
Alkyl	CH stretch	3157-2814	3122(α), 3135(β), (γ)
Carbonyl	C=O stretch	1720-1640	1677(α), 1680 (β), 1705(γ)
	C=O overtone	~3400	3459
Fingerprint region			
Nitro	NO ₂ asymmetric stretch	1510-1500	1497(α), 1501(β), 1510(γ)
	NO ₂ symmetric stretch	1390-1380	1387(α), 1389(β), 1387(γ)
	NO ₂ bending	800-500	807(α), 805(β), 807(γ)
Amide	NH ₂ out-of-plane bending	784, 1346	806(α), 783(β), 817(γ) 1326 (α), 1325(β), 1347(γ)
Furan	Out-of-plane CH vibration	735	736(α), 735(β), 736(γ)

References

- (1) Olszak TA, P. O., Blaton NM, De Ranter CJ, 5-Nitro-2-furaldehyde semicarbazone. *Acta Crystallographica* **1994**, Vol. 50, 948-950.
- (2) Pogoda, D.; Janczak, J.; Videnova-Adrabinska, V., New polymorphs of an old drug: conformational and synthon polymorphism of 5-nitrofurazone. *Acta Crystallographica Section B* **2016**, 72, (2), 263-273.
- (3) Moss, G., Basic terminology of stereochemistry (IUPAC Recommendations 1996). *Pure and applied chemistry* **1996**, 68, (12), 2193-2222.
- (4) Etter MC, M. J., Graph-Set Analysis of Hydrogen-Bond Patterns in Organic Crystals. *Acta Cryst* **1990**, 46, 256-262.
- (5) Jonathan W. Steed, J. L. A., *Supramolecular Chemistry, 2nd Edition*. ed.; **2009**; p 1002.
- (6) Stuart, B. H., Spectral Analysis. In *Infrared Spectroscopy: Fundamentals and Applications*, John Wiley & Sons, Ltd: **2005**; pp 45-70.

CHAPTER 4



The following chapter is the presentation and discussion of multicomponent crystals obtained.

4 Multicomponent crystals of nitrofurazone

The formation of multicomponent crystals with NFZ was extremely challenging. All the co-crystallisations with the selected co-formers or solvents failed, and mainly resulted in polymorph formation. The series of mineral acids and short chain carboxylic acids were used to offer a strong hydrogen bond donor species with the hope of breaking the amide homodimers and forming the amide-acid heterodimer (Table 4.1). It was also anticipated that applying mineral acids with very low pKa values (i.e. $\text{pKa} < 0$) would aid salt formation with the NFZ molecule via the protonation of the hydrazone moiety (Figure 4.1). Eventually three multicomponent crystals were obtained from this set of experiments and their single crystal data is summarized in Table 4.2.

Table 4.1 List of acid solvents used and their respective crystallizations

Solvents used	pKa	Results
HClO ₄ (dil)	≈ -10	co-crystal salt ¹
HClO ₄ (conc)	≈ -10	co-crystal salt ¹
H ₃ PO ₄ (dil)	2.12	solvate
H ₃ PO ₄ (conc)	2.12	solvate
H ₂ SO ₃ (dil)	1.81	β-polymorph
H ₂ SO ₃ (conc)	1.81	β-polymorph
HNO ₃ (dil)	< 1	β-polymorph
HNO ₃ (conc)	< 1	β-polymorph
H-COOH (FA)	3.75	β-polymorph
CH ₃ -COOH (AA)	4.76	β-polymorph
CH ₃ CH ₂ -COOH (PA)	4.87	solvate

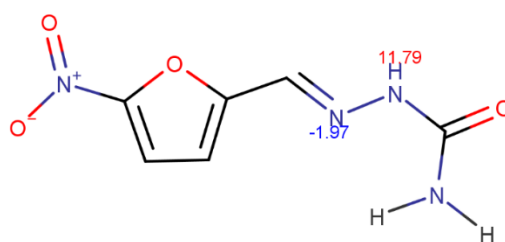


Figure 4.1 The pKa values of NFZ calculated with Marvin²

4.1 Crystal structure of 4NFZ·[H₃O⁺][ClO₄⁻]

Poor quality crystals were obtained after 3 months. Their morphology resembled very thin plates with multiple crystals clustered, thus the selection of a good quality crystal for single crystal data collection was extremely challenging (Figure 4.2).

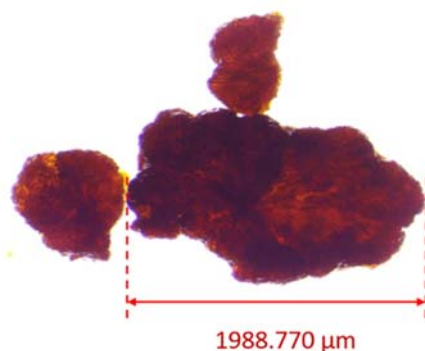


Figure 4.2 Photograph of uncut 4NFZ·[H₃O⁺][ClO₄⁻] co-crystal salt

A suitable crystal of 4NFZ·[H₃O⁺][ClO₄⁻] with dimensions 0.07 x 0.11 x 0.13 mm was selected for single crystal X-ray analysis. The compound crystallizes in the triclinic $P\bar{1}$ space group with four NFZ molecules, one H₃O⁺ and one ClO₄⁻ ions in the asymmetric unit. The acid donates its proton to a water molecule which subsequently forms a hydronium (H₃O⁺) ion. The amide homodimers were broken up and the four symmetrically independent NFZ molecules formed a virtually 4-fold arrangement around the hydronium ion (Figure 4.3). All four NFZ molecules are in the *sp-sp-ap* conformation. The molecular units of NFZ are labelled A, B, C and D in the ASU.

The four NFZ molecules hydrogen bond together via four N15-H15···O13 interactions that may be described by the $R_4^4(16)$ graph set. The central hydronium ion also hydrogen bonds to each NFZ forming $R_3^2(8)$ motifs. The four, almost coplanar NFZ tapes and the hydrogen bonded hydronium ion, dubbed as the *tetramer*, is the basic building unit of the crystal. The neighbouring tetramers are coplanar and held together via hydrogen bonds formed between the nitro oxygens and the hydrazone moieties, N11-H11···O2, described by the $R_2^2(18)$ graph set (Figure 4.4). Relevant crystallographic data and geometries of the hydrogen bonds are listed in Tables 4.2 and 4.3, respectively.

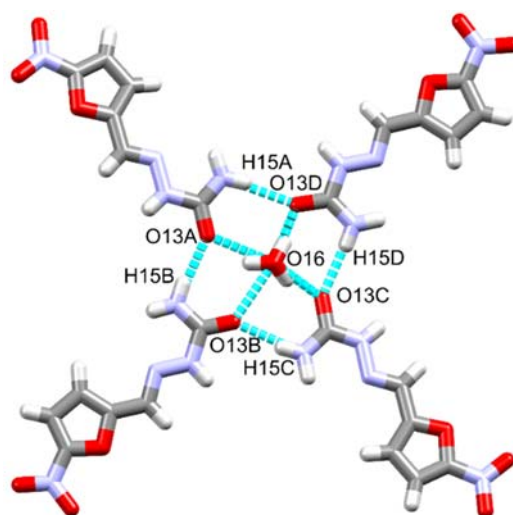


Figure 4.3 ASU of 4NFZ•[H₃O⁺][ClO₄⁻] showing the hydrogen bonds between the four symmetry independent NFZ molecules (labelled as A-D) and the hydronium ion (perchlorate anion is omitted for clarity)

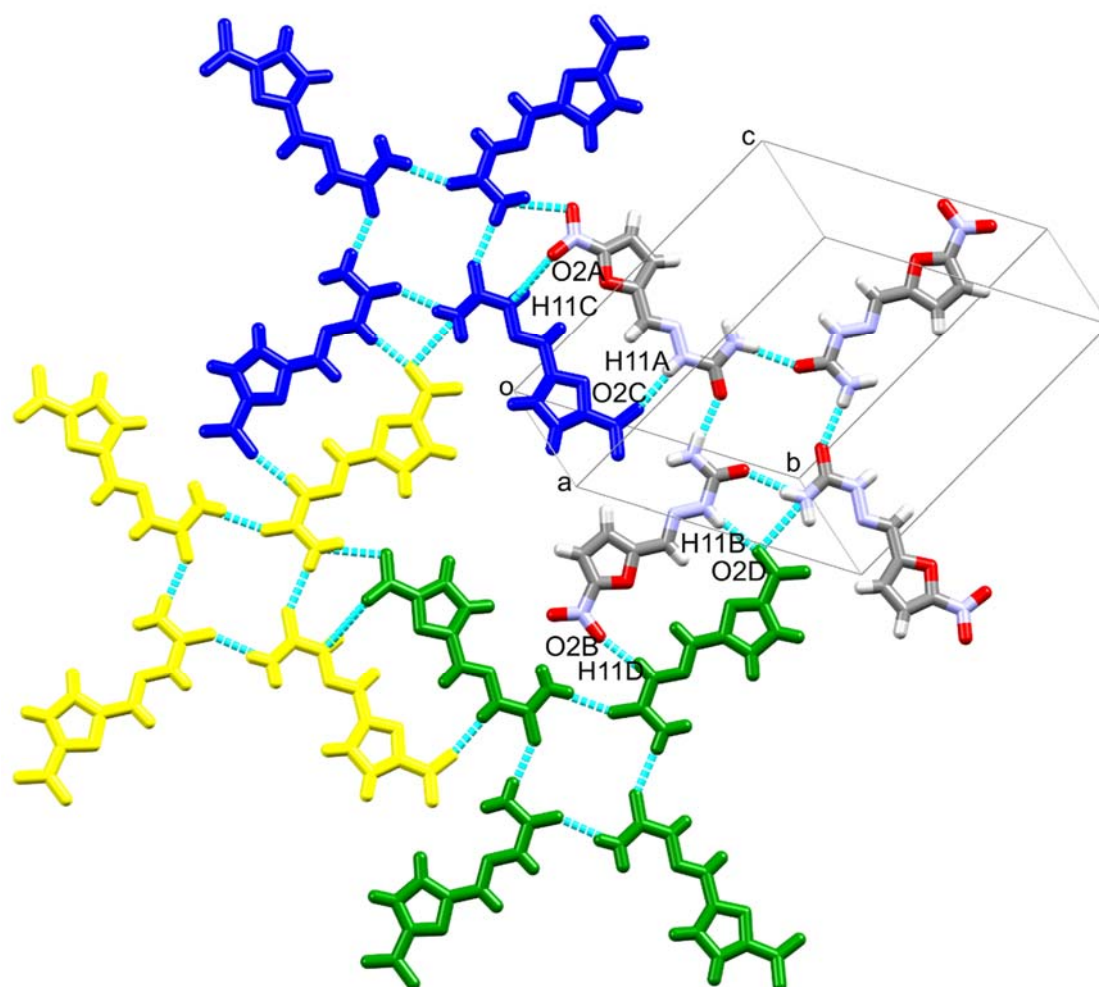


Figure 4.4 Hydrogen bonds between the neighbouring NFZ molecules to hold the tetramers together. (The hydronium ions and the perchlorate anions are omitted for clarity)

Table 4.2 Crystallographic data of the three multicomponent crystals of NFZ

	4NFZ•[H₃O⁺][ClO₄⁻]	NFZ•H₃PO₄	NFZ•PA
Molecular formula	C ₆ H ₆ N ₄ O ₄	C ₆ H ₉ N ₄ PO ₈	C ₉ H ₁₂ N ₄ O ₆
Formula weight	911.04	296.13	272.22
Temperature (K)	173(2)	173(2)	173(2)
Crystal system	Triclinic	Triclinic	Monoclinic
Space group	<i>P</i> $\bar{1}$	<i>P</i> $\bar{1}$	<i>P</i> 2 ₁ / <i>c</i>
a/Å	7.9863(16)	4.4913(9)	15.801(3)
b/Å	14.566(3)	10.893(2)	12.931(3)
c/Å	16.208(3)	12.672(3)	24.475(5)
α/°	77.88(3)	106.87(3)	90
β/°	80.90(3)	99.66(3)	90.04(3)
γ/°	87.87(3)	92.30(3)	90
Vol. /Å³	1820.2(7)	582.271	5000.8(17)
Z	2	2	16
MP /°C	223	221	241-248
ρ (gcm⁻³)	0.22	0.22	1.446
μ (mm⁻¹)	1.662	1.662	0.123
Dataset (<i>hkl</i>)	-16,16;-10,10;-10,10	-16,16;-10,10;-10,10	-21,21;-17,17;-32,32
F(000)	936.00	304.00	2272.00
Crystal size (mm)	0.07×0.11×0.13	0.29×0.39×0.56	0.12×0.13×0.15
Temperature (K)	173.15	173.15	173.15
Radiation [Å]	MoK α ,	MoK α , 0.71073	MoK α , 0.71073
Theta min-max[°]	1.300/25.073	1.710/28.423	28.423
Final R indices [I>2.0 (I)]	R ₁ = 0.0527 wR ₂ = 0.1408	R ₁ = 0.0298 wR ₂ = 0.0812	R ₁ = 0.0473 wR ₂ = 0.1265
Tot., uniq.data, R(int)	3976, 6451, 0.0456	13757, 2900, 0.0337	7474, 12422, 0.0802
N_{ref}, N_{par}	6472, 619	2906, 196	12444, 705
S	0.964	1.036	1.009
Max. and av. Shift/error	0.000/0.000	0.000/0.000	0.000/0.011
Min. and max. resd. dens	-0.442, 0.511	-0.317, 0.345	-0.442, 0.511

Table 4.3 The geometric parameters for intermolecular interactions in 4NFZ•[H₃O⁺][ClO₄⁻]

D-H...A	D-H (Å)	H...A (Å)	D...A (Å)	D-H...A (°)	Symmetry operators
MOLECULE A					
C8A-H8A...Cl17	0.950	2.912	3.736	145.79	-x, -y, -z +1
C8A-H8A...O20	0.950	2.566	3.455	155.91	-x, -y, -z +1
C9A-H9A...O19	0.950	2.465	3.107	124.84	
N11A-H11A...O2C	0.840	2.203	2.991	156.35	-1+x, -1+y, z
N14A-H14A...O3B	0.829	2.472	3.211	149.11	-1+x, y, z+1
N14A-H15A...O13D	0.841	2.164	2.995	169.77	
MOLECULE B					
C7B-H7B...O3C	0.950	2.501	3.426	164.41	-1+x, -1+y, z
C8B-H8B...O18	0.950	2.416	3.331	161.50	1-x, -y, -z
N11B-H11B...O2D	0.853	2.118	2.960	169.14	1+x, y, -1+z
N14B-H14B...O3C	0.877	2.357	3.190	158.68	-1+x, -1+y, z
N14B-H15B...O13A	0.828	2.095	2.915	170.81	
MOLECULE C					
C7C-H7C...O3D	0.950	2.548	3.458	160.48	1+x, y, -1+z
C8C-H8C...O21	0.950	2.479	3.217	134.53	2-x, 1-y, -z
N11C-H11C...O2A	0.829	2.412	3.063	135.92	-1+x, -1+y, z
N11C-H11C...O20	0.829	2.244	2.982	148.30	x, y+1, z
N14C-H14C...O2D	0.919	2.567	3.026	111.45	1+x, y, -1+z
N14C-H14C...O3D	0.919	2.272	3.167	164.10	1+x, y, -1+z
N14C-H14C...O13B	0.851	2.090	2.925	166.67	
MOLECULE D					
C8D-H8D...Cl17	0.950	2.942	3.697	137.36	1-x, 1-y, 1-z
C8D-H8D...O19	0.950	2.618	3.131	114.24	1-x, 1-y, 1-z
C8D-H8D...O21	0.950	2.580	3.509	166.14	1-x, 1-y, 1-z
N11D-H11D...O2B	0.877	2.095	2.958	167.98	-1+x, y, z+1
N14D-H14D...O3A	0.943	2.131	3.013	155.27	1+x, 1+y, z
N14D-H15D...O13C	0.802	2.224	3.024	175.06	
O16-H16A...O13A	0.900	1.969	2.772	147.66	
O16-H16B...O13C	0.902	1.591	2.439	155.05	
O16-H16C...O13D	0.905	1.613	2.508	169.33	

The perchlorate anions are embedded between the tetramer's tails, but no strong hydrogen bonds are observed between the ions and the surrounding molecules (Figure 4.5). The major structural function of the ClO_4^- anions is to connect the layers of tetramers together in the third dimension via weak hydrogen bonds (Figure 4.6).

The formation of $4\text{NFZ}\cdot[\text{H}_3\text{O}^+][\text{ClO}_4^-]$ was unexpected for multiple reasons. Firstly, based on the pKa differences between the acid ($\text{pKa}(\text{ClO}_4^-) \approx -10$) and $\text{pKa}(\text{NFZ})$ is -1.97), proton transfer was expected to happen. Hence, the crystallisation was carried out in dilute acid that contains water. On the other hand, protonation of the water molecule was not surprising because water is a stronger base than the NFZ ($\text{pKa}(\text{H}_2\text{O})$ is 14). The other interesting feature of the $4\text{NFZ}\cdot[\text{H}_3\text{O}^+][\text{ClO}_4^-]$ structure is its unusual stoichiometry and unique combination of Z' , Z'' and Z^c values, where Z' is defined as the number of formula units in the unit cell divided by the number of independent general positions; Z'' is the total number of chemical entities in the asymmetric unit; and Z^c is the number of different types of chemical units in the crystal.³ Z' defined for $4\text{NFZ}\cdot[\text{H}_3\text{O}^+][\text{ClO}_4^-]$ as 1, while $Z'' = 6$ and $Z^c = 3$.

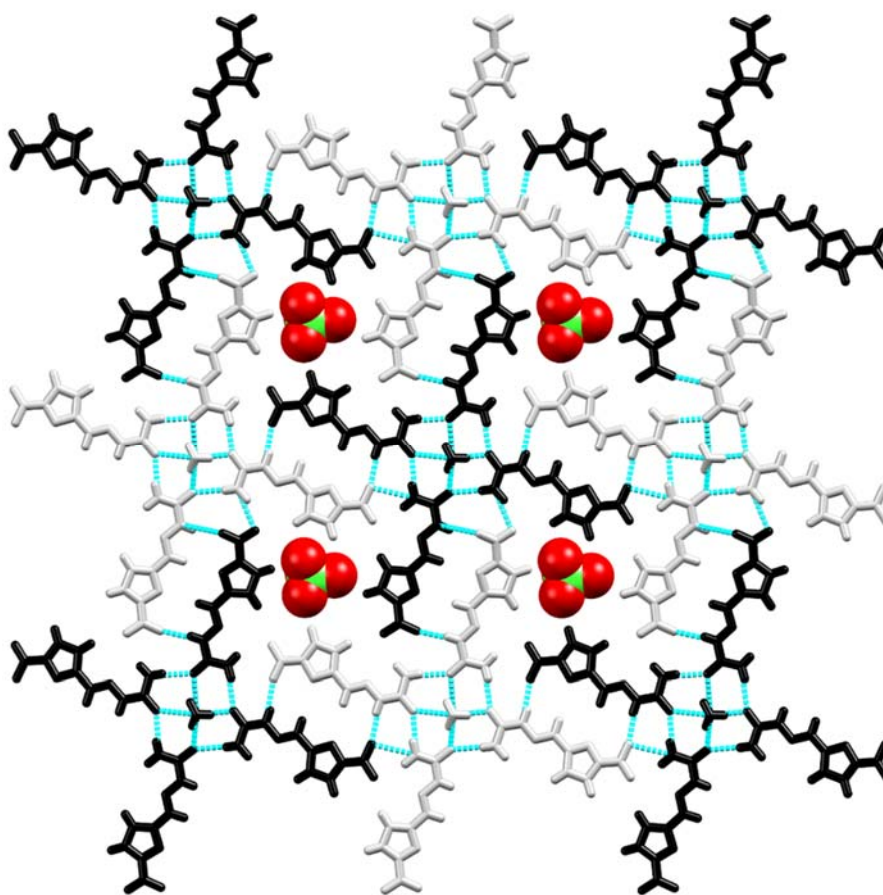


Figure 4.5 Embedded perchlorate ions in the layer of tetramers. (Perchlorate ions are presented in space fill view)

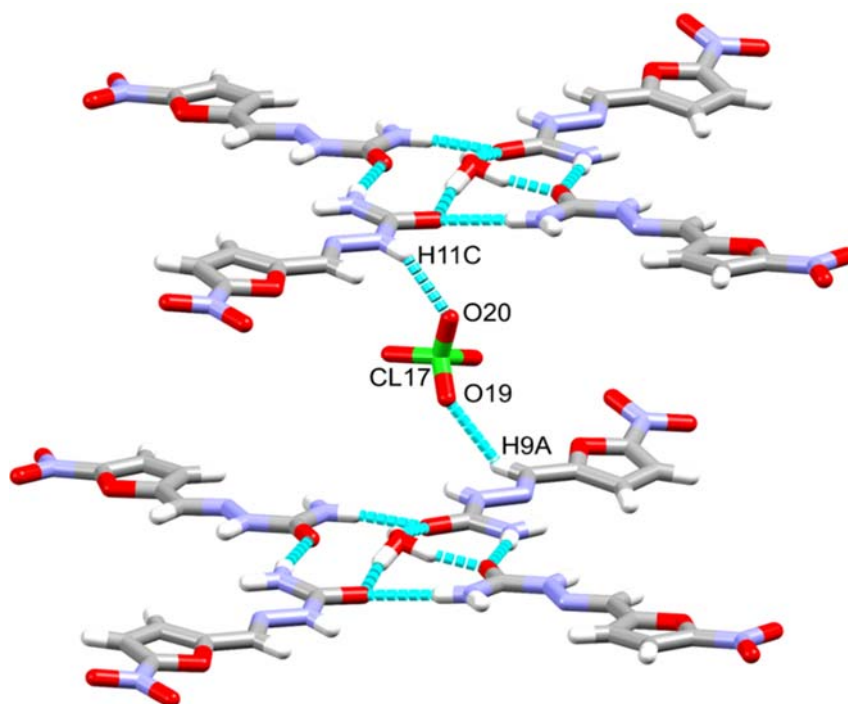


Figure 4.6 Hydrogen bonding of ClO_4^- between the layers of tetramers

4.2 Crystal structure of $\text{NFZ}\cdot\text{H}_3\text{PO}_4$

Crystals of $\text{NFZ}\cdot\text{H}_3\text{PO}_4$ were obtained after 4 months. Unlike the perchlorate co-crystal salt, $\text{NFZ}\cdot\text{H}_3\text{PO}_4$ crystals are blade shaped, elongated and not clustered. Their brittleness is observed when handled. Figure 4.7 shows the micrograph of an uncut crystal obtained from a solution of aqueous phosphoric acid and NFZ.

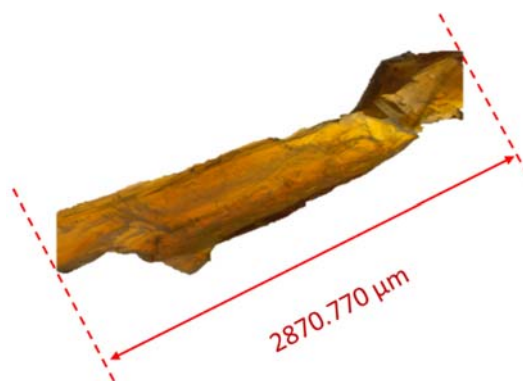


Figure 4.7 An uncut crystal of $\text{NFZ}\cdot\text{H}_3\text{PO}_4$

A suitable crystal of NFZ•H₃PO₄ with dimensions 0.29 × 0.39 × 0.56 mm was selected for single crystal X-ray analysis. The compound crystallized in the triclinic $P\bar{1}$ space group with one NFZ and one phosphoric acid molecule in the ASU (Figure 4.8). The crystallographic data for NFZ•H₃PO₄ are summarized in Table 4.2. Obtaining NFZ•H₃PO₄ in its current form, i.e. a solvate, was not entirely unexpected since the pK_a difference between the phosphoric acid (pK_a = 2.02) and the NFZ (pK_a = -1.97) does not suggest proton transfer. More interestingly, the crystallisation was carried out in dilute acid, thus, we expected a similar chemical outcome to that seen in the 4NFZ•[H₃O⁺][ClO₄⁻] structure.

The conformation of NFZ in the NFZ•H₃PO₄ crystal structure may be classified as *ap-sp-ap*. The designated torsion angle τ_1 (O5-C6-C9-H9) was found to be 176.04°, τ_2 (H9-C9••N11-H11) was 5.47° and τ_3 (H11-N11••N14-H14) was 168.72°. These values reveal the appearance of a new molecular conformation of NFZ that was not observed before in any crystal structures. The molecule still maintains its general planar fashion due to its rigid hydrazone sp² carbon. Figure 3.2 of chapter 3 clearly illustrates the conformer differences.

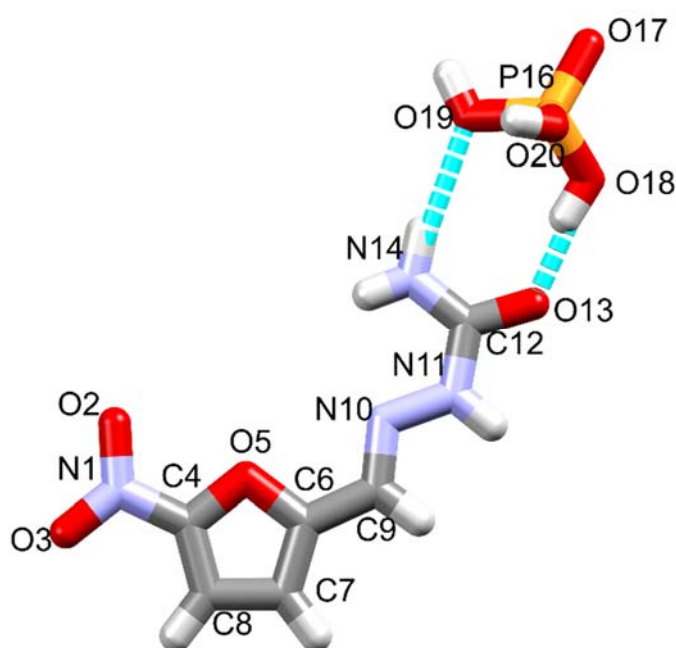


Figure 4.8 The asymmetric unit of NFZ•H₃PO₄

The typical amide-amide synthon formation was blocked by the inclusion of the phosphoric acid and hydrogen bonds of O18-H18···O13 and N14-H15-O19 were formed, creating $R_2^2(8)$ synthons. Rather, via N11-H11···O13 interactions, amide dimers are formed with the aid of the hydrazone moiety between the neighbouring NFZ molecules. The coplanarity of the neighbouring NFZ molecules gives rise to the quadruple hydrogen bond formation between the adjacent NFZ·H₃PO₄ units with the aid of C9-H9···O18 hydrogen bonds. The other prominent contact formed between adjacent NFZ molecules is the double hydrogen bond between the nitro and the amine functional group via N14-H15···O3 interaction with less ideal geometry and N14-H14···O2 interaction (Figure 4.9). The tapes of NFZ molecules are bonded together via phosphoric acid dimers formed via O19-H19···O17 interactions (Figure 4.10). Details of the hydrogen bonds are shown in Table 4.4.

The packing of NFZ·H₃PO₄ is layered, as a consequence of the planar molecular shape and the role of the phosphoric acids is to connect the planar structures in the third dimension. (Figure 4.11)

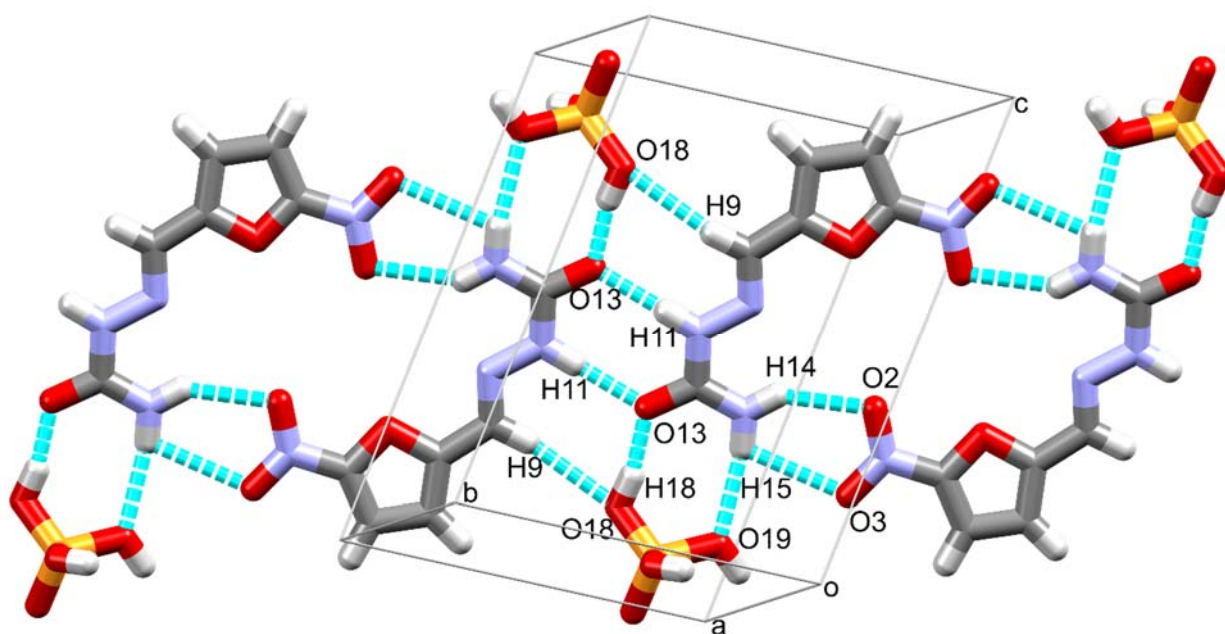


Figure 4.9 Hydrogen bonding between the coplanar NFZ molecules and the adjacent phosphoric acids

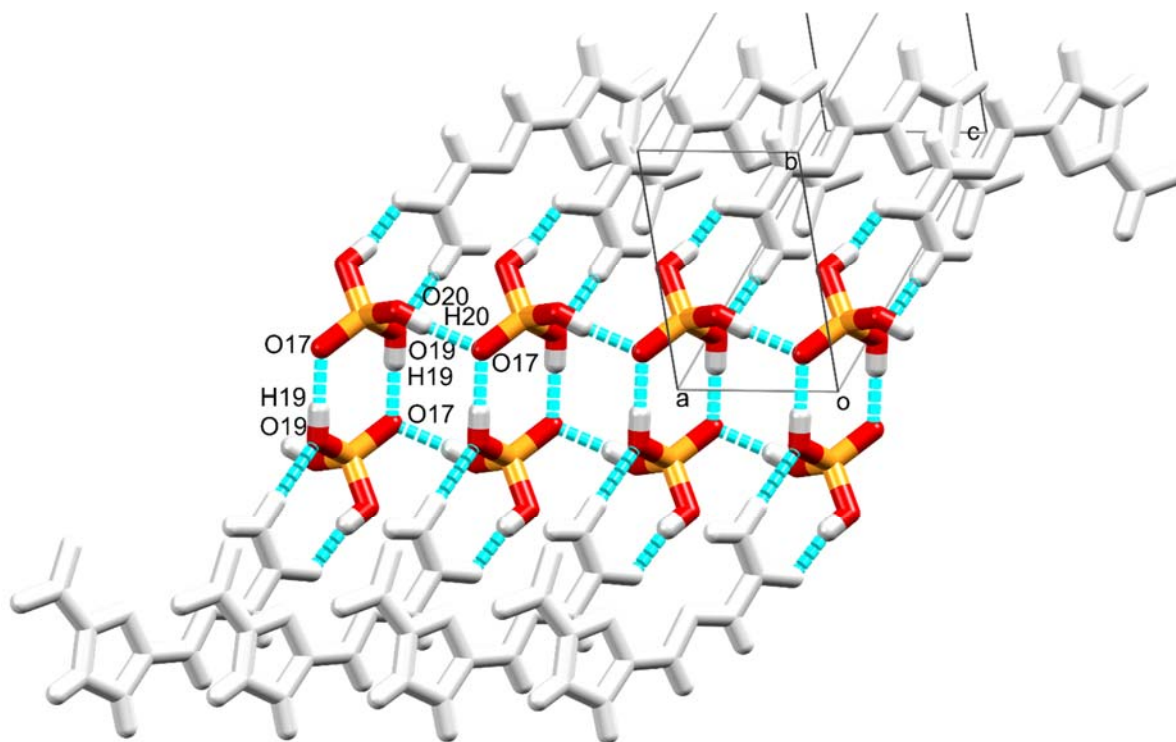


Figure 4.10 Hydrogen bonding between adjacent phosphoric acid molecules in $\text{NFZ}\cdot\text{H}_3\text{PO}_4$

Table 4.4 The geometric parameters for intermolecular interactions in $\text{NFZ}\cdot\text{H}_3\text{PO}_4$.

D-H...A	d(D-H) (Å)	d(H...A) (Å)	d(D...A) (Å)	<D-H...A(°)	Symmetry operators
C7-H7...O20	0.950	2.592	3.503	160.90	1-x, 1-y, 1-z
C8-H8...O20	0.950	2.477	3.360	154.62	-1+x, y, 1+z
C9-H9...O18	0.950	2.587	3.520	167.21	2-x, 1-y, 1-z
N11-H11...O13	0.881	1.983	2.862	175.91	2-x, 1-y, 1-z
N14-H15...O19	0.877	2.305	3.162	165.47	
N14-H14...O2	0.840	2.300	3.029	145.18	-x, -y, 1-z
O18-H18...O13	0.827	1.687	2.501	167.79	
O19-H19...O17	0.826	1.740	2.566	178.85	2-x, -y, -z
O20-H20...O17	0.774	1.797	2.568	174.96	-1+x, y, z

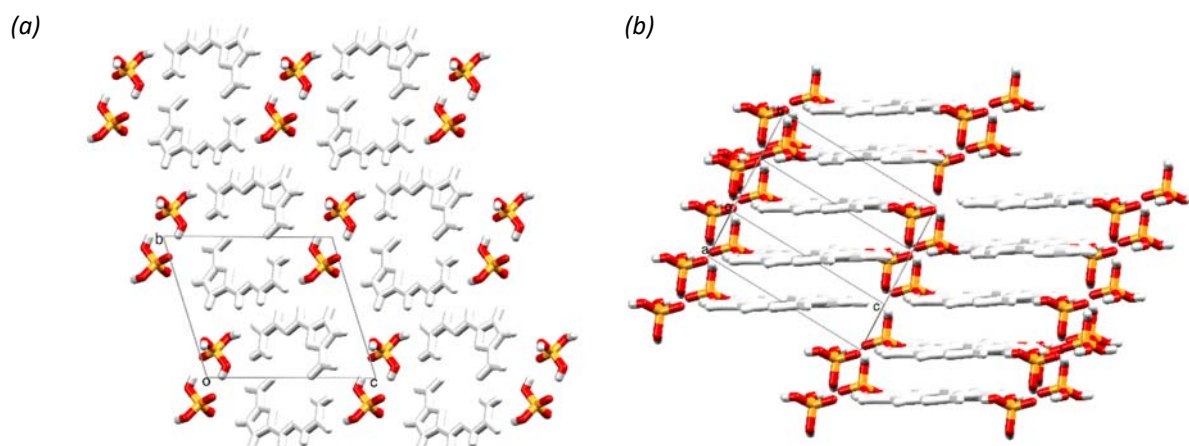


Figure 4.11 The packing of NFZ·H₃PO₄ viewed down *a* (a) and showing the layered nature of the structure (b)

4.3 Crystal structure of NFZ·PA

Crystals of the propionic acid inclusion of NFZ (NFZ·PA) were obtained in a shorter time of 5 months. They appear to have a rectangular morphology with a dark brown colouration. They were also not clustered like the perchlorate crystals. A micrograph of an uncut NFZ·PA crystal is shown in Figure 4.12.

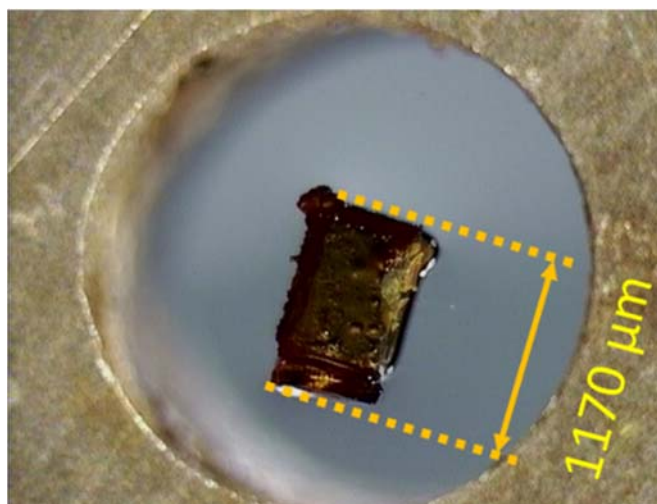


Figure 4.12 Uncut crystal of NFZ·PA

A suitable crystal of NFZ·PA with dimensions $0.12 \times 0.13 \times 0.15$ mm was selected for single crystal X-ray analysis. The compound crystallized in the $P2_1/c$ space group with four symmetrically independent NFZ and PA molecules in the ASU (Figure 4.13). The

crystallographic data are summarized in Table 4.2. No proton transfer was observed in the NFZ•PA crystal. All four NFZ molecules crystallized in the *sp-sp-ap* conformation.⁴

The hydrogen bonding is extensive in NFZ•PA. The ASU may be divided into two sections that contain two NFZs and two PA molecules each based on the hydrogen bonds observed. (Figure 4.14) The here defined NFZ pairs form amide dimers with each other via N14A-H14B···O13B and N14B-H14D···O13A between molecules A and B, and by N14C-H14F···O13D and N14D-H14G···O13C between molecules C and D, respectively. Also, each of the NFZ molecules form amide-acid heterosynthons with one PA via the respective O15-H15···O13 and N11-H11···O17 hydrogen bonds. Therefore, the ASU may be subdivided into two tetrameric units, each formed from two hydrogen-bonded NFZs and two related PAs.

Three additional interactions were noted between the molecules A and C (C7A-H7A···O2C and N14A-H14A···O3C) and between molecule C and the PA molecule related to B (C8C-H8C···O15B(PA)). The geometric details of the most prominent intermolecular interactions are listed in Table 4.5. The tetramers form sheets in the *ac* plane (Figure 4.15a) but no noticeable interactions can be found between the parallel layers (Figure 4.15b).

The layered nature of the structure is a plausible explanation why the crystallisation of the NFZ•PA crystals was extremely time consuming and challenging. NFZ has a similar molecular shape to dyes, which are typically planar. Therefore, growing crystals, i.e. 3D structures, is challenging if there are no functional groups that would form interactions into the third dimension. In light of this knowledge, the three discussed multicomponent crystals of NFZ present possible solutions to the problem. In the case of 4NFZ•[H₃O⁺][ClO₄⁻], the perchlorate anion is linking the layers of NFZ molecules into the third dimension. The same role may be described for the phosphoric acids in NFZ•H₃PO₄. In the NFZ•PA crystal the layers are held together with weak interactions, thus the formation of this crystal was the most unusual outcome.

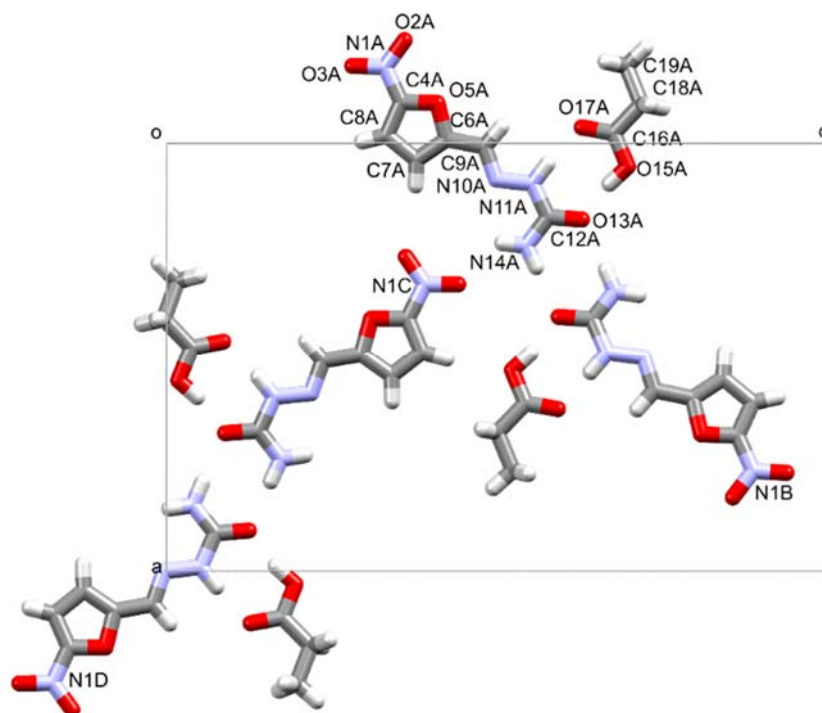


Figure 4.13 Asymmetric unit of NFZ•PA. Molecular units are labelled as A, B, C and D. Full numbering scheme of non-hydrogen atoms for unit A is shown

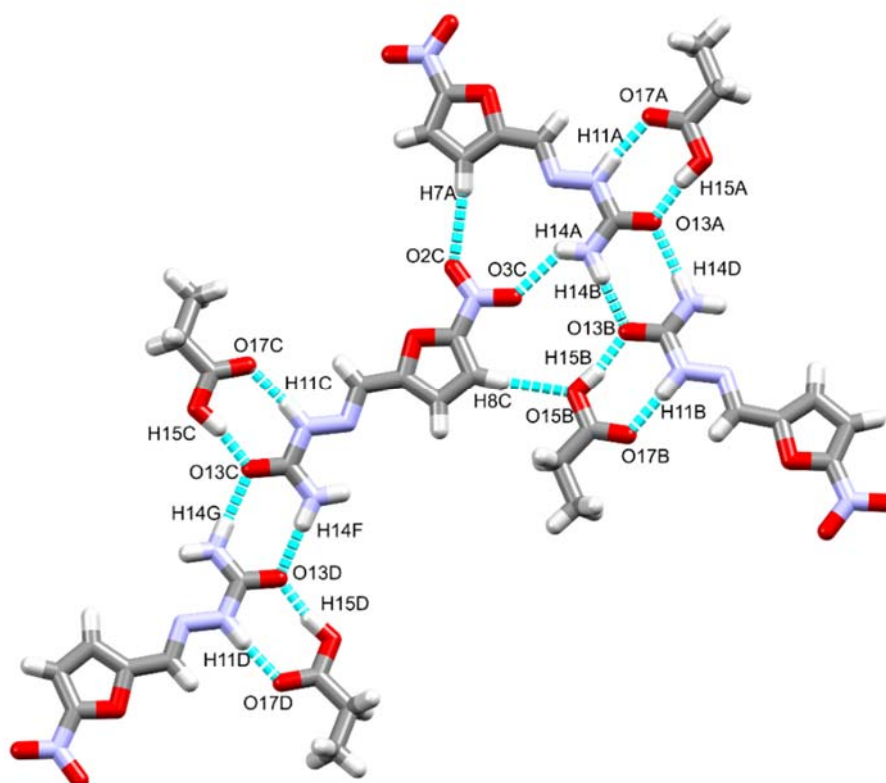


Figure 4.14 The complex hydrogen bond network in the ASU

Table 4.5 Hydrogen bonds in NFZ•PA

D-H...A	d(D-H) (Å)	d(H...A) (Å)	d(D...A) (Å)	<D-H...A (°)	Symmetry operators
C8A-H8A...O15D	0.950	2.507	3.451	172.63	-1+x, y, z
N11A-H11A...O17A	0.915	1.867	2.779	174.42	
O15A-H15A...O13A	0.959	1.690	2.641	170.38	
N14A-H14A...O3C	0.893	2.227	2.897	131.44	
N14A-H14B...O13B	0.864	2.020	2.883	176.88	
C8B-H8B...O15C	0.950	2.446	3.393	174.64	x, y, 1+z
N11B-H11B...O17B	0.950	1.836	2.783	173.96	
N14B-H14C...O3D	0.891	2.255	2.914	130.54	-1+x, y, 1+z
N14B-H14D...O13A	0.855	2.062	2.915	175.29	
O15B-H15B...O13B	0.948	1.705	2.643	169.69	
C7C-H7C...O2A	0.950	2.516	3.457	170.72	1+x, y, z
C8C-H8C...O15B	0.950	2.450	3.398	174.99	
N11C-H11C...O17C	0.941	1.859	2.798	174.88	
N14B-H14E...O3A	0.899	2.250	2.922	131.20	1+x, y, z
N14C-H14F...O13D	0.898	2.001	2.897	176.16	
C7D-H7D...O2B	0.950	2.531	3.466	168.07	x, y, -1+z
C8D-H8D...O15A	0.950	2.461	3.411	177.48	1+x, y, -1+z
N11D-H11D...O17D	0.934	1.857	2.790	175.67	
N14D-H14G...O13C	0.893	2.016	2.908	177.27	
N14D-H14H...O3B	0.894	2.205	2.903	134.60	x, y, -1+z
O15D-H15D...O13D	1.002	1.654	2.645	169.01	

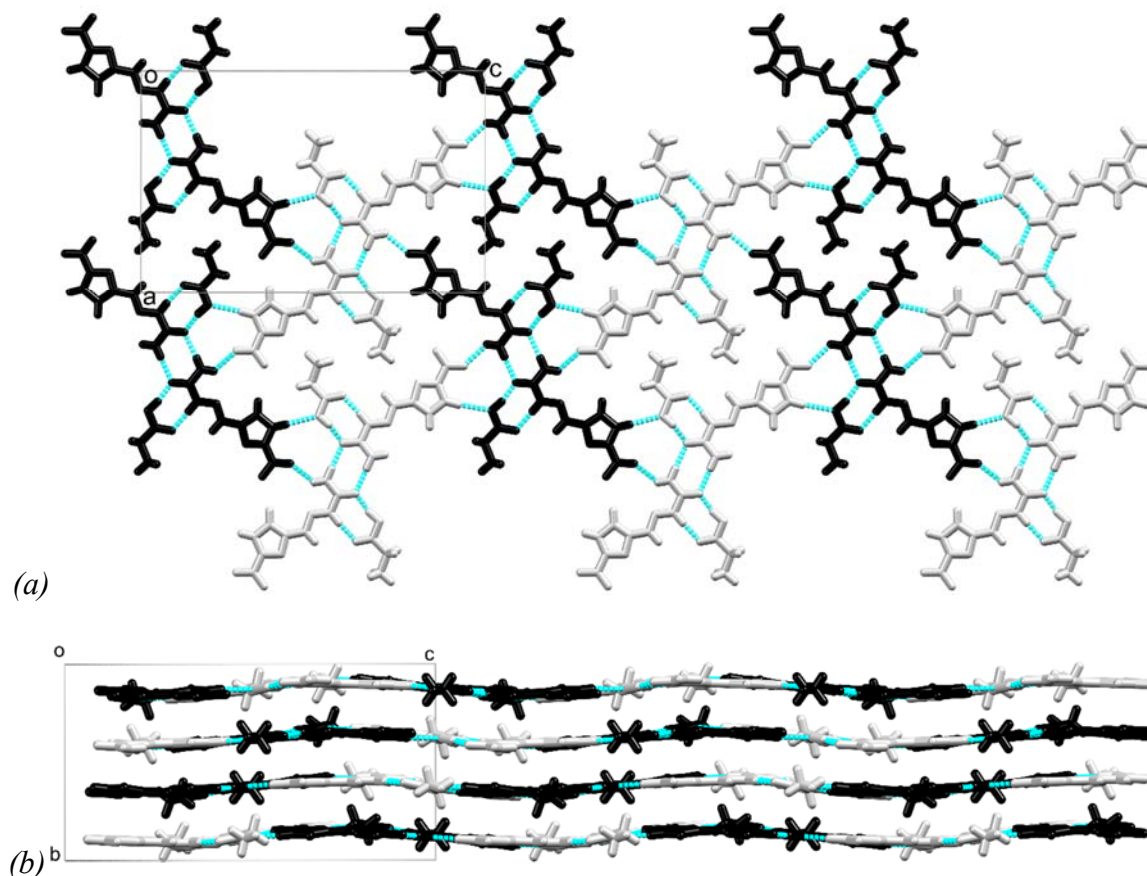


Figure 4.15 Packing of hydrogen-bonded tetramers of NFZ•PA viewed down *b* (a) and down *a* (b)

4.4 Bulk property analysis of multicomponent crystals of NFZ

Bulk properties of the three multicomponent crystals of NFZ were analysed using PXRD, DSC, TGA and FTIR spectroscopy.

4.4.1 Powder X-ray diffraction of multicomponent crystals of NFZ

The PXRD pattern of the $4\text{NFZ}\cdot[\text{H}_3\text{O}^+][\text{ClO}_4^-]$ crystals was recorded and compared to the generated powder pattern from the single crystal structure (green in Figure 4.16). The scarcity of the crystals and the poor crystallinity of the material resulted in signal poor PXRD patterns. Some peaks, however, can still be sufficient to show agreement with the generated pattern. The generated pattern is representative of the bulk of the solvent based crystallization (bulk pattern is blue in Figure 4.5). The generated pattern was also compared to the pattern of the material obtained from a 45 minute long liquid assisted grinding (LAG) to show that the $4\text{NFZ}\cdot[\text{H}_3\text{O}^+][\text{ClO}_4^-]$ co-crystal salt can also be prepared using mechanochemical methods.

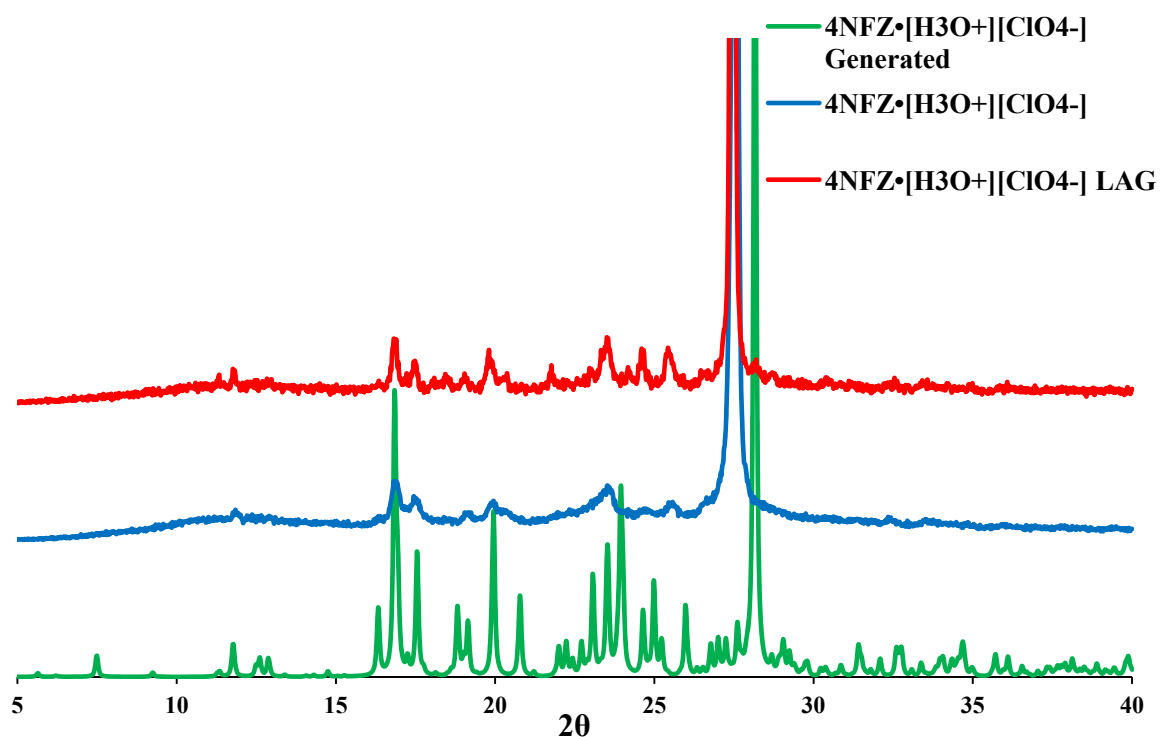


Figure 4.16 PXRD patterns of the samples prepared with different methods of 4NFZ·[H₃O⁺][ClO₄⁻]

The PXRD patterns of the NFZ·H₃PO₄ solvate were much more intense and this made the comparison easier. The selected single crystal was representative of the bulk material and the 45 mins LAG was also successful in reproducing the multicomponent crystal. The LAG did not yield 100% product and some remaining peaks from the starting materials can be seen on the pattern (Figure 4.17). The crystallisation of NFZ with PA yielded very few crystals, thus the PXRD pattern of the bulk crystals are signal poor. The single crystal pattern, the bulk of the solvent based crystallization and the formation of NFZ·PA by 45 mins LAG are represented as green blue and red, respectively (Figure 4.18).

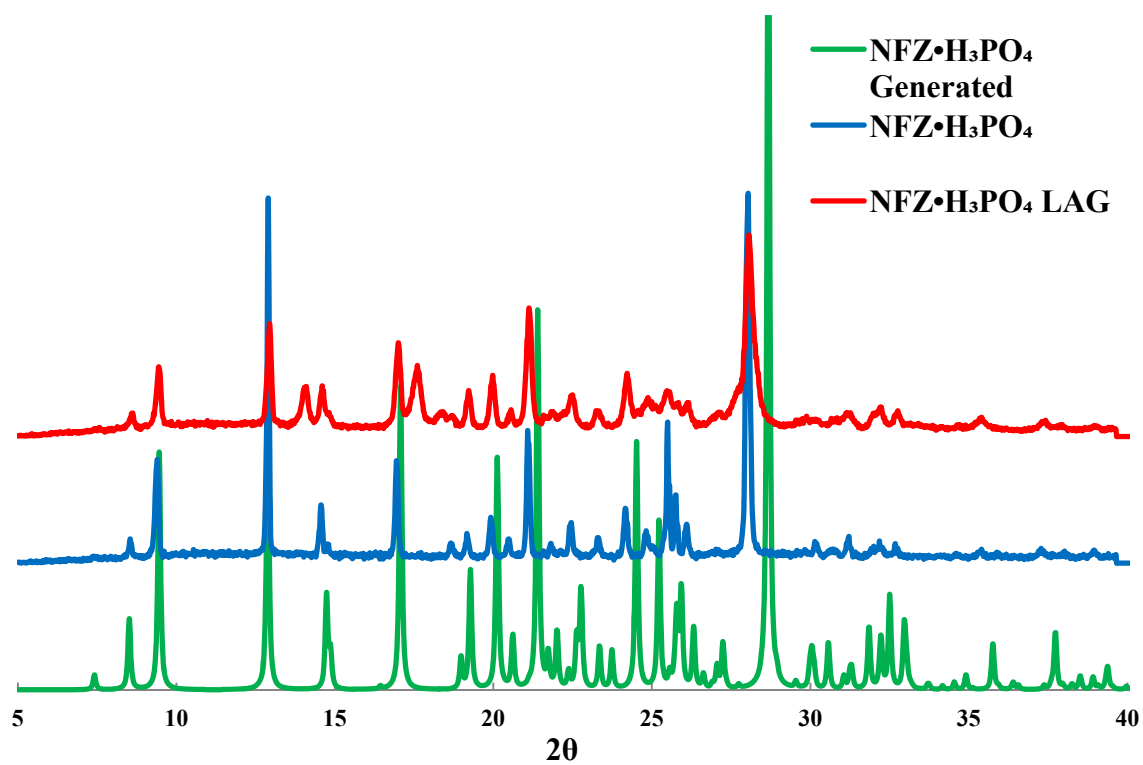


Figure 4.17 PXR D patterns of the samples prepared with different methods of $\text{NFZ}\cdot\text{H}_3\text{PO}_4$

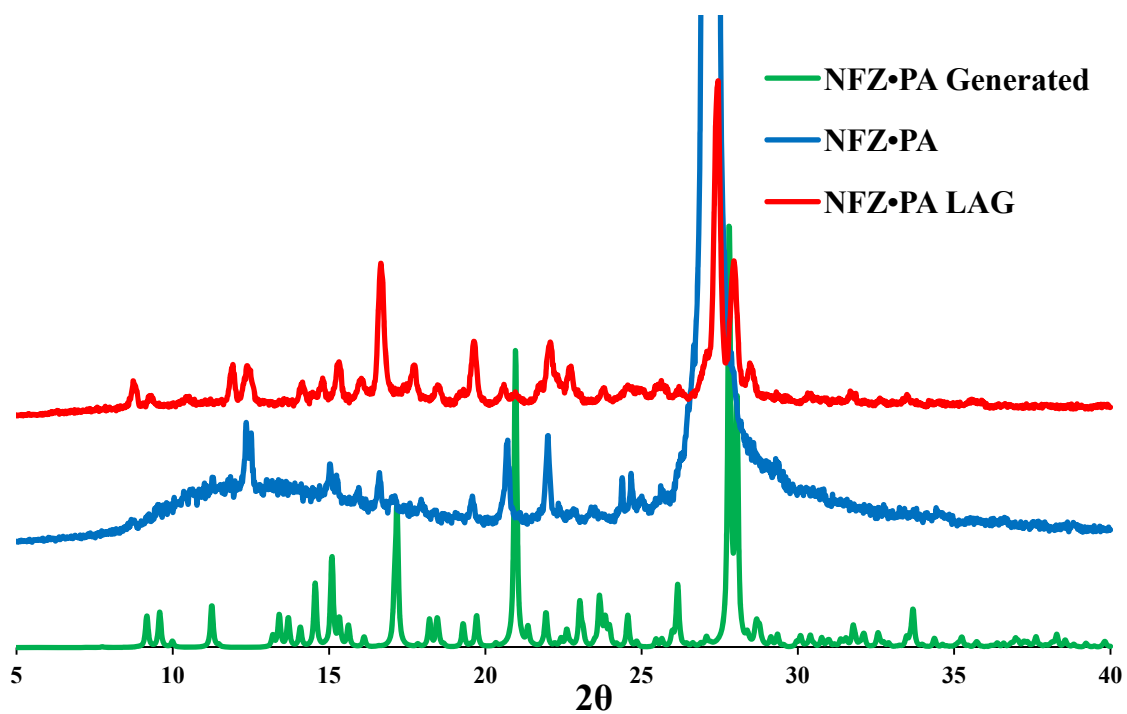


Figure 4.18 PXR D patterns of the samples prepared with different methods of $\text{NFZ}\cdot\text{PA}$

4.4.2 Thermal analysis of multicomponent crystals of NFZ

Crystals of NFZ with perchloric acid were obtained from some of the performed experiments and their melting points were recorded with DSC accordingly. Figure 4.19 shows the melting profile of $4\text{NFZ}\cdot[\text{H}_3\text{O}^+][\text{ClO}_4^-]$ crystals (green). Two thermal events are observed in the curve ($T_{\text{onset1}} = 182.07^\circ\text{C}$ and $T_{\text{peak1}} = 188.65^\circ\text{C}$; $T_{\text{onset2}} = 223.59^\circ\text{C}$ and $T_{\text{peak2}} = 237.74^\circ\text{C}$). The DSC curve of the compound obtained with LAG (blue) has two similar thermal events ($T_{\text{onset1}} = 174.80^\circ\text{C}$ and $T_{\text{peak1}} = 180.83^\circ\text{C}$; $T_{\text{onset2}} = 219.32^\circ\text{C}$ and $T_{\text{peak2}} = 236.99^\circ\text{C}$). The first endotherm may be related to the desolvation of the co-crystal salt and the second endotherm is most likely related to the melting of the NFZ. This theory is supported well by the TGA results (Figure 4.20). The curve shows a gradual mass loss via a three-step transformation. The first mass loss (calculated at 12.9 %) step corresponds to the theoretical value of 13.0 % that is related to the desolvation and losing the $[\text{H}_3\text{O}^+][\text{ClO}_4^-]$. This is followed by a complex thermal decomposition.

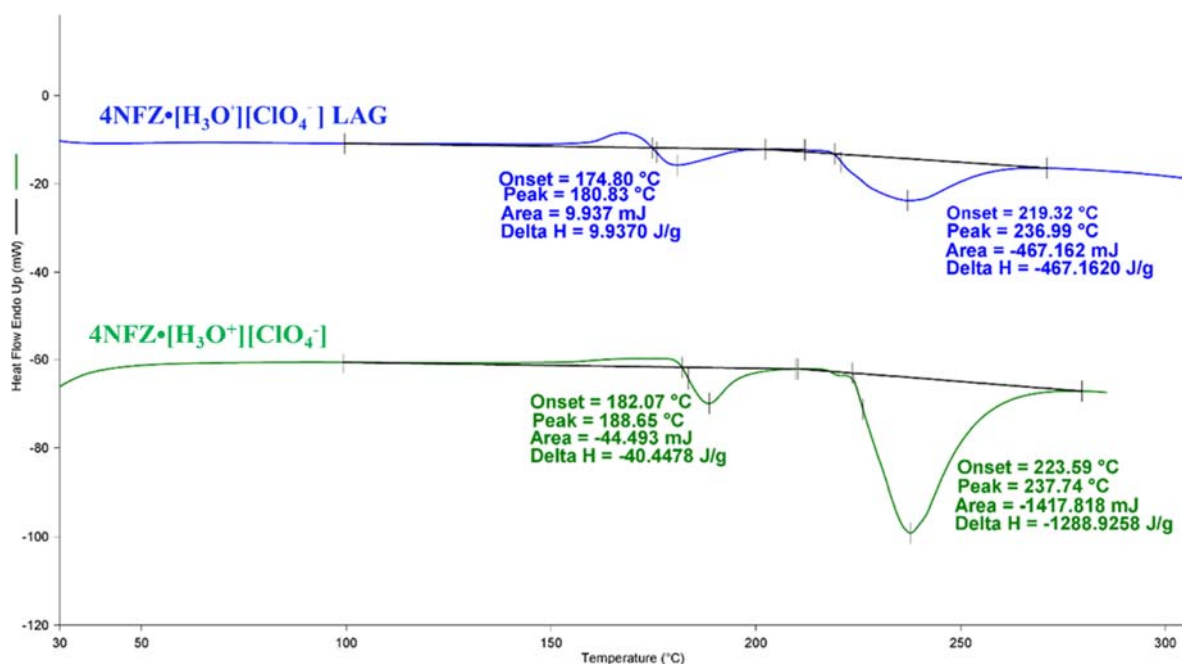


Figure 4.19 DSC curves of $4\text{NFZ}\cdot[\text{H}_3\text{O}^+][\text{ClO}_4^-]$ bulk material and samples obtained from LAG

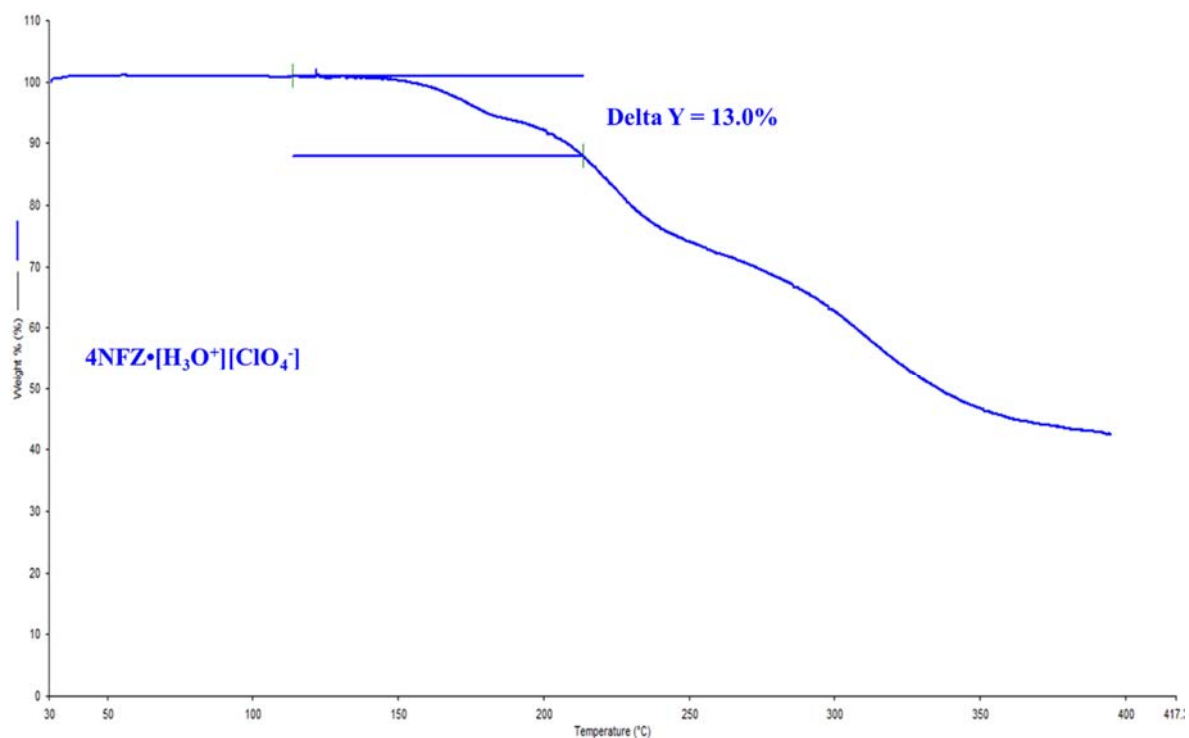


Figure 4.20: Thermal analysis curve showing steps of mass loss of $4\text{NFZ}\cdot[\text{H}_3\text{O}^+][\text{ClO}_4^-]$

Crystals of $\text{NFZ}\cdot\text{H}_3\text{PO}_4$ were obtained from some of the performed experiments and their thermal behaviour was recorded using DSC. (Figure 4.21) Similar to the DSC analysis of the $4\text{NFZ}\cdot[\text{H}_3\text{O}^+][\text{ClO}_4^-]$ crystals, two thermal events are observed ($T_{\text{onset}1} = 179.44^\circ\text{C}$ and $T_{\text{peak}1} = 186.83^\circ\text{C}$; $T_{\text{onset}2} = 222.73^\circ\text{C}$ and $T_{\text{peak}2} = 241.7^\circ\text{C}$). The analysis of the material obtained via LAG shows similar results to the bulk material of $\text{NFZ}\cdot\text{H}_3\text{PO}_4$ and proves that the compound can also be synthesized via grinding ($T_{\text{onset}1} = 179.97^\circ\text{C}$ and $T_{\text{peak}1} = 187.78^\circ\text{C}$; $T_{\text{onset}2} = 232.21^\circ\text{C}$ and $T_{\text{peak}2} = 244.28^\circ\text{C}$). The TGA result reveals a complex, multi-step decomposition process (Figure 4.22). The rough estimate of the overall mass loss in the initial phase is 32 % and this corresponds well to the loss of the H_3PO_4 moiety.

The DSC and the TGA curves of $\text{NFZ}\cdot\text{PA}$ are shown in Figure 4.23. (These data were collected on a TA instrument with a heating rate of $10^\circ\text{C}/\text{min}$.) The DSC curve shows two thermal events, where the first one ($T_{\text{onset}} = 80.48^\circ\text{C}$ and $T_{\text{peak}} = 87.22^\circ\text{C}$), is related to the desolvation of the $\text{NFZ}\cdot\text{PA}$ crystals, while the second endotherm ($T_{\text{onset}} = 240.60$ and $T_{\text{peak}} = 244.38$) can be related to the melting of the NFZ. The TGA results support the desolvation process; the 26.21 % mass loss agrees well with the loss of the PA moiety. The DSC results of the new crystals are summarized in Table 4.6 and the TGA results are listed in Table 4.7.

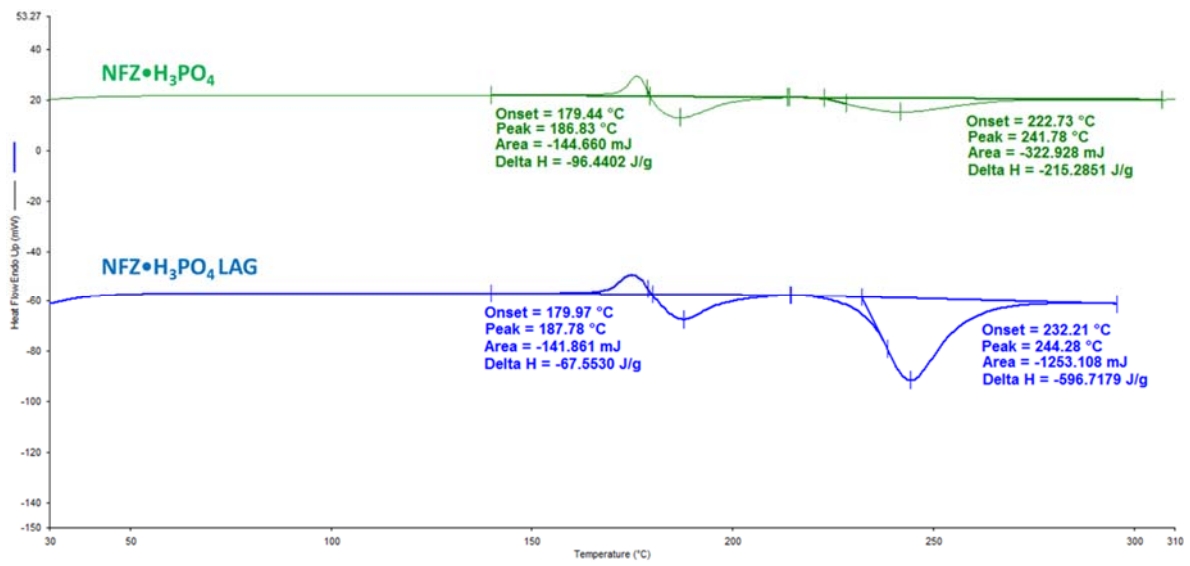


Figure 4.21 DSC curve of NFZ•H₃PO₄ bulk material and NFZ•H₃PO₄ LAG

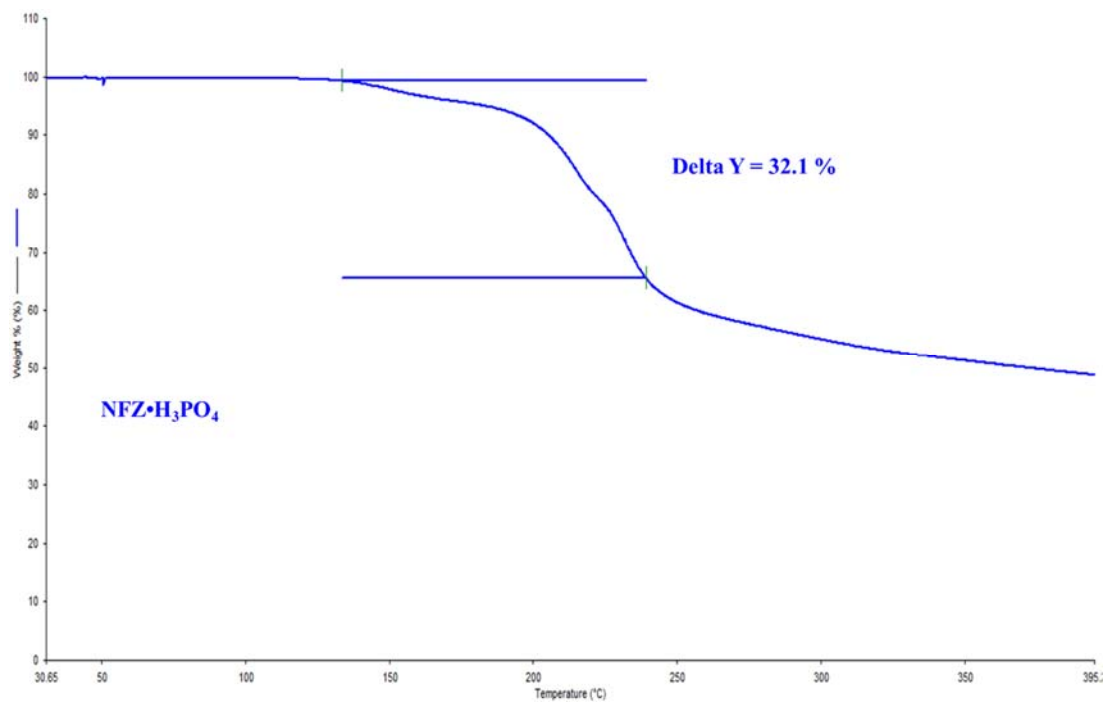


Figure 4.22 Thermal analysis curve showing weight loss in NFZ•H₃PO₄ bulk material

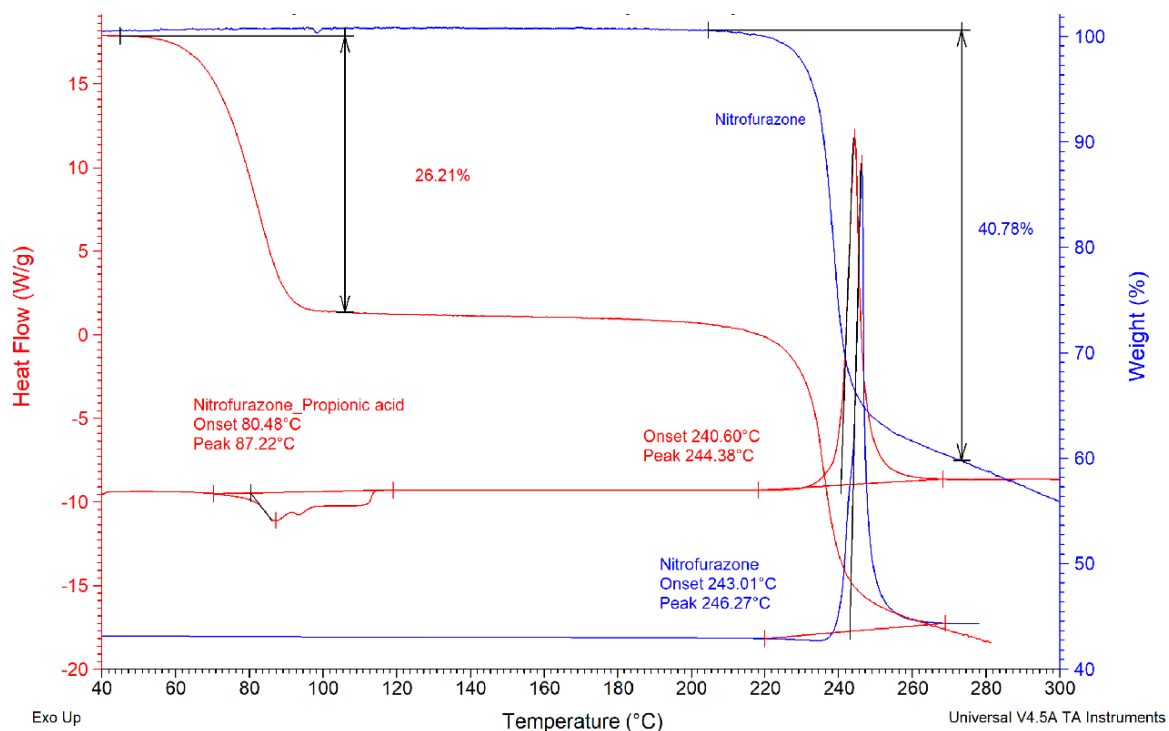


Figure 4.23 DSC and DTA curves of NFZ•PA

Table 4.6 DSC data of multicomponent crystals of NFZ

Crystal	T _{onset} (°C)	T _{peak} (°C)
4NFZ•[H ₃ O ⁺][ClO ₄ ⁻]	182.07	188.65
	223.59	237.74
NFZ•H ₃ PO ₄	179.97	187.78
	221.07	241.78
NFZ•PA	80.48	87.22
	240.60	244.38

Table 4.7 TGA data of multicomponent crystals of NFZ

Mass	Calculated mass loss (%)	Observed mass loss (%)
4NFZ•[H ₃ O ⁺][ClO ₄ ⁻]		
	[H ₃ O ⁺][ClO ₄ ⁻]	13.0
NFZ•H ₃ PO ₄		
	H ₃ PO ₄	33.1
NFZ•PA		
	PA	27.2

4.4.3 FTIR analysis of the multicomponent crystals of NFZ

FTIR spectroscopy was exclusively used in the comparison and determination of the new crystal structures of NFZ. It is important to note that three species are present in the $4\text{NFZ}\cdot[\text{H}_3\text{O}^+][\text{ClO}_4^-]$ crystal, each possessing unique vibrational modes. Hydrogen bonding as well as ionic interactions come into play, as they intensify the stiffness of the covalent bonds.⁵ Moreover, the ionic species present (i.e. H_3O^+ and ClO_4^-), have a unique symmetry which also influences the overall vibrational frequencies. In this scenario, the tetrahedral (T_d) symmetry of ClO_4^- gives a broad and strong peak at a frequency 1071 cm^{-1} . The trivial lowering is due to $\text{N11-H11}\cdots\text{O20}$ and $\text{C9-H9}\cdots\text{O19}$ intermolecular associations between the anion and the NFZ tapes. Literature also confirms that tetrahedral anions typically have two vibrational modes, that is, symmetric stretching and bending, respectively. Some examples of T_d symmetry anions with their respective stretching and bending vibrational frequencies are as follows: PO_4^{3-} (1017 cm^{-1} , 567 cm^{-1}), CrO_4^{2-} (890 cm^{-1} , 378 cm^{-1}) and MnO_4^- (902 cm^{-1} , 386 cm^{-1}).⁵ The 621 cm^{-1} absorption frequency may be attributed to Cl-O asymmetric bending. The C=O frequency has shifted to 1639 cm^{-1} , largely due to the inflexibility of the hydrogen bonded carbonyls.

The other interesting thing about the spectral peaks of $4\text{NFZ}\cdot[\text{H}_3\text{O}^+][\text{ClO}_4^-]$ is the unusually expansive peak in the $3600\text{-}3100\text{ cm}^{-1}$ range. This is probably due to the ionized water molecule. The spectral bands of H_2O and H_3O^+ can be difficult to discriminate as their characteristic band range falls in the same region. Notable differences are seen in the fingerprint region and at peaks 593 and 549 cm^{-1} . The doublet in the starting material spectrum (blue) seems to have been overshadowed by the broadened absorption band in the crystal spectrum (red). Moreover, a double peak is observed in $4\text{NFZ}\cdot[\text{H}_3\text{O}^+][\text{ClO}_4^-]$ at 3453 cm^{-1} and 3416 cm^{-1} while a single peak is observed in the starting material. Another distinguishing peak in the spectrum of $4\text{NFZ}\cdot[\text{H}_3\text{O}^+][\text{ClO}_4^-]$ is seen at 3331 cm^{-1} . Relatively sharper peaks are observed in the starting material as compared to the new salt. FTIR successfully identifies the peaks of the new crystal structure. Infra-red spectra of $4\text{NFZ}\cdot[\text{H}_3\text{O}^+][\text{ClO}_4^-]$ and the starting material are shown in Figure 4.27. Molecular vibrations observed in the infra-red spectrum of ClO_4^- is shown in Table 4.8.

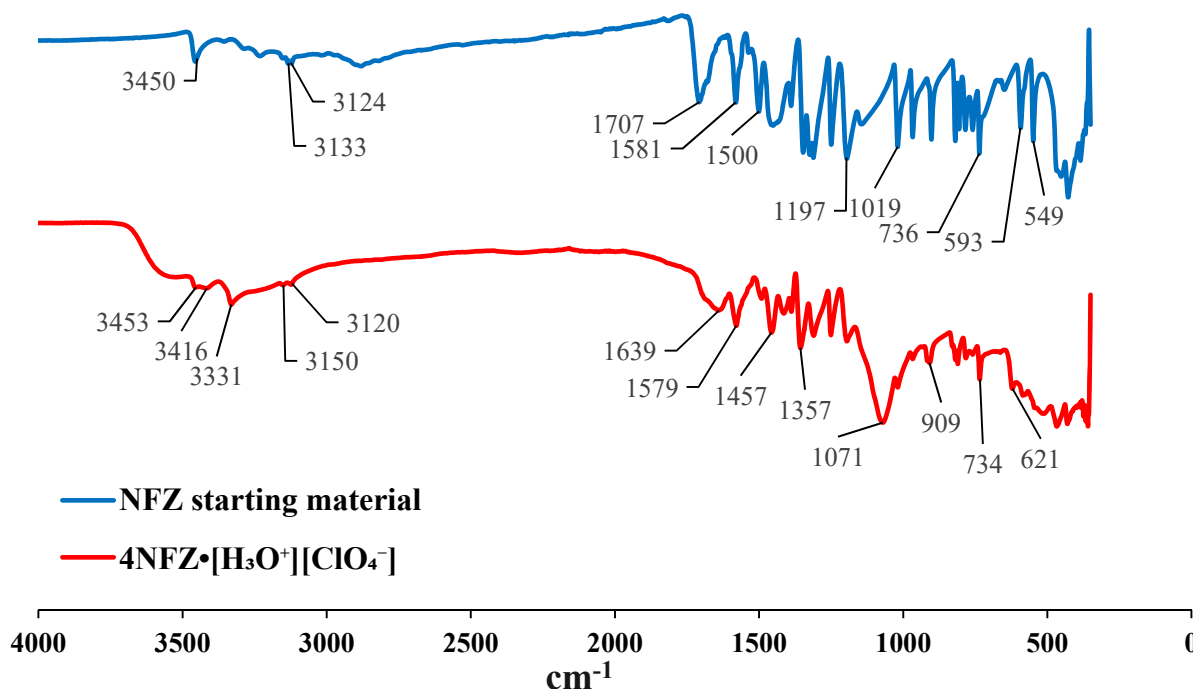


Figure 4.24 FTIR spectra of NFZ and $4\text{NFZ}\cdot[\text{H}_3\text{O}^+][\text{ClO}_4^-]$

Vibrational modes of $\text{NFZ}\cdot\text{H}_3\text{PO}_4$ were investigated and the spectra can be observed in Figure 4.25. We expect to find at least one characteristic broad band in the functional group region in the range of $2700\text{-}2100\text{ cm}^{-1}$. That band is associated with a $\text{P}(\text{O})\text{OH}$ group of the phosphoric acid molecule.⁵ Firstly, we observed gentle sloping of the spectrum in the functional group region as anticipated. Literature reports that the broad band range in the $1100\text{-}950\text{ cm}^{-1}$ is associated with aqueous phosphoric acid.⁶ Since this is in aqueous medium, we cannot expect a similar absorption band in the case of unprotonated acid in our $\text{NFZ}\cdot\text{H}_3\text{PO}_4$ crystal, but there is room left for anomalous behaviour. In our case, we can expect the intermolecular interactions to come into play and reduce the vibrational modes by making the P-OH bonds stiffer, thereby affecting the band accordingly. We also observed a distinguished peak at 3367 cm^{-1} . This particular frequency band does not appear in the starting material. We know from literature that phosphorus groups absorb highly in that region. Broad bands observed from the peak at 1500 cm^{-1} going up signify the presence of hydrogen bonds. We observed an extensively broad band which was generally smooth with hardly any peaks within the specified frequencies.

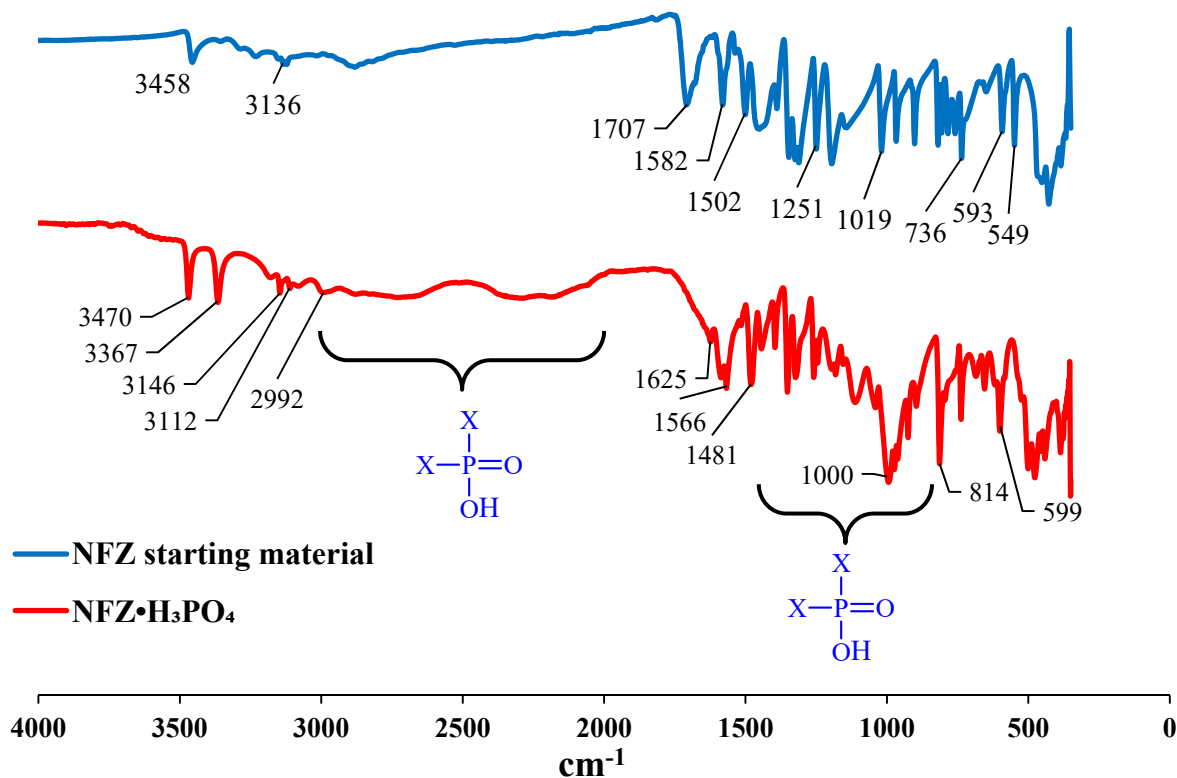


Figure 4.25 FTIR spectra of NFZ and NFZ·H₃PO₄

FTIR was used to measure the infra-red absorptions of the NFZ·PA crystals. Nate Schultheiss and co-workers state that neutral carboxyl group with its proton intact shows a sharp carbonyl π bond stretching band at ca. 1700 cm⁻¹ and a relatively weak sigma bond stretch at approximately 1200 cm⁻¹ if it forms an O-H...N hydrogen bond.⁷ We therefore anticipate the neutral carboxyl (C=O) bands for the NFZ·PA co-crystal since propionic acid (PA) did not deprotonate. Unlike the example in literature, propionic acid (PA) in the NFZ·PA co-crystal forms a hydrogen bond with the neutral NFZ tape via O-H...O, and the absorption band is observed at 1689 cm⁻¹. The hydrogen in the latter interaction is more strongly held by the oxygen compared to the less electronegative nitrogen in the former interaction. The O-H covalent bond of the O-H...O becomes stiffer, thus increasing its infrared radiation absorption. This accounts for the lower wavenumber of 1689 cm⁻¹. The 1198 cm⁻¹ frequency is probably due to the weak sigma bond stretch (Figure 4.26).

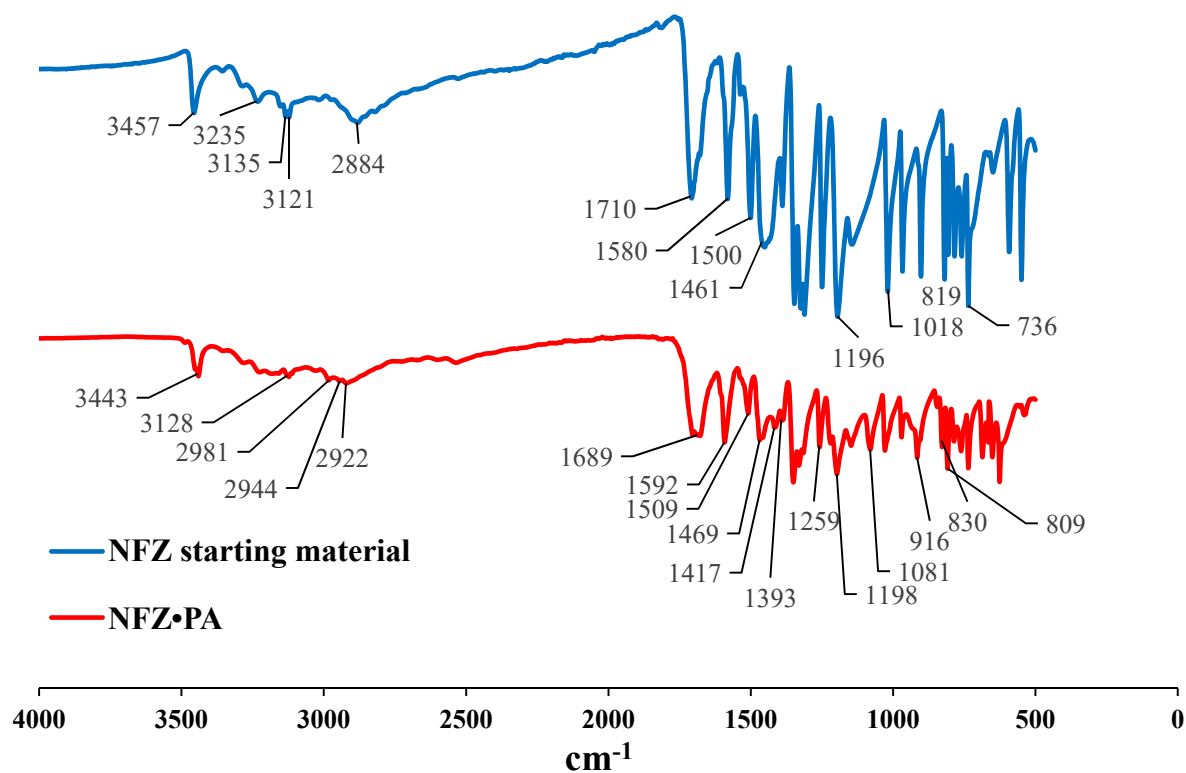


Figure 4.26 FTIR spectra of NFZ and NFZ•PA


Table 4.8 Molecular vibrations observed in the spectra of ClO_4^- , H_3PO_4 and PA

Ion/functional group	Assignment	Expected	Observed
IR peaks in cm^{-1}			
ClO_4^-	Cl-O strong asymmetric stretching	1170-1050	1071
	Cl-O weak asymmetric bending	635-610	621
H_3PO_4	P(O)OH	2700-2100	2909-1979
	P=O	1200-1100	1182-995
Carboxylic acid (PA)	C=O (free)	1760	n/a
	C=O (h-bonded)	1700	1689
	C-O stretching	1240	1259
	O-H in plane bending	1430	1417
	O-H oop bending	930	916

References

- (1) Grothe, E.; Meekes, H.; Vlieg, E.; ter Horst, J. H.; de Gelder, R., Solvates, Salts, and Cocrystals: A Proposal for a Feasible Classification System. *Crystal Growth & Design* **2016**, 16, (6), 3237-3243.
- (2) Calculator Plugins were used for structure property prediction and calculation, Marvin 16.4.25., 2016, ChemAxon (<http://www.chemaxon.com>). # The pKa prediction is done on the basis of the partial charge distribution calculated for the atoms in the molecule and this method provides an efficient and robust way to locate the most acidic and basic sites.
- (3) Steed, K. M.; Steed, J. W., Packing Problems: High Z' Crystal Structures and Their Relationship to Cocrystals, Inclusion Compounds, and Polymorphism. *Chemical Reviews* **2015**, 115, (8), 2895-2933.
- (4) Moss, G., Basic terminology of stereochemistry (IUPAC Recommendations 1996). *Pure and applied chemistry* **1996**, 68, (12), 2193-2222.
- (5) Stuart, B. H., Spectral Analysis. In *Infrared Spectroscopy: Fundamentals and Applications*, John Wiley & Sons, Ltd: **2005**; pp 45-70.
- (6) Arai, Y.; Sparks, D. L., ATR-FTIR spectroscopic investigation on phosphate adsorption mechanisms at the ferrihydrite-water interface. *Journal of Colloid and Interface Science* **2001**, 241, (2), 317-326.
- (7) Schultheiss, N.; Newman, A., Pharmaceutical cocrystals and their physicochemical properties. *Crystal growth and design* **2009**, 9, (6), 2950-2967.

CHAPTER 5



The following chapter is the presentation of the
CSD study of the semicarbazone moiety

5 CSD analysis of the semicarbazone moiety

A Cambridge Structural Database (version 5.39, February 2018) search was carried out in order to (1) investigate the molecular interaction preferences of the NFZ molecule and its fragments and (2) determine the most commonly occurring conformer of the semicarbazone moiety with the aid of mapping the torsional frequency distribution for the functional group using τ_1 , τ_2 , and τ_3 molecular descriptors (See Figure 3.2, page 44).

5.1 Hydrogen bonding of the semicarbazone fragment

During this work, it was noted that the NFZ molecule forms interactions mainly via the semicarbazone moiety, which possesses 5 possible hydrogen bonding sites (Figure 5.1). The grouping of the hydrogen bonding functionalities allows us to section the semicarbazone moiety into two smaller functional groups, namely hydrazone and amide.

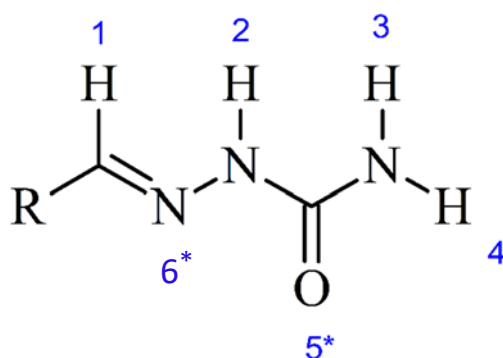


Figure 5.1 Possible bonding sites in the semicarbazone functionality. Site1-4 are hydrogen bond donors and 5* and 6* are hydrogen bond acceptors

The dataset for the bonding preferences of the semicarbazone chain was retrieved with the aid of *ConQuest* 1.22.¹ A general search was done for the carbonyl, amine, amide, semicarbazone and whole NFZ molecule with the restrictions; 3D coordinates determined, no errors, only single crystal structures, not polymeric and only organics. The amide fragment yielded 4245 hits, while the semicarbazone chain had 60 hits. The results of the relevant fragments summarized in Figure 5.2 show the frequency of occurrence of each functional group and how the number of hits decreases as the chain size increases.

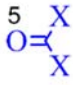
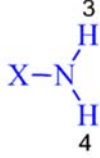
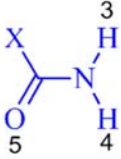
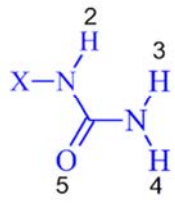
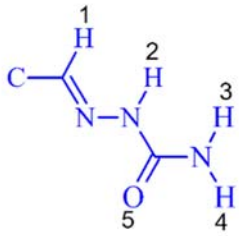
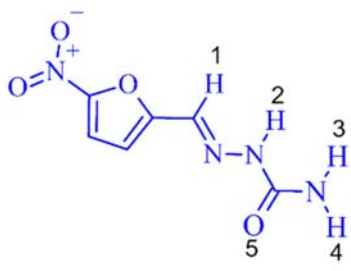
Fragment	Bonding sites	CSD Hits
	1	189723
	2	35894
	3	4245
	4	829
	5	60
	5	3

Figure 5.2 CSD hits for the selected fragments

In order to investigate the occurrence of specific interactions involving these fragments, a hydrogen bond motif search was done on the selected datasets using Mercury.² Figure 5.3 gives the overall outcome of the search. Individual synthons were searched, with the aim of investigating the likelihood of certain interactions occurring, based on the functional groups present on the co-formers that were used in the attempted co-crystallisations and inclusion formation with NFZ. A systematic search was done separately for all identified synthons; first for the amide, then the semicarbazone moiety, and eventually with the whole NFZ molecule. It was observed that the likelihood of obtaining a certain contact as the chain grew decreases. Figure 5.3 *a) to h)* summarizes the hits for the possible hydrogen bond motifs of the selected fragments and the NFZ molecule.

The amide-amide dimer is observed in 10.8 % of all structures that possess an amide group and only in 7.81 % of all structures that have a semicarbazone segment (Table 5.1). It is interesting to note that the formation of the amide-amide dimer when the whole NFZ molecule is included in the search was found in the structure of the β -polymorph only, i.e. WERVEU01 or β -RT and β -LT structures (Figure 5.3a). Since we observed a relatively low probability of the formation of the amide-amide dimer, it therefore attests to the difficulty encountered during co-crystallizations of NFZ with amide co-formers.

In the next step, a search for the interaction in the amide fragment with any type of hydrogen bond donor was conducted. (Figure 5.3b-h) These selected groups were carboxylic acid, carbonyl and ether to represent the selected co-formers in our experiments and the carboxylic and the amide interactions with the fragments were analysed in different possible geometrical arrangements (Figure 5.3b, f and g). Of all the structures containing an amide fragment, it was concluded that 91.13% display at least one hydrogen bond interaction. However, the observed number of hits for the selected interaction with the semicarbazone moiety decreased from 3831 to only 59. These results support the common observation that complex molecules with many hydrogen bonding possibilities exhibit highly unpredictable behaviour during co-crystallisation experiments.³ As such, the lack of expected new solid forms from the co-crystallisation of NFZ with various co-formers is not an uncommon occurrence.

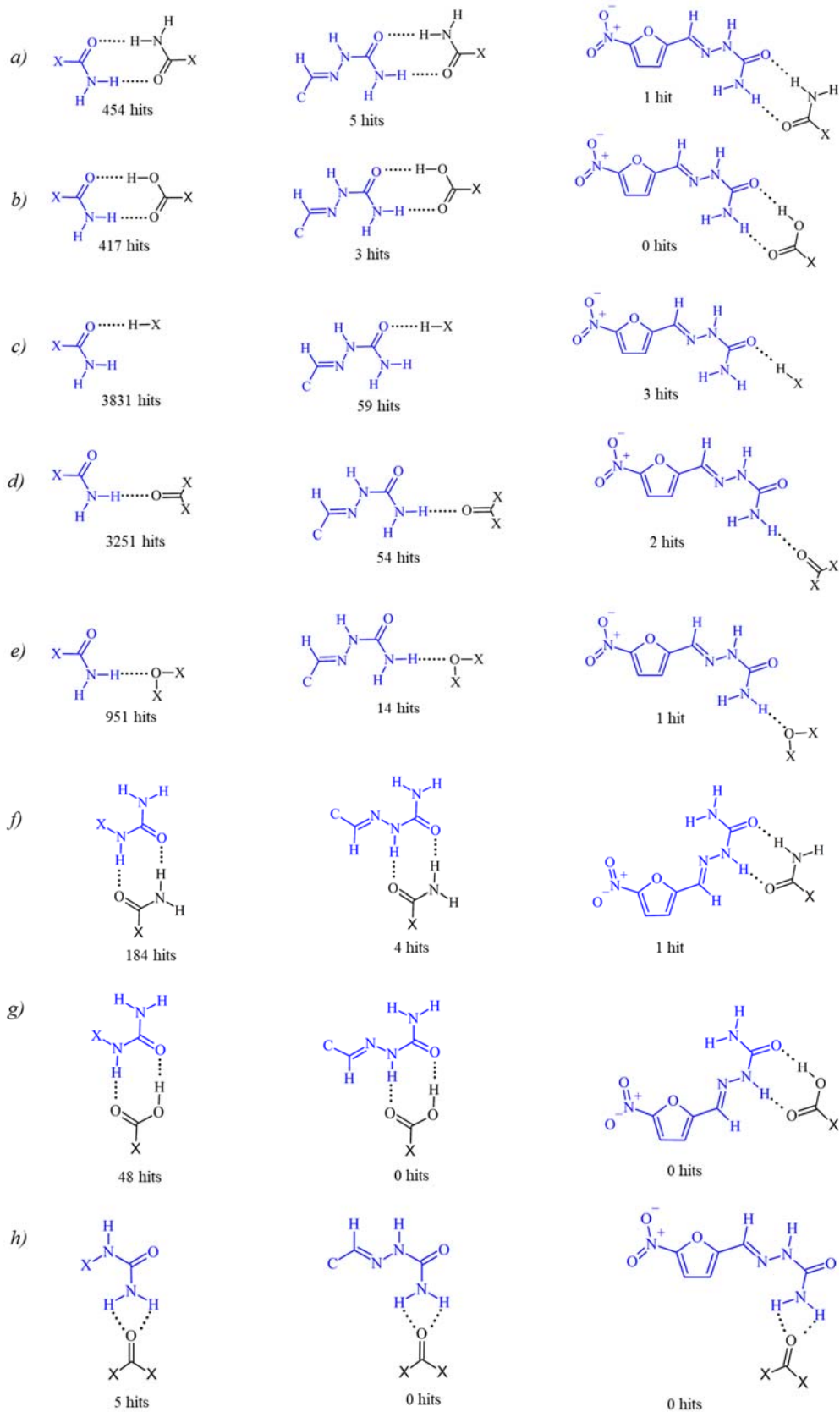


Figure 5.3 Hits obtained from the hydrogen bond motif search, where X is any atom

Table 5.1 Frequency of occurrence for each synthon pair, where X is any atom

	NFZ fragment	Amide	Semicarbazone	NFZ
a	XCONH ₂	10.8%	7.81%	0.00%
b	XCOOH	9.92%	4.69%	0.00%
c	H-X	91.13%	92.19%	100.00%
d	X ₂ C=O	77.33%	84.38%	66.70%
e	X-O-X	22.62%	0.53%	33.33%
f	XCONH	4.38%	4.69%	0.00%
g	XCOOH	1.14%	0	0.00%
h	X ₂ C=O (bifurcated)	0.12%	0.00%	0.00%

5.2 Conformational analysis

Molecules with many freely rotatable bonds can adopt several conformations; hence, they can form a variety of crystalline solids. Therefore, possible molecular conformation is an important factor in drug discovery because of its influence of biological and physical properties. Despite having an infinite number of possible theoretical conformations, molecules usually exhibit only a few energetically favourable arrangements. Geometrical data of the semicarbazone moiety was collected by searching the CSD (version 5.39, February 2018) with the aid of *ConQuest*.² The search, included the following restrictions: only single crystal structures, 3D coordinates determined, no errors, not polymeric and only organic structures. 60 structures with an overall 166 motifs were found (Table 5.2). The polar histograms of each of the defined torsion angles (τ_1 , τ_2 , and τ_3 molecular descriptors, see on Figure 3.2, page 44) are shown in Figures 5.4-5.6 (X in Figures 5.4-5.6 represent any atom). Generally, the torsion angles are planar with τ_1 and τ_3 distributed mainly around $\pm 0^\circ$ and $\pm 180^\circ$, which correspond to the synperiplanar and antiperiplanar orientation respectively. However, τ_2 is centred only around $\pm 0^\circ$ showing that it only occurs in the synperiplanar orientation.

There are some outlier structures. For τ_1 , structures UWIREZ, PIWFUW, PIWFUW01, EKILQZ and VILPIQ with the synperiplanar conformation, display a wide variation in the torsion angle. The semicarbazone chain in these structures is attached to an sp³ carbon with the effect that τ_1 cannot adopt a planar conformation because of the staggered arrangement. Also, despite the semicarbazone being attached to a sp² carbon in PAVZAP, TUBREN and DUNZAN, the chain is slightly rotated out of the plane. This may be due to the bulky groups in the structure which introduce strain in the molecular conformation. τ_3 is mainly in the

antiperiplanar orientation; and only WERVEU, ZINZIH and XUTVOZ have the synperiplanar arrangement. WERVEU is the α -polymorph of nitrofurazone. Table 5.2 summarizes relevant information for the crystal structures possessing the semicarbazone moiety. The conformer frequency distribution is shown in Figure 5.7.

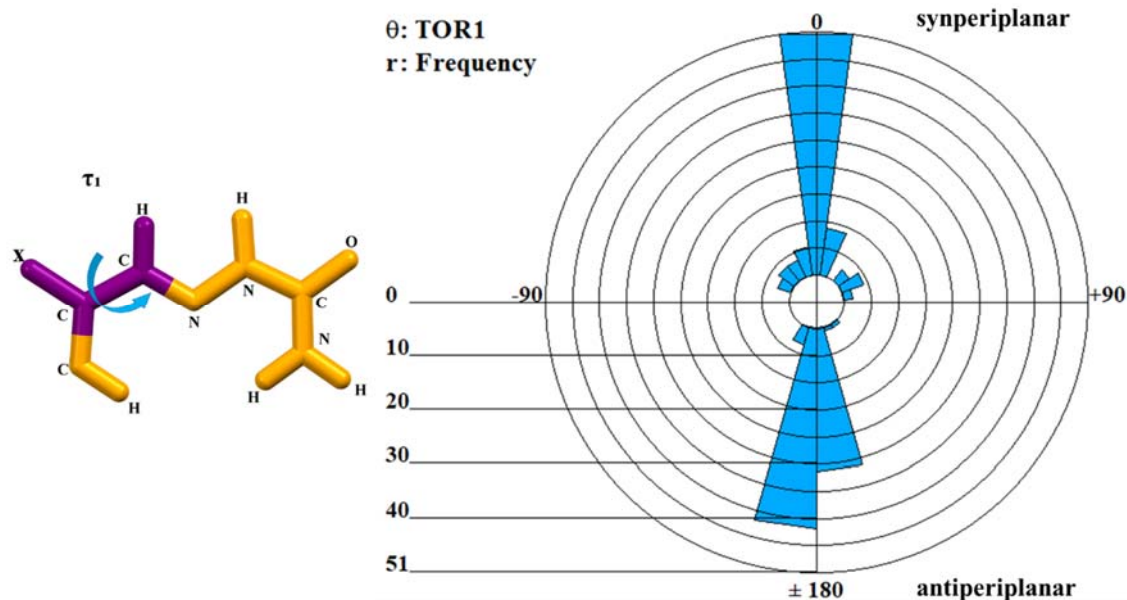


Figure 5.4 Polar histogram showing τ_1 frequency distribution

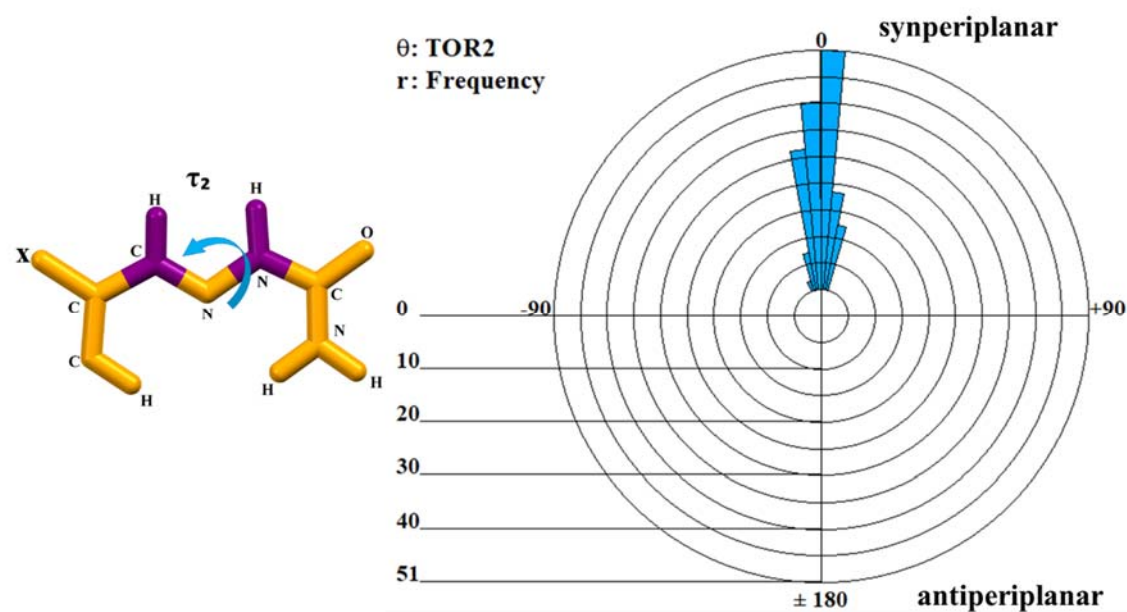


Figure 5.5 Polar histogram showing τ_2 frequency distribution

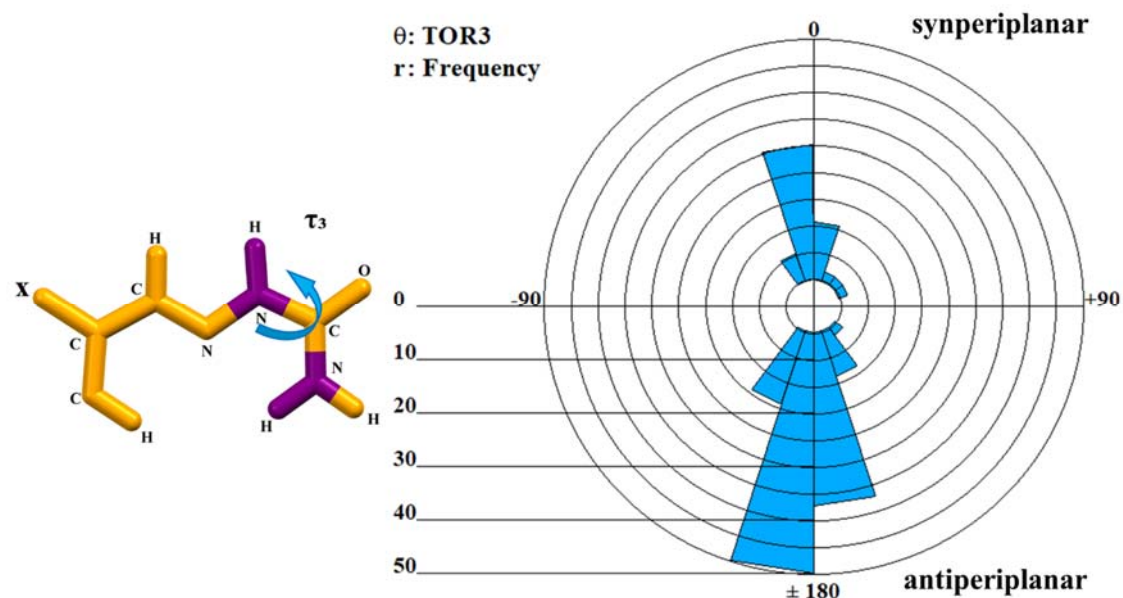


Figure 5.6 Polar histogram showing τ_3 frequency distribution

Table 5.2 Relevant torsion angles and their resulting conformation (continued to page 94)

<i>Refcode</i>	<i>Sp. Grp</i>	<i>Fragment</i>	τ_1	τ_2	τ_3	<i>Class</i>
BZALSC01	$P2_1/c$	1	6.118	-8.06	2.229	<i>sp-sp-ap</i>
BZALSC01	$P2_1/c$	2	-175.454	-8.06	2.229	<i>ap-sp-sp</i>
BZALSC10	$P2_1/c$	1	5.522	3.659	158.158	<i>sp-sp-ap</i>
BZALSC10	$P2_1/c$	2	-176.56	3.659	158.158	<i>ap-sp-ap</i>
DODGEI	$P1_12_1/b$	1	-174.576	10.501	-19.229	<i>sp-sp-sp</i>
DODGEI	$P1_12_1/b$	2	5.314	10.501	-19.229	<i>sp-sp-sp</i>
DUMZAN	$P3_12_1$	1	-161.039	1.066	179.26	<i>sp-sp-ap</i>
DUMZAN	$P3_12_1$	2	19.471	1.066	179.26	<i>sp-sp-ap</i>
EDELUV	$P\bar{1}$	1	178.111	-11.639	12.359	<i>sp-sp-ap</i>
EDELUV	$P\bar{1}$	2	-2.418	-11.639	12.359	<i>sp-sp-sp</i>
EKILOZ	$P2/c$	1	79.441	-0.479	-173.708	<i>sc-sp-ap</i>
EKILOZ	$P2/c$	2	-68.837	-4.61	177.848	<i>ac-sp-ap</i>
EKILOZ	$P2/c$	3	-38.775	-0.479	-173.708	<i>ac-sp-ap</i>
EKILOZ	$P2/c$	4	50.119	-4.61	177.848	<i>ac-sp-ap</i>
EKILOZ	$P2/c$	5	-159.138	-0.479	-173.708	<i>ap-sp-ap</i>
EKILOZ	$P2/c$	6	168.841	-4.61	177.848	<i>sp-sp-ap</i>
ETIXOU	$P2_1/c$	1	-167.888	-1.565	-157.461	<i>sp-sp-ap</i>
ETIXOU	$P2_1/c$	2	11.192	-1.565	-157.461	<i>sp-sp-ap</i>
EVERED	$Pca2_1$	1	174.938	2.954	-1.75	<i>sp-sp-ac</i>
EVERED	$Pca2_1$	2	-179.421	0.536	-156.631	<i>ap-sp-ap</i>
EVERED	$Pca2_1$	3	-3.061	2.954	-1.75	<i>sp-sp-sp</i>
EVERED	$Pca2_1$	4	-2.265	0.536	-156.631	<i>sp-sp-ap</i>
EVERED01	$Pca2_1$	1	173.773	-9.123	177.454	<i>sp-sp-ap</i>
EVERED01	$Pca2_1$	2	-178.212	6.637	-177.645	<i>ap-sp-ap</i>

EVERED01	$Pca2_1$	3	-4.528	-9.123	177.454	<i>sp-sp-ap</i>
EVERED01	$Pca2_1$	4	-1.546	6.637	-177.645	<i>sp-sp-ap</i>
EVERED02	$Pca2_1$	1	-179.093	15.305	-20.536	<i>ap-sp-sp</i>
EVERED02	$Pca2_1$	2	172.494	2.178	-5.335	<i>sp-sp-ap</i>
EVERED02	$Pca2_1$	3	-1.91	15.305	-20.536	<i>sp-sp-sp</i>
EVERED02	$Pca2_1$	4	-5.722	2.178	-5.335	<i>sp-sp-sp</i>
FUDQIE	$P2_1/a$	1	15.87	0.582	178.598	<i>sp-sp-ap</i>
FUDQIE	$P2_1/a$	2	-165.889	0.582	178.598	<i>ap-sp-ap</i>
FUNDUN	$P2_1/c$	1	-178.594	-5.04	-13.382	<i>ap-sp-sp</i>
FUNDUN	$P2_1/c$	2	-0.17	-5.04	-13.382	<i>sp-sp-sp</i>
GAQDOT	$P\bar{1}$	1	-178.596	0.256	-11.797	<i>sp-sp-ap</i>
GAQDOT	$P\bar{1}$	2	-177.773	-2.457	178.704	<i>ap-sp-ap</i>
GAQDOT	$P\bar{1}$	3	1.388	0.256	-11.797	<i>sp-sp-sp</i>
GAQDOT	$P\bar{1}$	4	1.86	-2.457	178.704	<i>sp-sp-ap</i>
GUHXOY	$C2/c$	1	-3.222	-2.536	-1.56	<i>sp-sp-ap</i>
GUHXOY	$C2/c$	2	178.24	-2.536	-1.56	<i>ap-sp-ap</i>
GUHXOY01	$I2/a$	1	3.941	-6.797	-177.933	<i>sp-sp-ap</i>
GUHXOY01	$I2/a$	2	-177.613	-6.797	-177.933	<i>ap-sp-ap</i>
GUHXOY02	$I2/a$	1	3.941	-6.797	-177.933	<i>sp-sp-ap</i>
GUHXOY02	$I2/a$	2	-177.613	-6.797	-177.933	<i>ap-sp-ap</i>
GUMNIN	$P\bar{1}$	1	4.482	0.12	-169.56	<i>sp-sp-ap</i>
GUMNIN	$P\bar{1}$	2	177.16	0.12	-169.56	<i>ap-sp-ap</i>
HAXHOG	$P2_1/c$	1	4.121	8.294	-175.615	<i>sp-sp-ap</i>
HAXHOG	$P2_1/c$	2	-172.783	8.294	-175.615	<i>ap-sp-ap</i>
IJOXAH	$P2_1/c$	1	171.293	1.359	-11.426	<i>sp-sp-ap</i>
IJOXAH	$P2_1/c$	2	-7.982	1.359	-11.426	<i>sp-sp-sp</i>
JOWSIZ	$P\bar{1}$	1	178.933	-2.49	176.911	<i>sp-sp-ap</i>
JOWSIZ	$P\bar{1}$	2	1.915	-2.49	176.911	<i>sp-sp-ap</i>
KEZKIK	$P\bar{1}$	1	1.116	-6.962	179.813	<i>sp-sp-ap</i>
KEZKIK	$P\bar{1}$	2	-176.177	-6.571	-174.642	<i>ap-sp-ap</i>
KEZKIK	$P\bar{1}$	3	-179.692	-6.962	179.813	<i>ap-sp-ap</i>
KEZKIK	$P\bar{1}$	4	2.135	-6.571	-174.642	<i>sp-sp-ap</i>
KUHGEA	$P2_1/n$	1	-0.27	-2.171	-16.39	<i>sp-sp-ap</i>
KUHGEA	$P2_1/n$	2	-179.452	-2.171	-16.39	<i>ap-sp-ap</i>
LATFER	$P2_1/c$	1	-6.775	-4.786	17.934	<i>sp-sp-ap</i>
LATFER	$P2_1/c$	2	172.694	-4.786	17.934	<i>ap-sp-ap</i>
LATFIV	$P2_1/a$	1	-170.174	10.209	-11.973	<i>sp-sp-ap</i>
LATFIV	$P2_1/a$	2	9.115	10.209	-11.973	<i>sp-sp-sp</i>
MOPBUP	$P2_1/c$	1	-3.476	0.259	157.042	<i>sp-sp-ap</i>
MOPBUP	$P2_1/c$	2	175.959	0.259	157.042	<i>ap-sp-ap</i>
MOPCAW	$C2/c$	1	4.964	-14.261	-160.544	<i>sp-sp-ap</i>
MOPCAW	$C2/c$	2	-175.603	-14.261	-160.544	<i>ap-sp-ap</i>
MUKXEV	$P\bar{1}$	1	-173.148	11.062	141.205	<i>sp-sp-ac</i>
MUKXEV	$P\bar{1}$	2	173.323	-8.644	10.708	<i>ap-sp-sp</i>
MUKXEV	$P\bar{1}$	3	174.42	-2.822	-11.844	<i>ap-sp-sp</i>

MUKXEV	$P\bar{1}$	4	-174.276	10.839	175.696	<i>ap-sp-ap</i>
MUKXEV	$P\bar{1}$	5	7.459	11.062	141.205	<i>sp-sp-sc</i>
MUKXEV	$P\bar{1}$	6	-7.977	-8.644	10.708	<i>sp-sp-sp</i>
MUKXEV	$P\bar{1}$	7	-2.954	-2.822	-11.844	<i>sp-sp-sp</i>
MUKXEV	$P\bar{1}$	8	3.209	10.839	175.696	<i>sp-sp-ap</i>
PAVZAP	$C2/c$	1	148.354	-16.85	174.229	<i>sc-sp-ap</i>
PAVZAP	$C2/c$	2	-31.214	-16.85	174.229	<i>ac-sp-ap</i>
PIWFUW	$P2_12_12_1$	1	-44.923	-7.808	-178.722	<i>sc-sp-ap</i>
PIWFUW	$P2_12_12_1$	2	-58.717	2.055	-176.522	<i>ac-sp-ap</i>
PIWFUW	$P2_12_12_1$	3	67.318	14.367	-177.636	<i>ac-sp-ap</i>
PIWFUW	$P2_12_12_1$	4	68.727	-7.808	-178.722	<i>ac-sp-ap</i>
PIWFUW	$P2_12_12_1$	5	53.717	2.055	-176.522	<i>ac-sp-ap</i>
PIWFUW	$P2_12_12_1$	6	-176.508	14.367	-177.636	<i>ap-sp-ap</i>
PIWFUW	$P2_12_12_1$	7	-164.592	-7.808	-178.722	<i>ap-sp-ap</i>
PIWFUW	$P2_12_12_1$	8	-172.964	2.055	-176.522	<i>ap-sp-ap</i>
PIWFUW	$P2_12_12_1$	9	-52.658	14.367	-177.636	<i>ac-sp-ap</i>
PIWFUW01	$P2_12_12_1$	1	-44.923	-7.808	-178.722	<i>sc-sp-ap</i>
PIWFUW01	$P2_12_12_1$	2	-58.717	2.055	-176.522	<i>ac-sp-ap</i>
PIWFUW01	$P2_12_12_1$	3	67.318	14.367	-177.636	<i>ac-sp-ap</i>
PIWFUW01	$P2_12_12_1$	4	68.727	-7.808	-178.722	<i>ac-sp-ap</i>
PIWFUW01	$P2_12_12_1$	5	53.717	2.055	-176.522	<i>ac-sp-ap</i>
PIWFUW01	$P2_12_12_1$	6	-176.508	14.367	-177.636	<i>ap-sp-ap</i>
PIWFUW01	$P2_12_12_1$	7	-164.592	-7.808	-178.722	<i>ap-sp-ap</i>
PIWFUW01	$P2_12_12_1$	8	-172.964	2.055	-176.522	<i>ap-sp-ap</i>
PIWFUW01	$P2_12_12_1$	9	-52.658	14.367	-177.636	<i>ac-sp-ap</i>
TAKREC	$C2/c$	1	175.352	-1.252	156.046	<i>sp-sp-ap</i>
TAKREC	$C2/c$	2	-4.172	-1.252	156.046	<i>sp-sp-ap</i>
TAKREC01	$P\bar{1}$	1	-175.305	-5.559	-152.45	<i>ap-sp-ap</i>
TAKREC01	$P\bar{1}$	2	-178.219	-9.865	55.036	<i>ap-sp-ac</i>
TAKREC01	$P\bar{1}$	3	3.319	-5.559	-152.45	<i>sp-sp-ap</i>
TAKREC01	$P\bar{1}$	4	2.408	-9.865	55.036	<i>sp-sp-ac</i>
TAKREC02	$C2/c$	1	176.78	7.599	147.232	<i>sp-sp-ac</i>
TAKREC02	$C2/c$	2	-2.84	7.599	147.232	<i>sp-sp-ap</i>
TIVGOU	$P\bar{1}$	1	-179.314	0.077	-174.008	<i>sp-sp-ap</i>
TIVGOU	$P\bar{1}$	2	177.714	0.988	179.364	<i>sp-sp-ap</i>
TIVGOU	$P\bar{1}$	3	0.61	0.077	-174.008	<i>sp-sp-ap</i>
TIVGOU	$P\bar{1}$	4	15.858	0.988	179.364	<i>sp-sp-ap</i>
TUBQOW	$P2_1/a$	1	171.214	3.48	30.25	<i>sp-sp-ap</i>
TUBQOW	$P2_1/a$	2	-9.409	3.48	30.25	<i>sp-sp-ac</i>
TUBQUC	$P2_1/c$	1	-0.034	-15.672	-6.667	<i>sp-sp-ap</i>
TUBQUC	$P2_1/c$	2	178.169	-15.672	-6.667	<i>ap-sp-sp</i>
TUBRAJ	$P2_1/a$	1	17.064	0.196	-21.094	<i>sp-sp-sp</i>
TUBRAJ	$P2_1/a$	2	-163.247	0.196	-21.094	<i>ap-sp-sp</i>
TUBREN	$P2_1/a$	1	-19.183	-1.369	171.284	<i>sp-sp-ap</i>
TUBREN	$P2_1/a$	2	161.321	-1.369	171.284	<i>ap-sp-ap</i>

UMAKIE	$P2_1/a$	1	167.294	-9.182	171.851	<i>sp-sp-ap</i>
UMAKIE	$P2_1/a$	2	-10.22	-9.182	171.851	<i>sp-sp-ap</i>
UWIREZ	$P2_1$	1	68.15	5.427	-179.892	<i>sc-sp-ap</i>
UWIREZ	$P2_1$	2	-38.889	5.427	-179.892	<i>ac-sp-ap</i>
UWIREZ	$P2_1$	3	-165.133	5.427	-179.892	<i>ap-sp-ap</i>
VILPIQ	$P2_1$	1	-154.655	3.763	179.273	<i>ap-sp-ap</i>
VILPIQ	$P2_1$	2	79.28	3.763	179.273	<i>sp-sp-ap</i>
VILPIQ	$P2_1$	3	-36.123	3.763	179.273	<i>ac-sp-ap</i>
VORKET	$P2_1/c$	1	-9.662	-11.179	166.634	<i>sp-sp-ap</i>
VORKET	$P2_1/c$	2	167.886	-11.179	166.634	<i>ap-sp-ap</i>
VORKET01	$P2_1/c$	1	9.807	11.536	-167.326	<i>sp-sp-ap</i>
VORKET01	$P2_1/c$	2	-167.896	11.536	-167.326	<i>ap-sp-ap</i>
WERVEU	$P2_1/a$	1	177.457	-10.14	-161.818	<i>ap-sp-ap</i>
WERVEU	$P2_1/a$	2	-2.758	-10.14	-161.818	<i>sp-sp-ap</i>
WERVEU01	$P2_1$	1	5.348	8.586	-15.69	<i>sp-sp-sp</i>
WERVEU01	$P2_1$	2	-174.361	8.586	-15.69	<i>ap-sp-sp</i>
WERVEU02	$P2_1/c$	1	-1.062	1.433	-1.715	<i>sp-sp-sp</i>
WERVEU02	$P2_1/c$	2	-178.363	1.433	-1.715	<i>ap-sp-sp</i>
WIGPAF	$P\bar{1}$	1	-173.108	2.113	-149.444	<i>sp-sp-ac</i>
WIGPAF	$P\bar{1}$	2	3.762	2.113	-149.444	<i>sp-sp-sc</i>
XAXXUQ	$P\bar{1}$	1	2.41	-4.566	-2.412	<i>sp-sp-ap</i>
XAXXUQ	$P\bar{1}$	2	-177.954	-4.566	-2.412	<i>ap-sp-sp</i>
XUTVIT	$P2_1/c$	1	-2.238	7.128	-7.986	<i>sp-sp-ap</i>
XUTVIT	$P2_1/c$	2	177.185	7.128	-7.986	<i>ap-sp-sp</i>
XUTVOZ	$P\bar{1}$	1	176.836	-1.509	14.429	<i>ap-sp-sp</i>
XUTVOZ	$P\bar{1}$	2	-3.642	-1.509	14.429	<i>sp-sp-sp</i>
YAGFIX	$P2_1/c$	1	7.33	-1.108	-151.271	<i>sp-sp-ap</i>
YAGFIX	$P2_1/c$	2	-171.318	-1.108	-151.271	<i>ap-sp-ap</i>
YAVVAU	$P2/c$	1	177.36	-10.513	9.118	<i>ap-sp-sp</i>
YAVVAU	$P2/c$	2	-0.888	-10.513	9.118	<i>sp-sp-sp</i>
YEFGIB	$P2_1/c$	1	178.206	0.67	-176.513	<i>sp-sp-ap</i>
YEFGIB	$P2_1/c$	2	-167.313	8.543	172.502	<i>ap-sp-ap</i>
YEFGIB	$P2_1/c$	3	-5.149	0.67	-176.513	<i>sp-sp-ap</i>
YEFGIB	$P2_1/c$	4	15.651	8.543	172.502	<i>sp-sp-ap</i>
YEFGIB	$P2_1/c$	5	-4.926	-3.046	-174.28	<i>sp-sp-ap</i>
YEFGIB	$P2_1/c$	6	0.9	5.258	175.78	<i>sp-sp-ap</i>
YEFGIB	$P2_1/c$	7	174.036	-3.046	-174.28	<i>ap-sp-ap</i>
YEFGIB	$P2_1/c$	8	-176.533	5.258	175.78	<i>ap-sp-ap</i>
YEFGOH	$P2_1/c$	1	2.319	7.451	154.868	<i>sp-sp-ap</i>
YEFGOH	$P2_1/c$	2	-179.966	7.451	154.868	<i>sp-sp-ap</i>
YIFTOX	$P2_1/c$	1	174.711	-0.628	-160.651	<i>sp-sp-ap</i>
YIFTOX	$P2_1/c$	2	-6.993	-0.628	-160.651	<i>sp-sp-ap</i>
YIFVUF	$P2_1/c$	1	-4.018	1.662	-166.483	<i>sp-sp-ap</i>
YIFVUF	$P2_1/c$	2	178.319	1.662	-166.483	<i>ap-sp-ap</i>
YOYNOP	$P2_1/a$	1	9.941	-2.714	42.537	<i>sp-sp-ac</i>

YOYNOP	$P2_1/a$	2	-167.953	-2.714	42.537	<i>ap-sp-ac</i>
YOYNOP01	$P2_1/c$	1	10.524	4.262	-169.823	<i>sp-sp-ap</i>
YOYNOP01	$P2_1/c$	2	-168.574	4.262	-169.823	<i>ap-sp-ap</i>
ZAMZUI	$P2_1/n$	1	178.179	-2.12	-170.134	<i>ap-sp-ap</i>
ZAMZUI	$P2_1/n$	2	-1.215	-2.12	-170.134	<i>sp-sp-sp</i>
ZINZIH	$P\bar{1}$	1	178.501	2.646	169.21	<i>sp-sp-sp</i>
ZINZIH	$P\bar{1}$	2	-2.616	2.646	169.21	<i>sp-sp-ap</i>

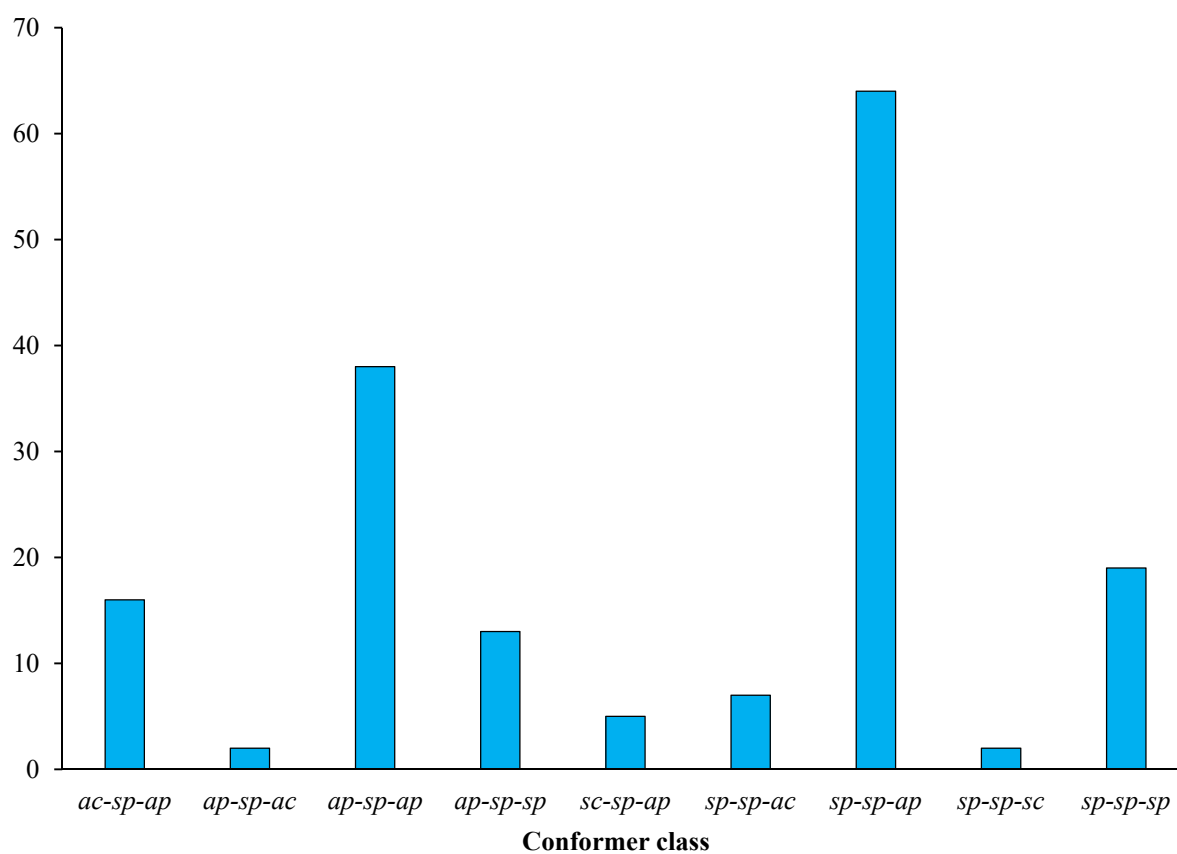


Figure 5.7 Occurrence of semicarbazone conformers in the CSD

The most popular conformation of the torsion angles was found to be as the *sp-sp-ap* conformer and the second most popular conformer was found to be the *ap-sp-ap* (Figure 5.7). These solid state findings were tested by conducting conformational analysis of the NFZ molecule with gas phase DFT calculations*.⁴⁻¹⁰ The five lowest energy conformers and their relative energies are shown in Figure 5.8. The *sp-sp-ap* conformer that was observed in polymorphs β and γ , was found to have the lowest energy, while the α -polymorph has the highest energy *ap-sp-sp* conformation. The energy of the *ap-sp-ap* conformer was also found to be the lowest (although confirmation of the actual energy value needs further investigation) and this conformation was observed in 38 of the 166 hits. The higher energy *ap-ap-sp* and the *sp-ap-ap* conformers were also not observed in any of the solid state structures. It is interesting to note that the structure of NFZ•H₃PO₄ adopted the *ap-sp-ap* conformation, and hence this is the only example in which the NFZ takes up this low energy conformer.

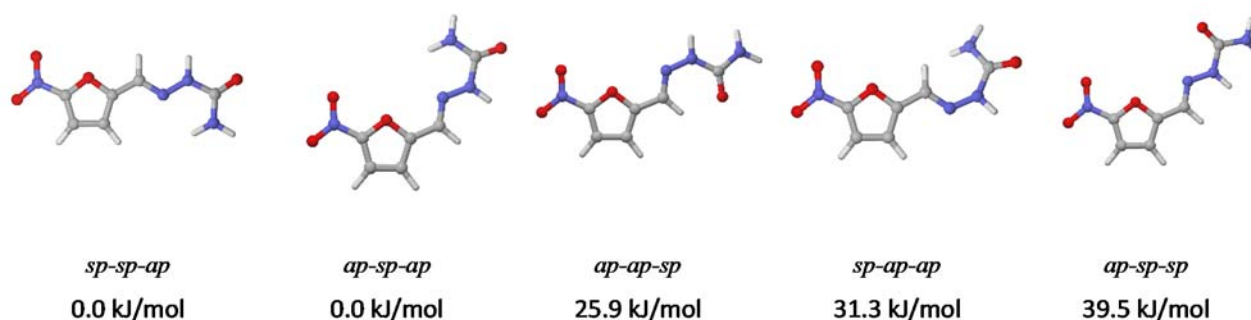



Figure 5.8 Low energy molecular conformations of NFZ obtained from gas phase calculations

*DFT calculations were done using ORCA 4.⁴ The PBE functional was used,⁵ together with the def2-TZVP basis set.⁶ The D3 dispersion correction of Grimme, with the Becke–Johnson damping function (D3BJ), was added.^{7,8} The resolution of identity approximation⁹ was applied using the def2 Coulomb fitting auxiliary basis of Weigend.¹⁰ This level of theory is denoted as PBE-D3(BJ)/def2-TZVP. All configurations studied were local minima (confirmed through the absence of imaginary frequencies in the vibrational spectrum). Electronic energies are given as relative values in kJ/mol.

References

- (1) Bruno, I. J.; Cole, J. C.; Edgington, P. R.; Kessler, M.; Macrae, C. F.; McCabe, P.; Pearson, J.; Taylor, R., New software for searching the Cambridge Structural Database and visualizing crystal structures. *Acta Crystallographica Section B* **2002**, 58, (3 Part 1), 389-397.
- (2) Macrae, C. F.; Bruno, I. J.; Chisholm, J. A.; Edgington, P. R.; McCabe, P.; Pidcock, E.; Rodriguez-Monge, L.; Taylor, R.; van de Streek, J.; Wood, P. A., Mercury CSD 2.0 - new features for the visualization and investigation of crystal structures. *Journal of Applied Crystallography* **2008**, 41, (2), 466-470.
- (3) Gavezzotti, A., Are crystal structures predictable? *Accounts of Chemical Research* **1994**, 27, (10), 309-314.
- (4) Neese, F., The ORCA program system. *Wiley Interdisciplinary Reviews: Computational Molecular Science* **2012**, 2, (1), 73-78.
- (5) Perdew, J. P.; Burke, K.; Ernzerhof, M., Generalized gradient approximation made simple. *Physical Review Letters* **1996**, 77, (18), 3865.
- (6) Weigend, F.; Ahlrichs, R., Balanced basis sets of split valence, triple zeta valence and quadruple zeta valence quality for H to Rn: Design and assessment of accuracy. *Physical Chemistry Chemical Physics* **2005**, 7, (18), 3297-3305.
- (7) Grimme, S.; Ehrlich, S.; Goerigk, L., Effect of the damping function in dispersion corrected density functional theory. *Journal of Computational Chemistry* **2011**, 32, (7), 1456-1465.
- (8) Grimme, S.; Antony, J.; Ehrlich, S.; Krieg, H., A consistent and accurate ab initio parametrization of density functional dispersion correction (DFT-D) for the 94 elements H-Pu. *The Journal of Chemical Physics* **2010**, 132, (15), 154104.
- (9) Neese, F., An improvement of the resolution of the identity approximation for the formation of the Coulomb matrix. *Journal of Computational Chemistry* **2003**, 24, (14), 1740-1747.
- (10) Weigend, F., Accurate Coulomb-fitting basis sets for H to Rn. *Physical Chemistry Chemical Physics* **2006**, 8, (9), 1057-1065.

CHAPTER 6



The following chapter is the presentation of the summary and conclusion of the research

6 Summary and conclusion

Over half of known drugs have poor solubility in the human circulatory system. Several approaches to counter the challenge of poor bioavailability of drugs have gained momentous interest, namely production of multicomponent crystals such as salts and co-crystals which have improved physicochemical properties.

The foremost objective of this research was (i) to produce a series of crystals of nitrofurazone via methodical varying of co-crystallizing co-former compounds without changing its molecular structure and (ii) to understand and compare their supramolecular stability by comparing their physicochemical properties. As the first step in multicomponent crystal formation, the functional groups of the NFZ molecule were investigated and synthon engineering principles were used to select a series of possible co-formers with complementary functional groups. The aim was to form (i) the amide-amide homosynthon and (ii) the amide-carboxylic acid heterosynthon via the semicarbazone functionality.

In the initial run of the crystallization experiments, a series of carboxylic acids and substituted amides were used. In all these crystallisations, multicomponent crystal formation was futile and only polymorphs of nitrofurazone (i.e. either α , β or γ) were formed and their crystallographic data were obtained at low temperature. Parallel to these experiments, NFZ was exposed to a variety of general organic solvents with accessible hydrogen bond donor or hydrogen bond acceptor functional groups. The same result of only formation of the three polymorphs was obtained from the solvents. Designated torsion angles, i.e. τ_1 , τ_2 and τ_3 of the polymorphs were used to classify the conformers according to IUPAC rules. The α -polymorph was found to contain from the *ap-sp-sp* conformer whereas β - and γ -polymorphs contained the *sp-sp-ap* conformer. Conformations exhibited in these polymorphs took the preferred *sp-sp-ap* molecular orientation of semicarbazones.

Series of mineral acids and short chain carboxylic acids were used to provide strong hydrogen bonding functional groups with the hope of breaking the amide homodimers and forming the amide-acid heterodimer. Three multicomponent crystals, $4\text{NFZ}\cdot[\text{H}_3\text{O}^+][\text{ClO}_4^-]$, $\text{NFZ}\cdot\text{H}_3\text{PO}_4$ and $\text{NFZ}\cdot\text{PA}$ were obtained eventually from this set of experiments. Bulk property analyses of all crystals of NFZ were carried out using PXRD, DSC, TGA and FTIR spectroscopy. The $4\text{NFZ}\cdot[\text{H}_3\text{O}^+][\text{ClO}_4^-]$ structure exhibited an unusual stoichiometry and exclusive combination of Z' , Z'' and Z^x values. All four NFZ molecules in the perchlorate crystal were in the *sp-sp-ap*

conformation. A new conformation of NFZ, *ap-sp-ap*, was observed in the NFZ•H₃PO₄ solvate. Typical amide-amide synthon formation was inhibited in this structure by the inclusion of the acid. Similarly to NFZ•H₃PO₄, no protonation occurred in the NFZ•PA crystal. All four NFZ molecules in NFZ•PA crystallized in the *sp-sp-ap* conformation. Its tetramers formed sheets, but no interactions were found between the sheets. This layered nature of the structure was the most plausible explanation of why the crystallisation of NFZ•PA crystals was really challenging. In the case of 4NFZ•[H₃O⁺][ClO₄⁻], the perchlorate anion links the layers of NFZ molecules into the third dimension, while phosphoric acids in NFZ•H₃PO₄ facilitate the same structural role. In the NFZ•PA crystal the layers are held together with weak interactions, thus the formation of this crystal was the most unusual outcome. NFZ has a typically planar molecular shape similar to that of dyes. Therefore, growing crystals is difficult if there are no functional groups that would form interactions into the third dimension. In light of this knowledge, the three discussed multicomponent crystals of NFZ present good examples of the problems which may arise when dye-like compounds are crystallized.

The solid state behaviour of the semicarbazone moiety was studied with the aid of data retrieved from the Cambridge Structural Database. The aim was to (i) investigate the intermolecular interactions preferred by the moiety and to (ii) determine the most commonly occurring conformer with the aid of mapping torsional frequency distribution for the functional group using τ_1 , τ_2 and τ_3 molecular descriptors. From the synthon and the moiety searches, it was concluded that the probability of obtaining a contact decreased as the NFZ semicarbazone fragment grew. Secondly, the torsional flexibility of the semicarbazone moiety was investigated and the most popular conformers were found to be the *sp-sp-ap* followed by *ap-sp-ap*. These solid state findings were further tested by conducting conformational analysis of the NFZ molecule with gas phase DFT calculations. The *sp-sp-ap* conformer observed in β - and γ -polymorphs was found to have the lowest energy, along with the *ap-sp-ap* conformer. The higher energy conformers (i.e. *ap-ap-sp* and *sp-ap-ap*), were not observed in any of the solid state structures. Interestingly, the structure of NFZ•H₃PO₄ adopted the *ap-sp-ap* conformation, and it is the only structure where NFZ took the low energy conformer, thereby showing that solid state findings agreed with the energy calculations.

APPENDIX



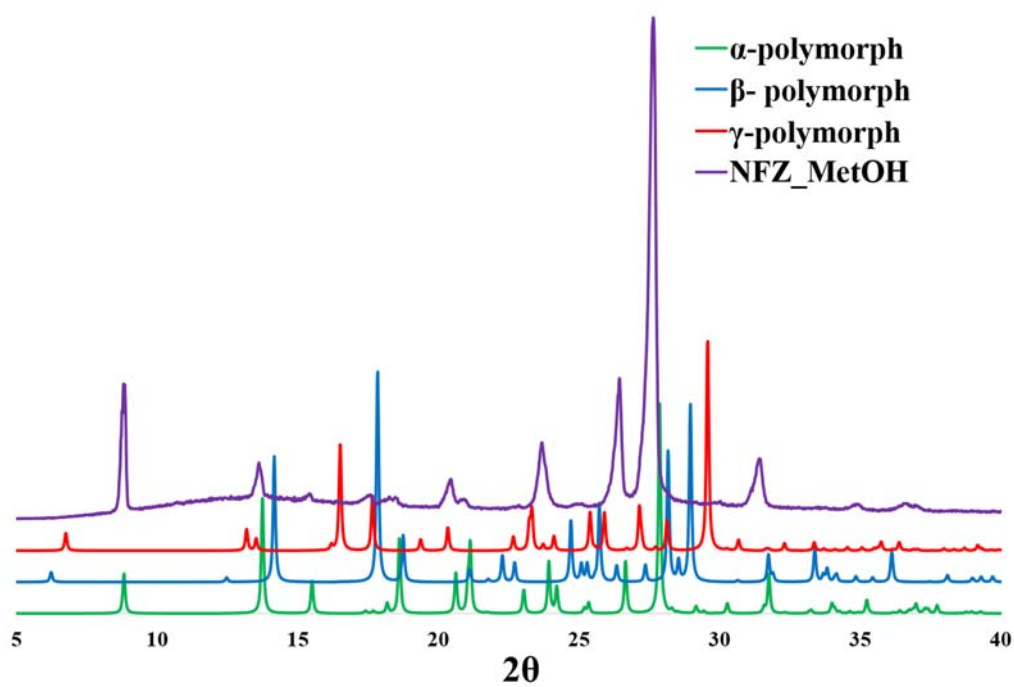


Figure A 1 PXRD patterns of α , β , and γ -polymorphs and the crystal obtained from methanol

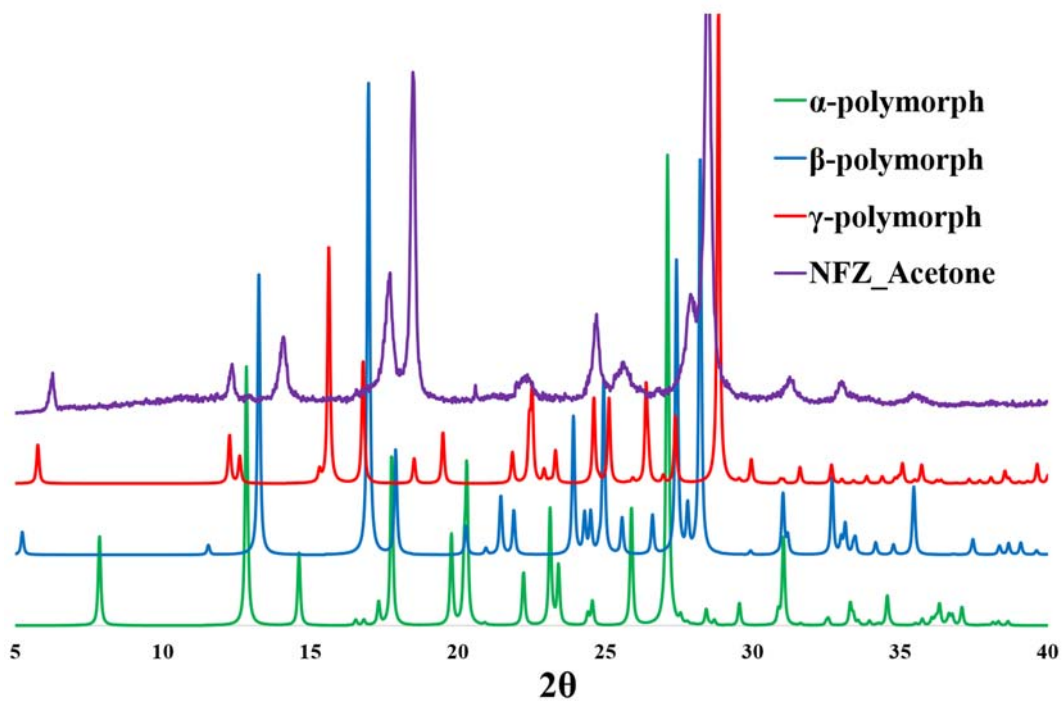


Figure A 2 PXRD patterns of α , β , and γ -polymorphs and the crystal obtained from acetone

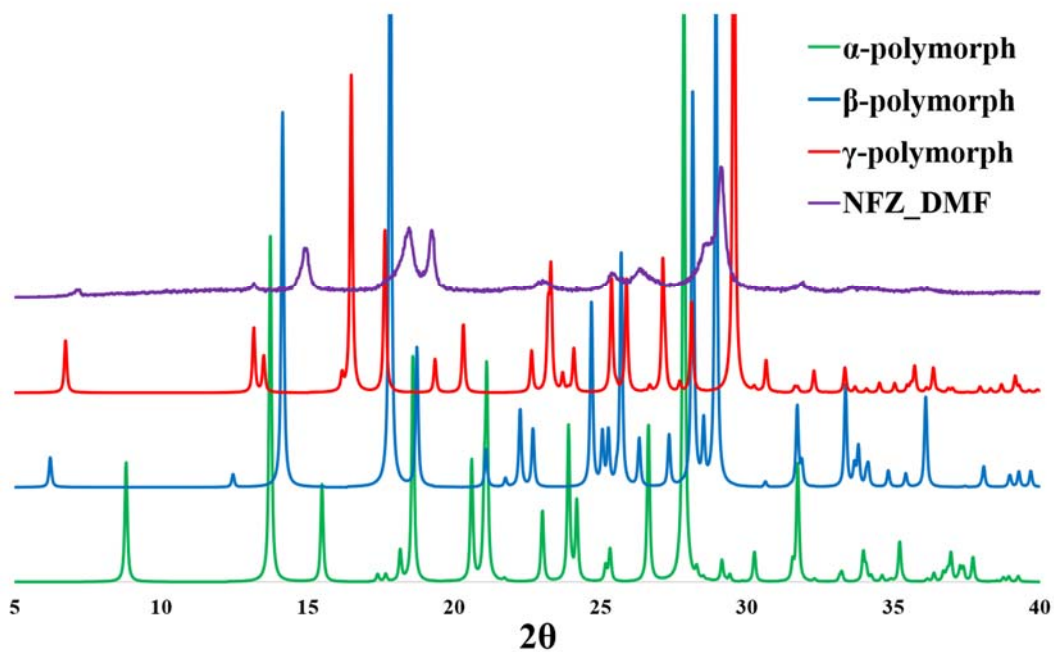


Figure A 3 PXR D patterns of α , β , and γ -polymorphs and the crystal obtained from dimethylformamide

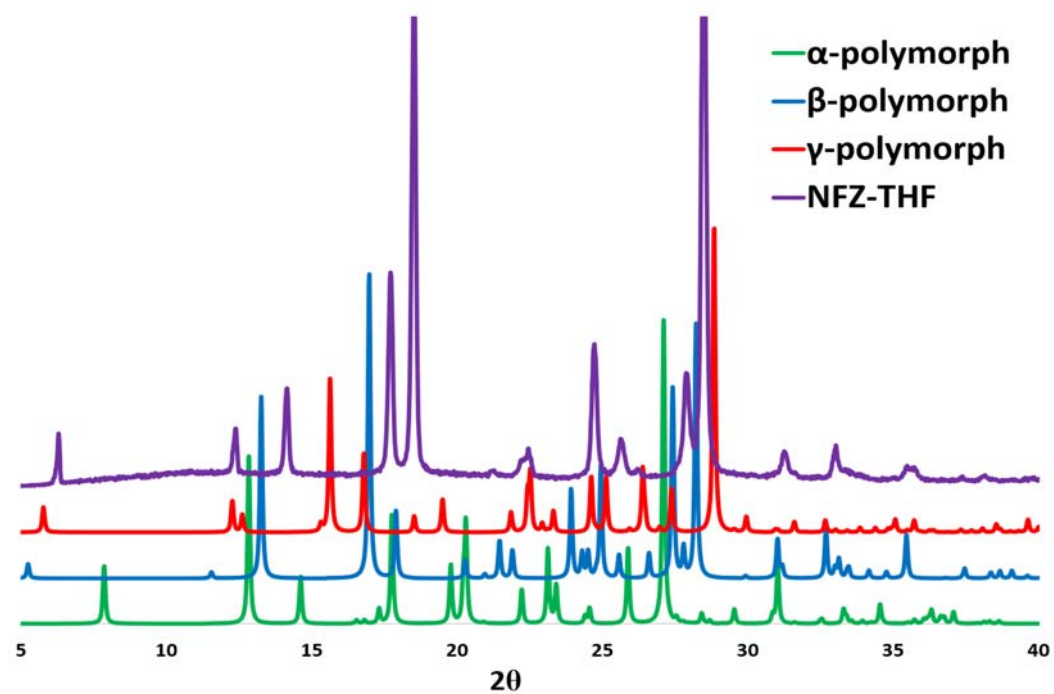


Figure A 4 PXR D patterns of α , β , and γ -polymorphs and the crystal obtained from tetrahydrofuran

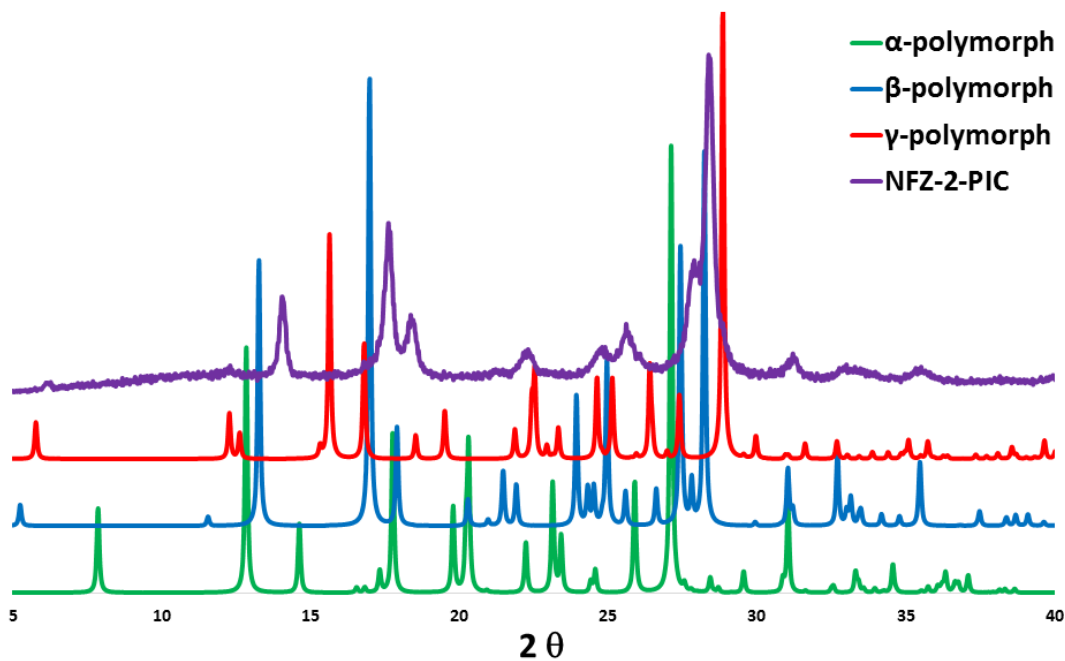


Figure A 5 PXRD patterns of α , β , and γ -polymorphs and the crystal obtained from 2-picoline

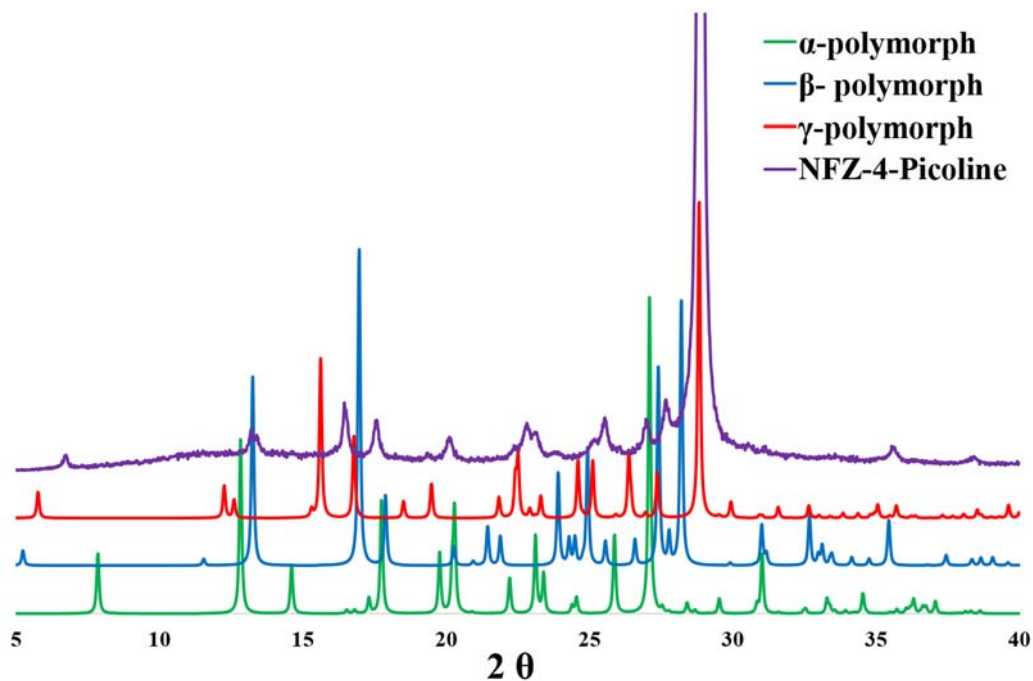


Figure A 6 PXRD patterns of α , β , and γ -polymorphs and the crystal obtained from 4-picoline

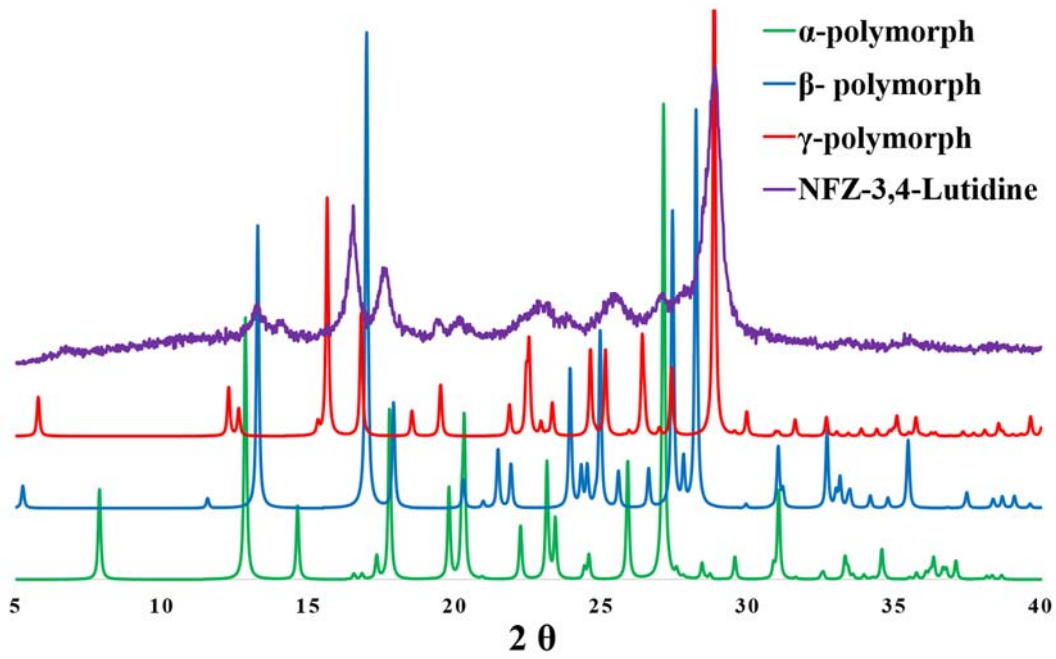


Figure A 7 PXR D patterns of α , β , and γ -polymorphs and the crystal obtained from 3,4-lutidine

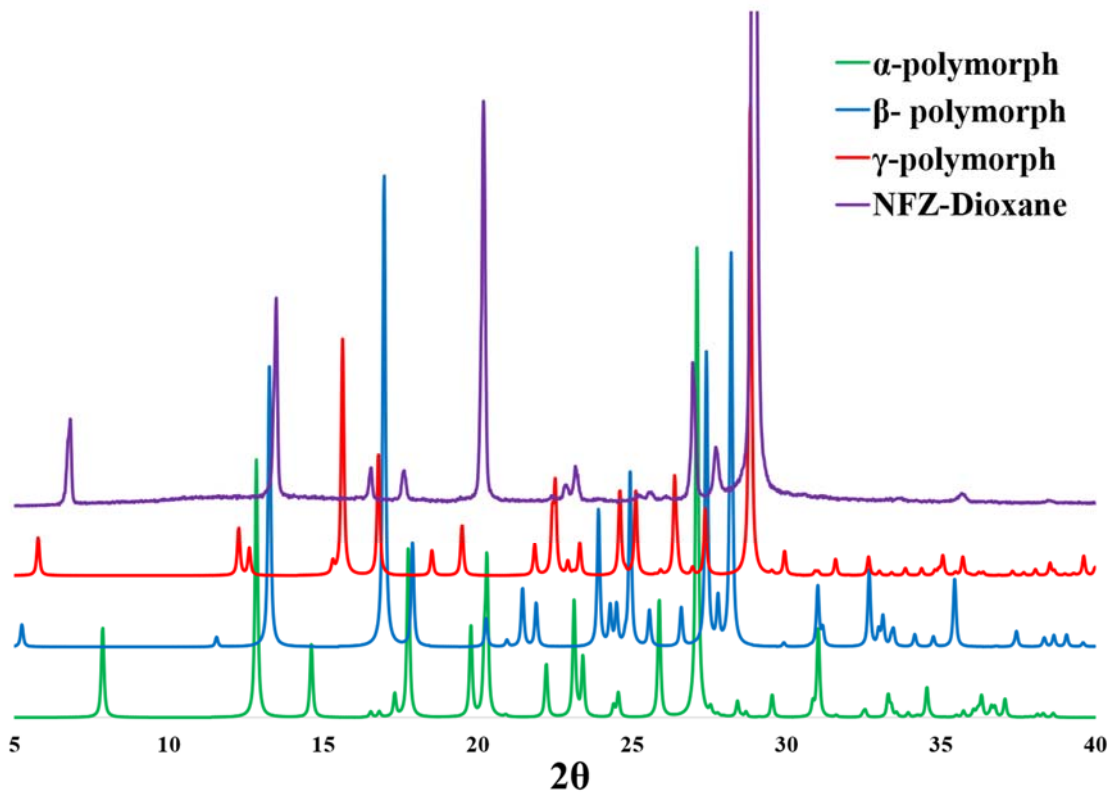


Figure A 8 PXR D patterns of α , β , and γ -polymorphs and the crystal obtained from dioxane

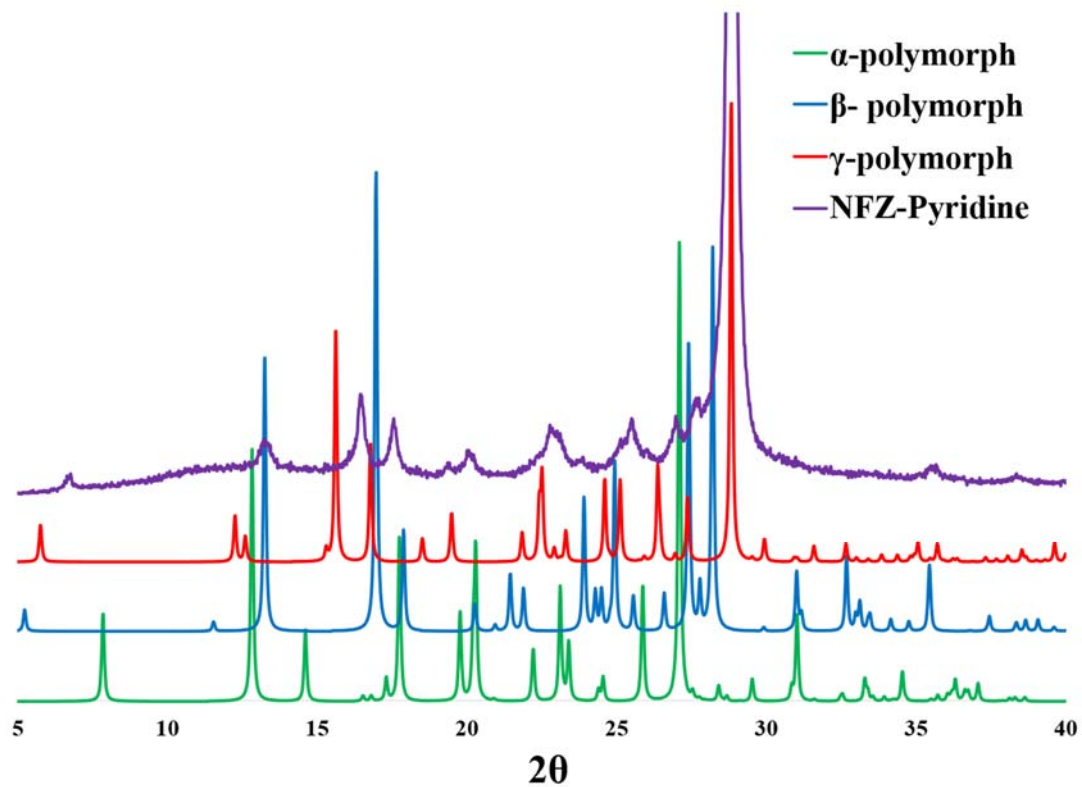


Figure A 9 PXR D patterns of α , β , and γ -polymorphs and the crystal obtained from pyridine

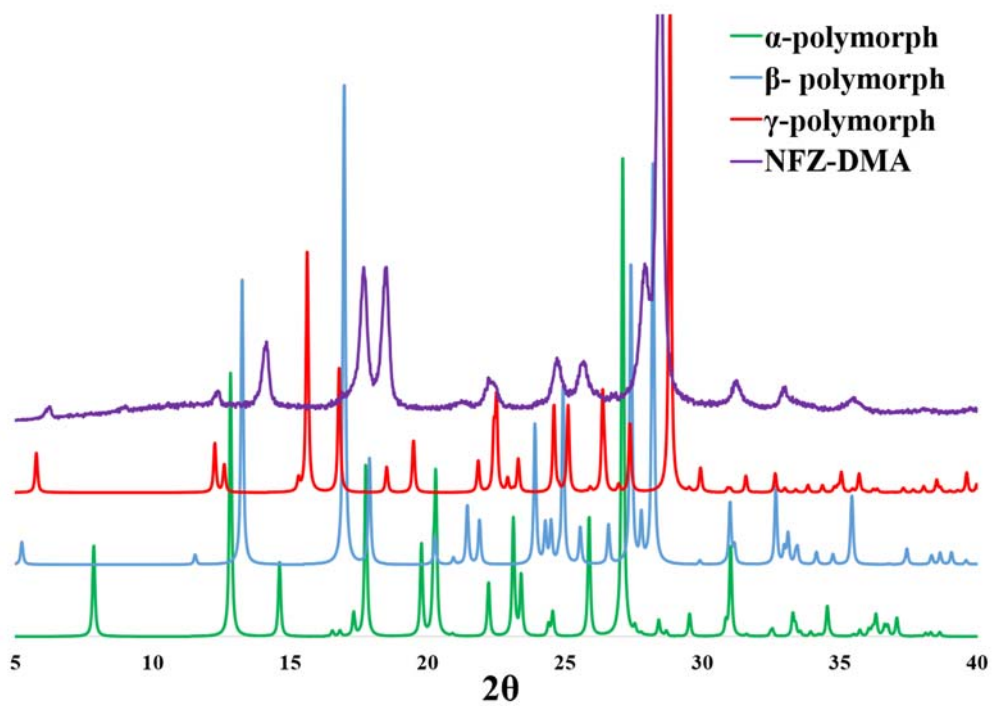


Figure A 10 PXR D patterns of α , β , and γ -polymorphs and the crystal obtained from dimethylacetamide

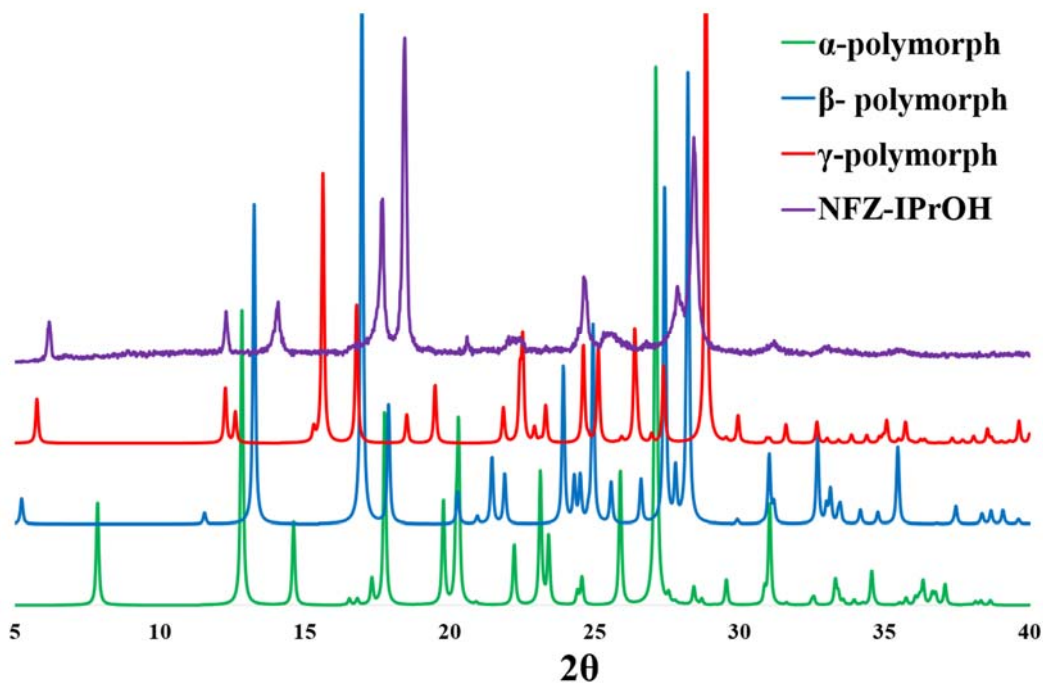


Figure A 11 PXR D patterns of α , β , and γ -polymorphs and the crystal obtained from isopropanol

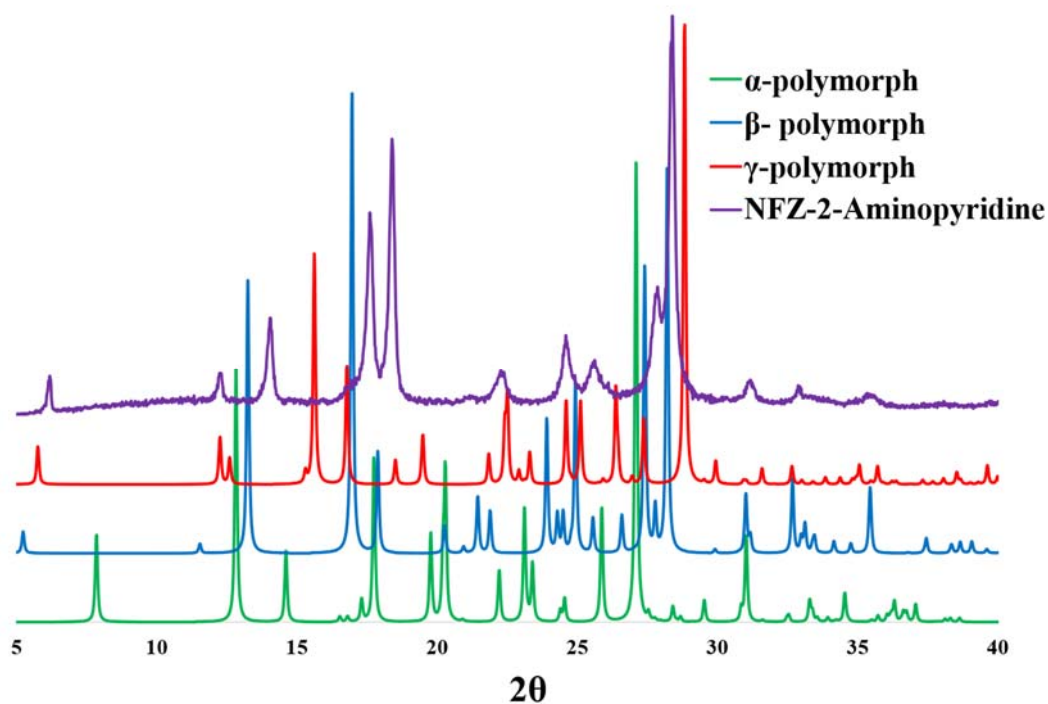


Figure A 12 PXR D patterns of α , β , and γ -polymorphs and the crystal obtained from 2-aminopyridine

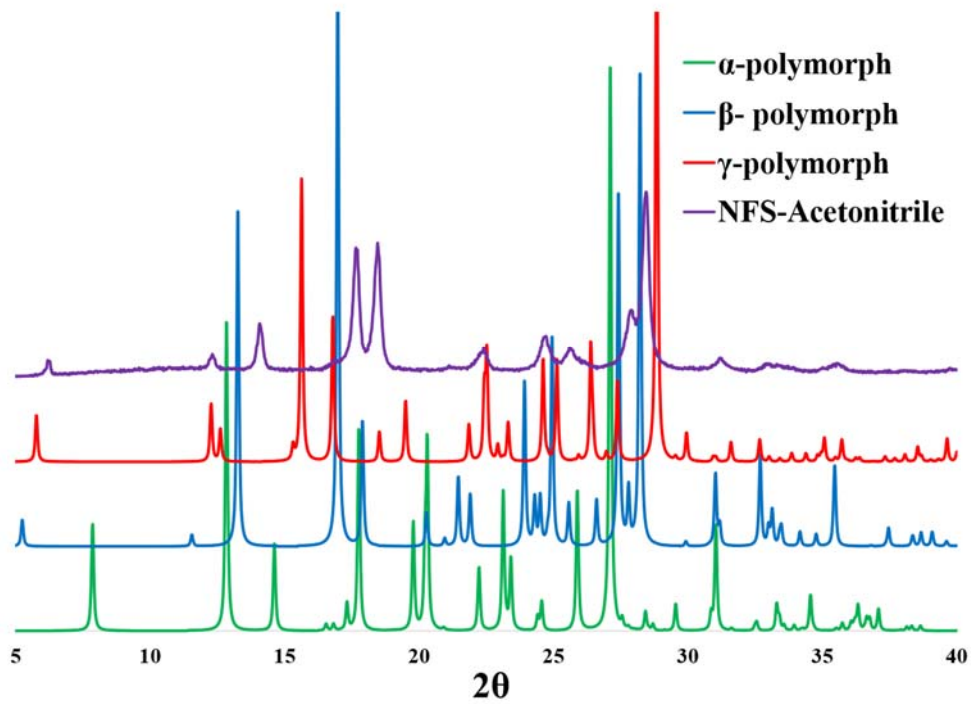


Figure A 13 PXR D patterns of α , β , and γ -polymorphs and the crystal obtained from acetonitrile

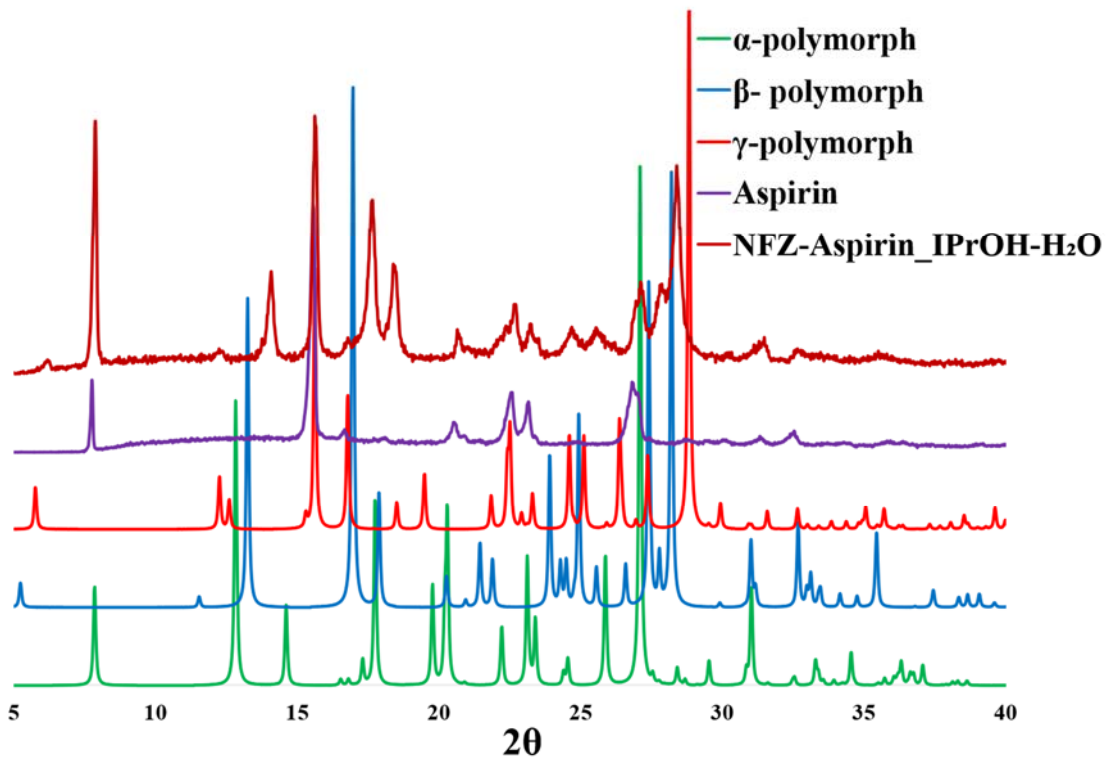


Figure A 14 PXR D patterns of α , β , and γ -polymorphs and the crystal obtained from aspirin:isopropanol:H₂O

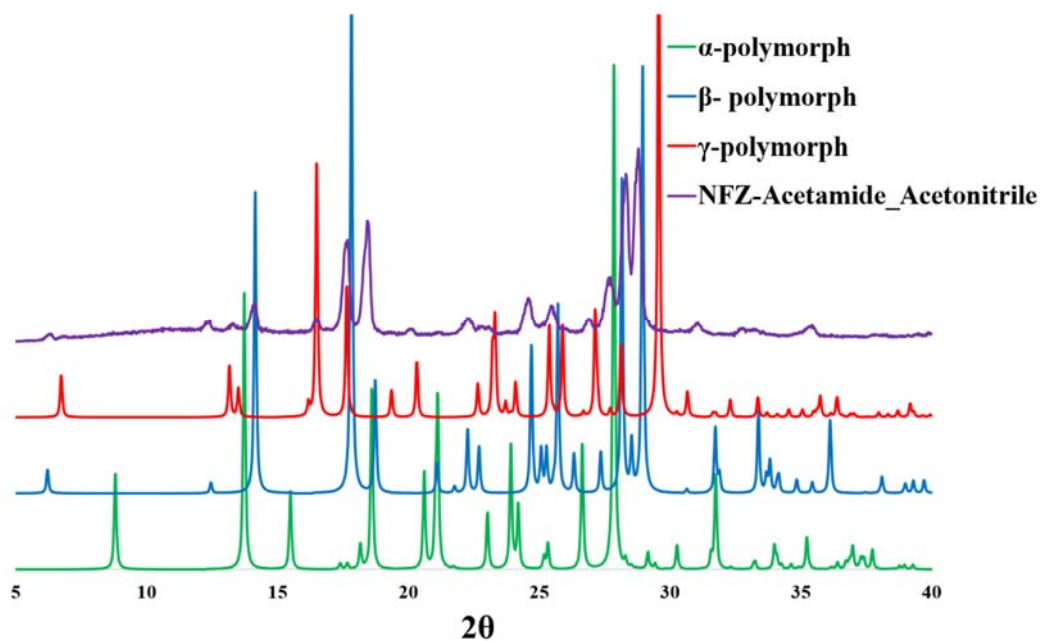


Figure A 15 PXR D patterns of α , β , and γ -polymorphs and the crystal obtained from acetamide:cetonitrile

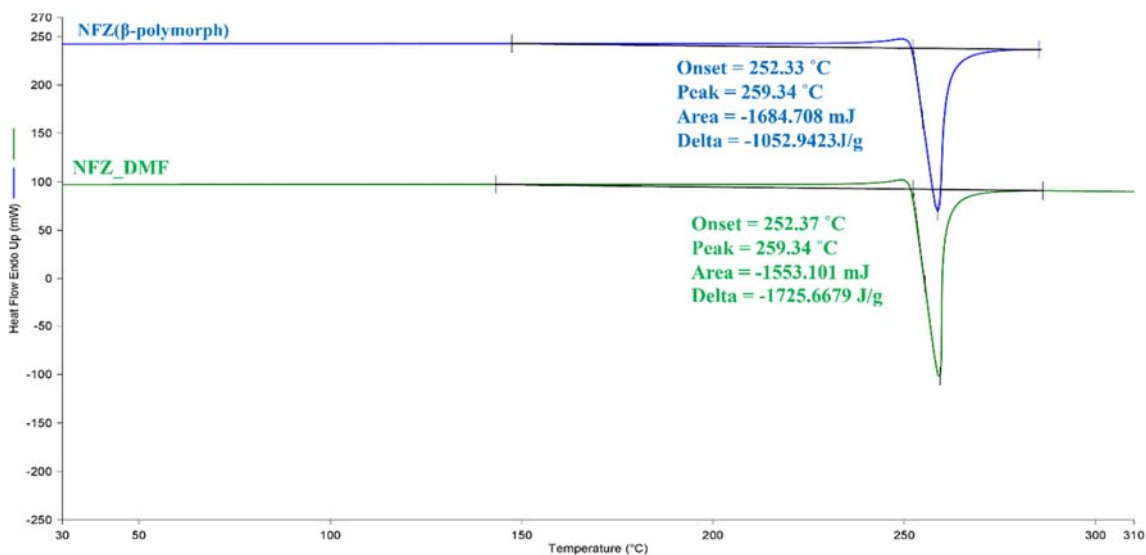


Figure A 16 DSC curves showing NFZ starting material and NFZ crystals obtained from dimethylformamide

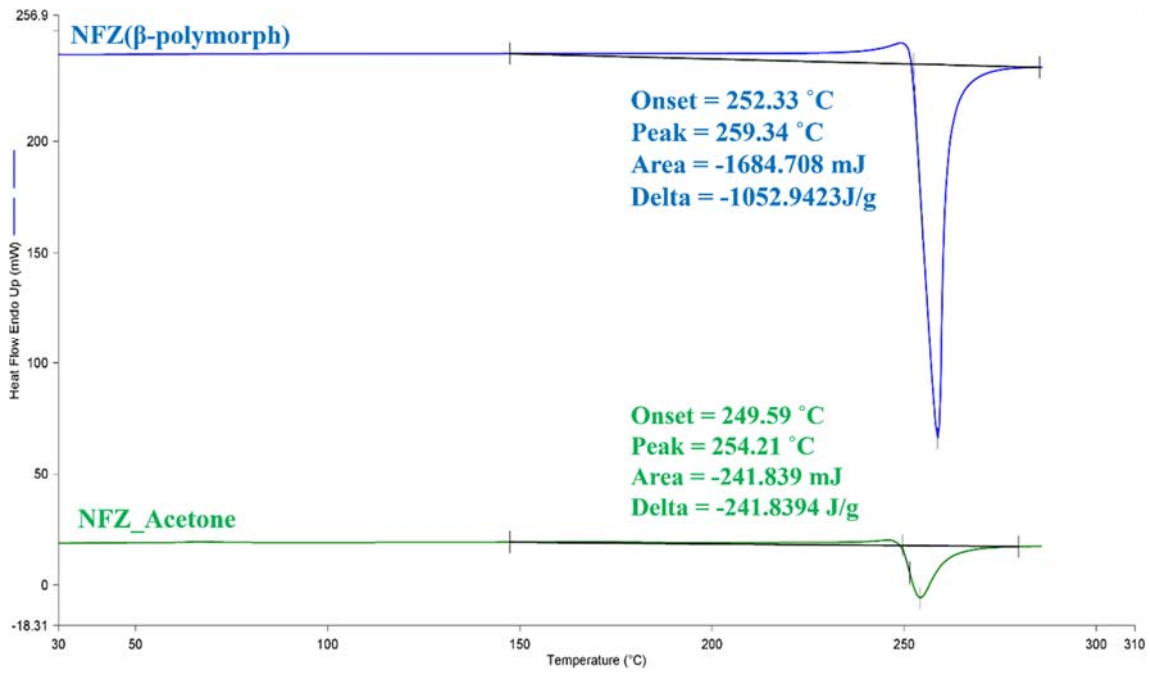


Figure A 17 DSC curves showing NFZ starting material and NFZ crystals obtained from acetone

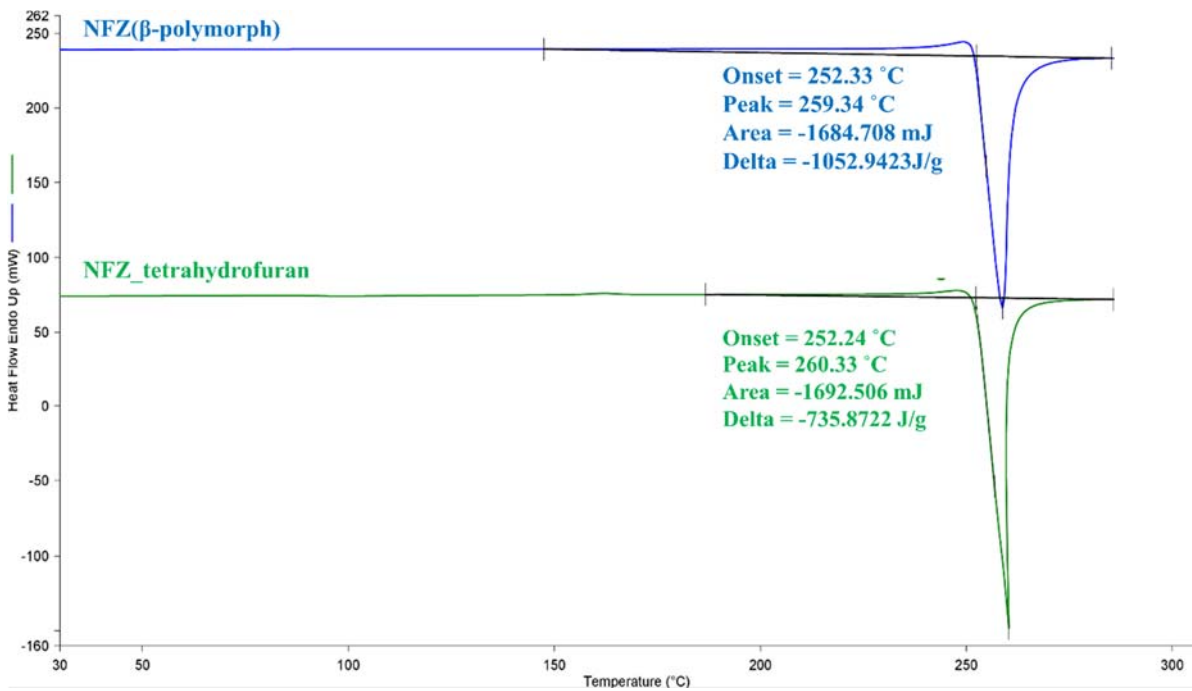


Figure A 18 DSC curves showing NFZ starting material and NFZ crystals obtained from tetrahydrofuran

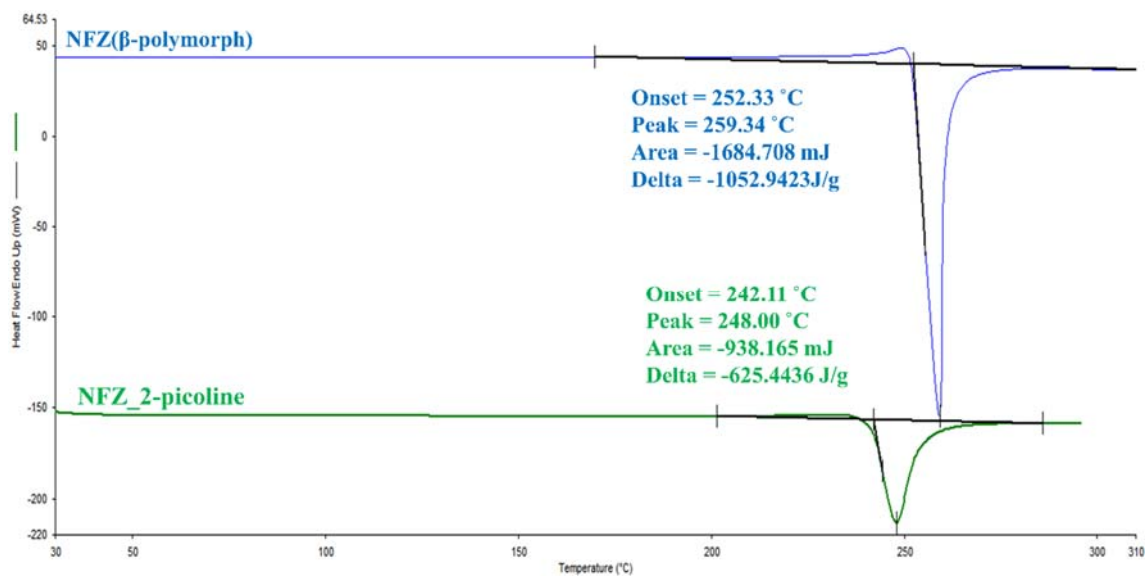


Figure A 19 DSC curves showing NFZ starting material and NFZ crystals obtained from 2-picoline

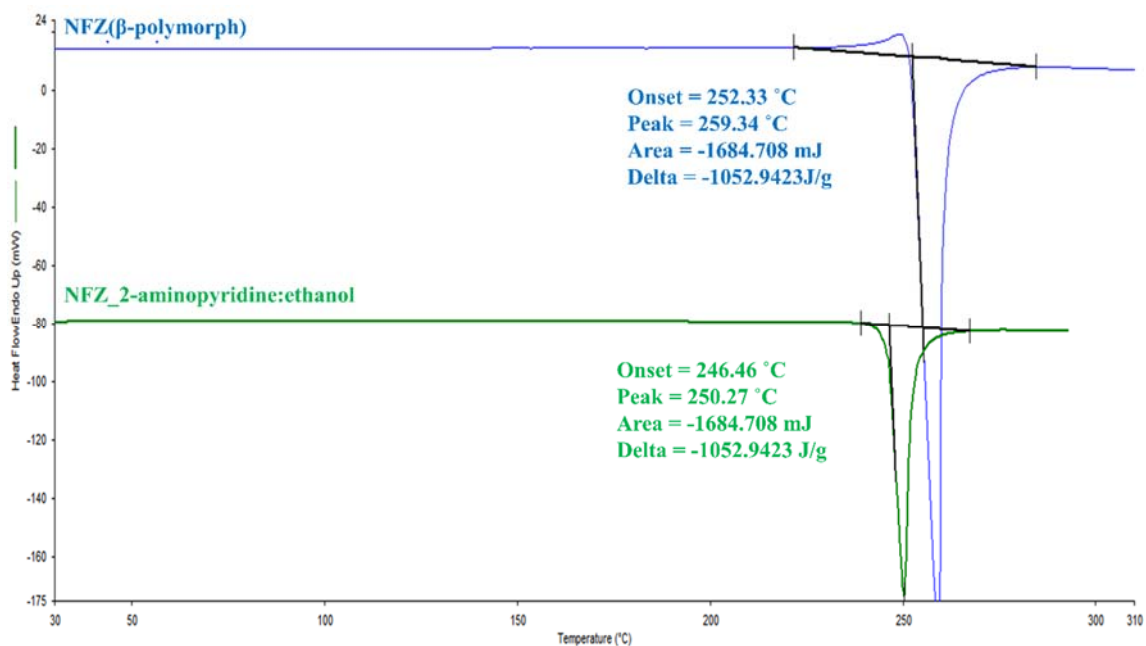


Figure A 20 DSC curves showing NFZ starting material and NFZ crystals obtained from 2-aminopyridine-ethanol

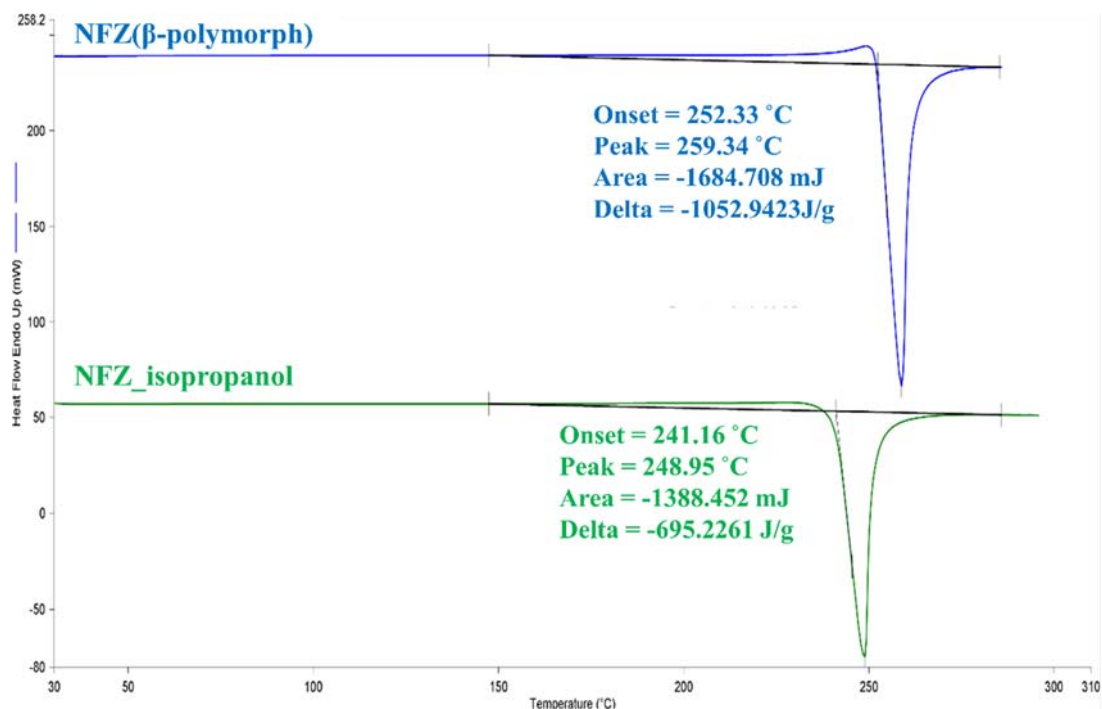


Figure A 21 DSC curves showing NFZ starting material and NFZ crystals obtained from isopropanol

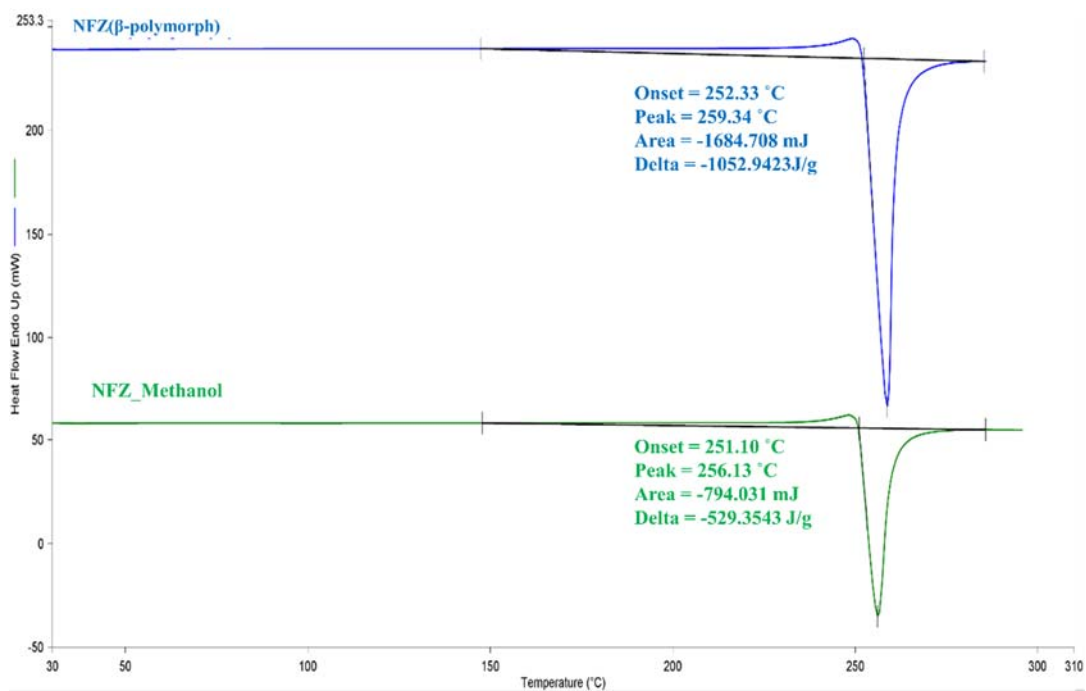


Figure A 22 DSC curves showing NFZ starting material and NFZ crystals obtained from methanol

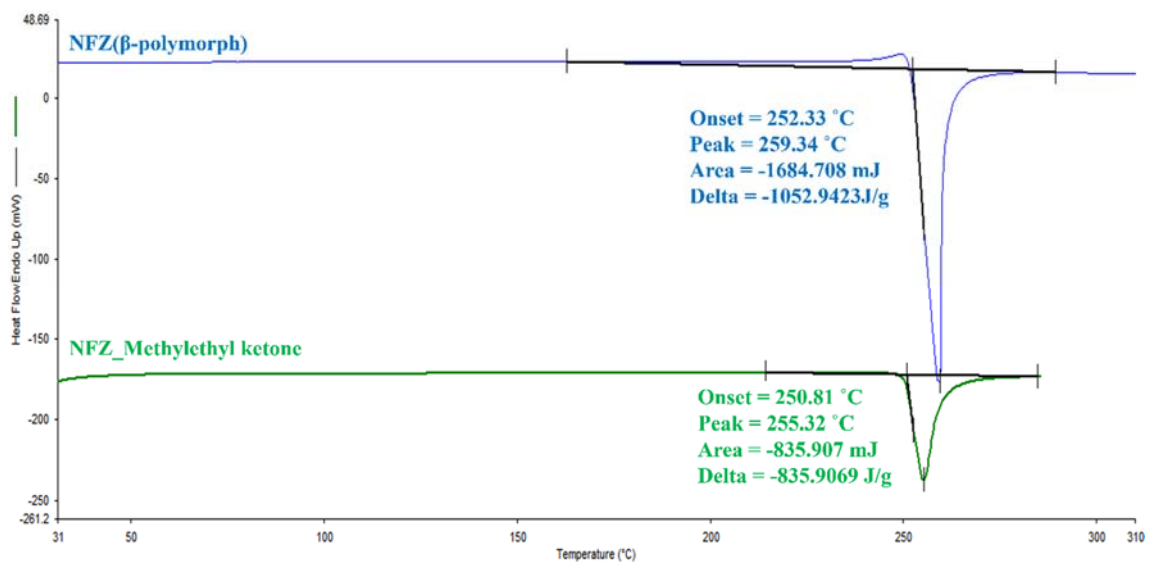


Figure A 23 DSC curves showing NFZ starting material and NFZ crystals obtained from methylethylketone

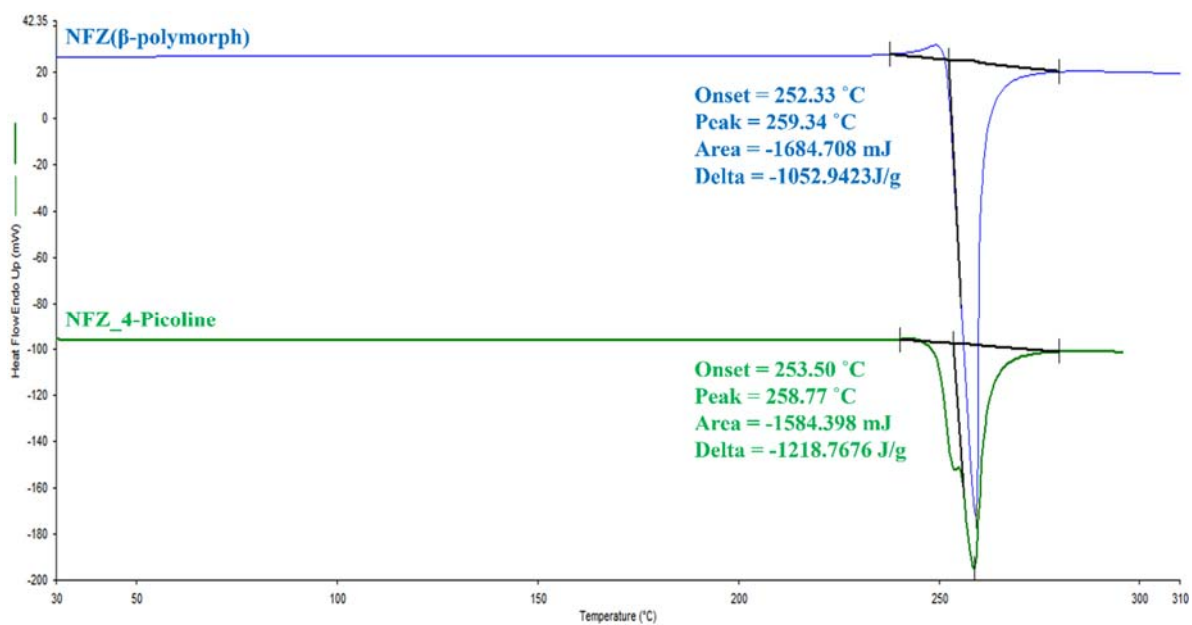


Figure A 24 DSC curves showing NFZ starting material and NFZ crystals obtained from 4-picoline

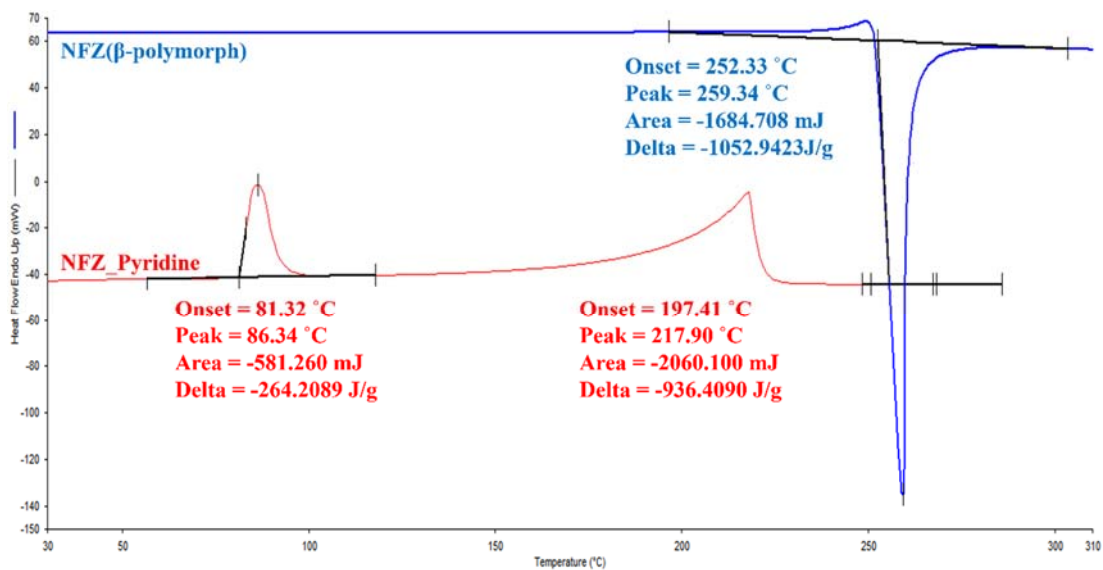


Figure A 25 DSC curves showing NFZ starting material and NFZ crystals obtained from pyridine

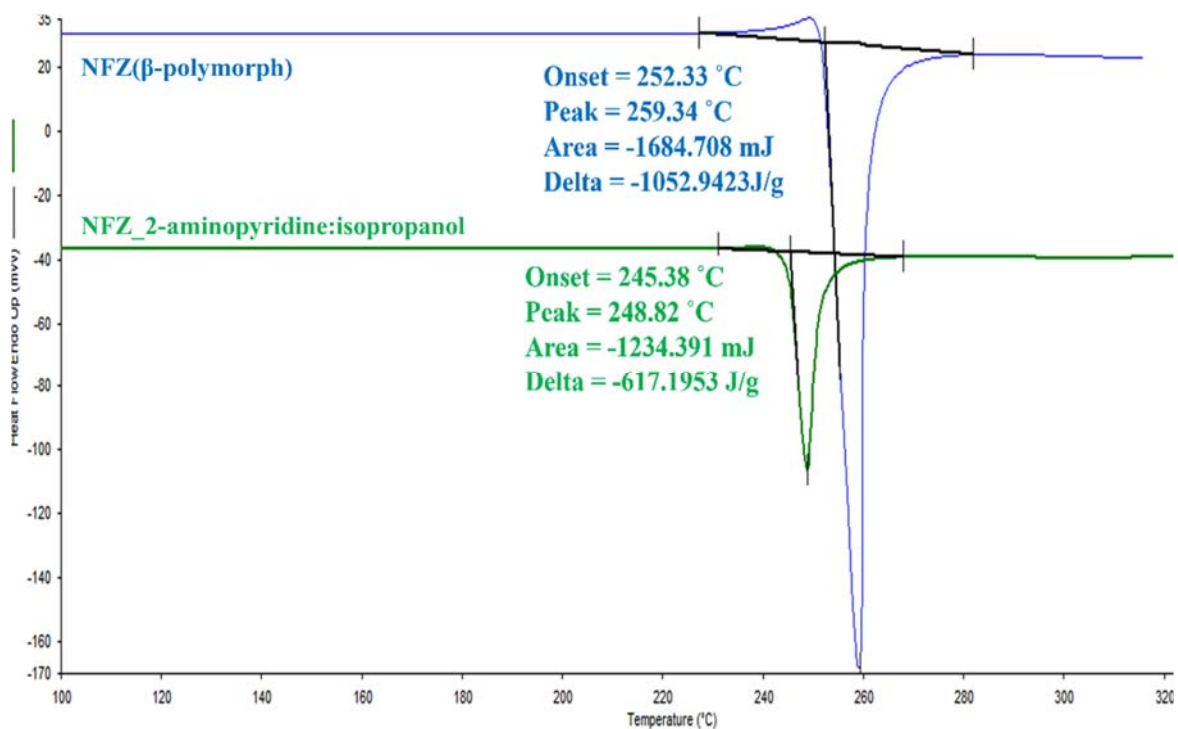


Figure A 26 DSC curves showing NFZ starting material and NFZ crystals obtained from 2-aminopyridine-isopropanol

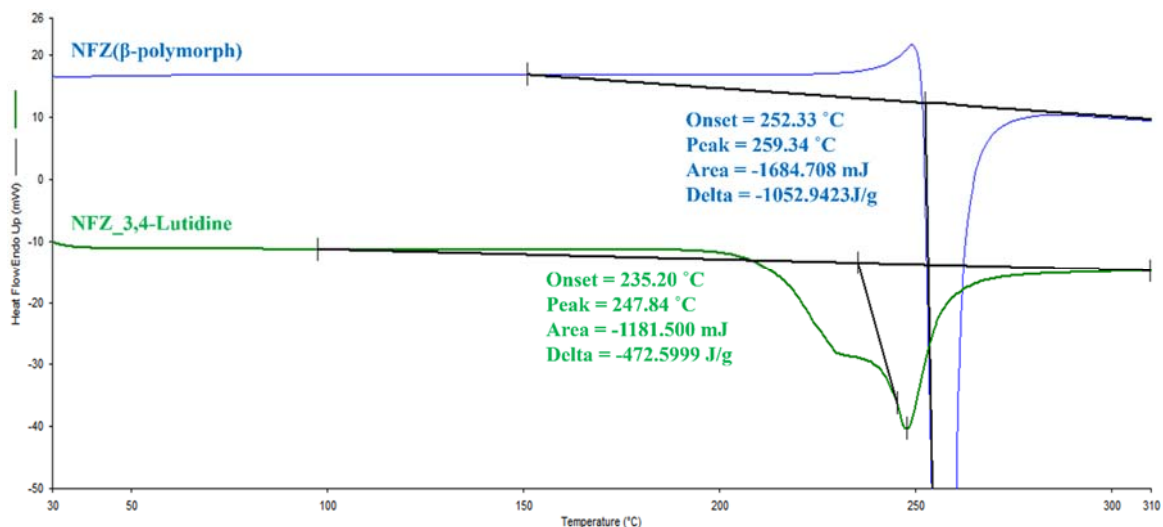


Figure A 27 DSC curves showing NFZ starting material and NFZ crystals obtained from 3,4-lutidine

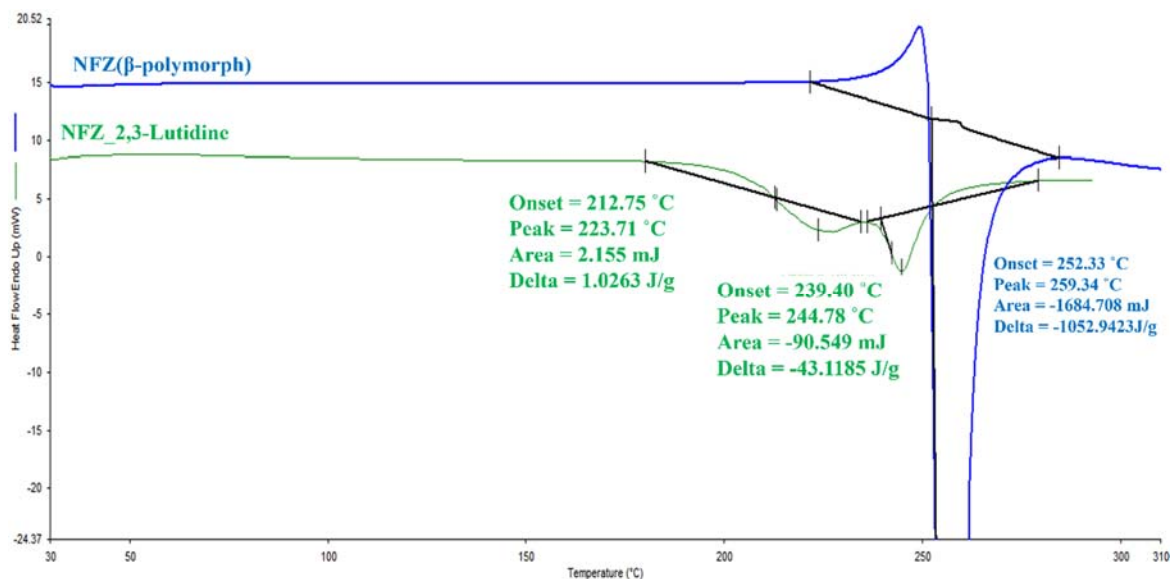


Figure A 28 DSC curves showing NFZ starting material and NFZ crystals obtained from 2,3-lutidine

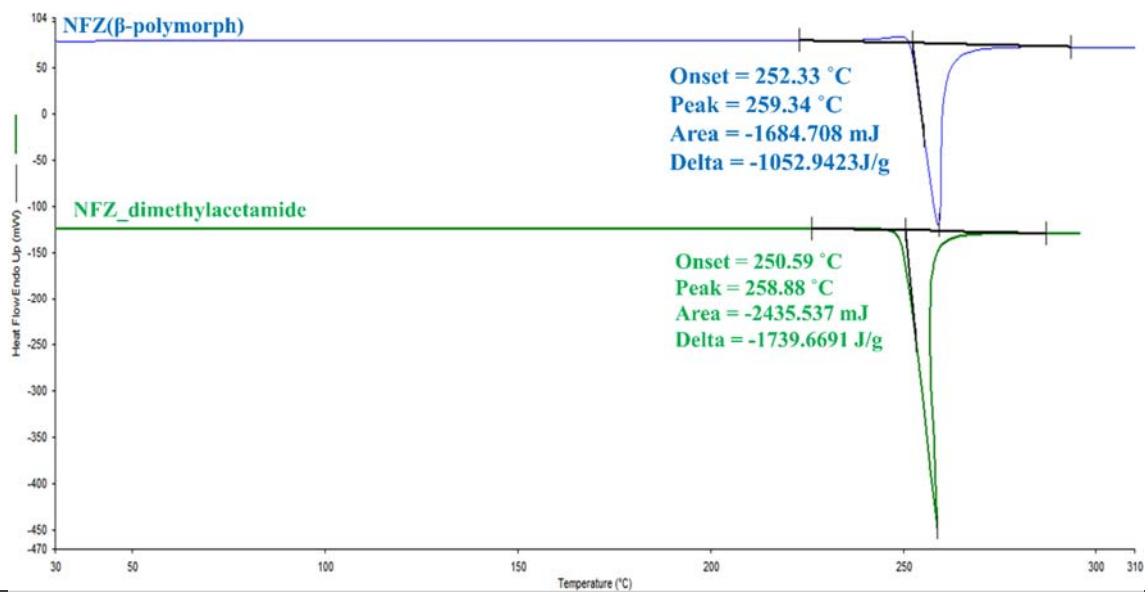


Figure A 29 DSC curves showing NFZ starting material and NFZ crystals obtained from dimethylacetamide

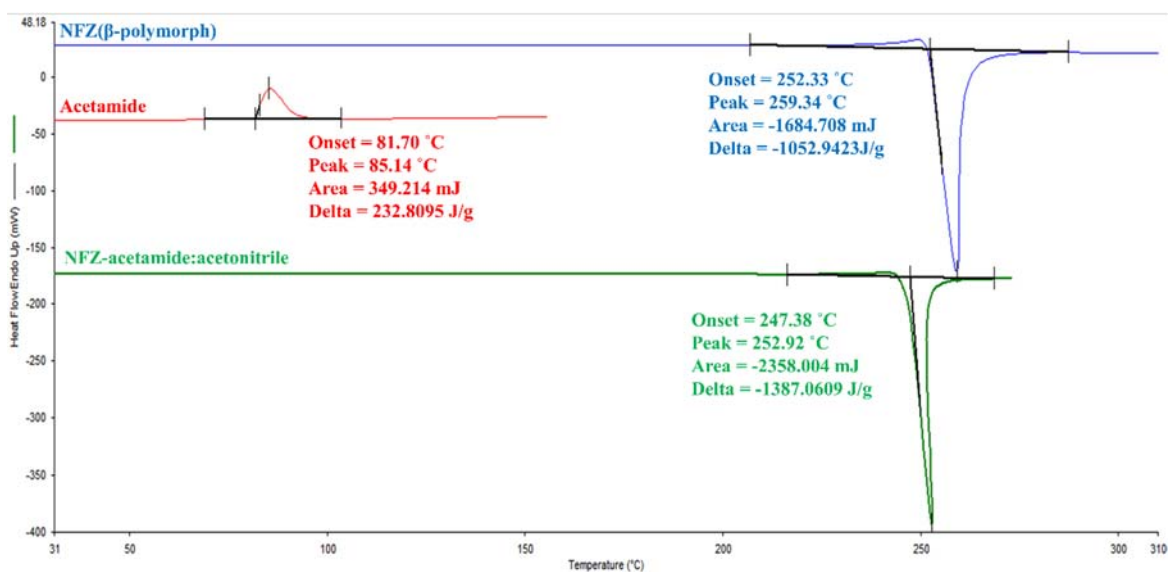


Figure A 30 DSC curves showing NFZ starting material and NFZ crystals obtained from acetamide:acetonitrile

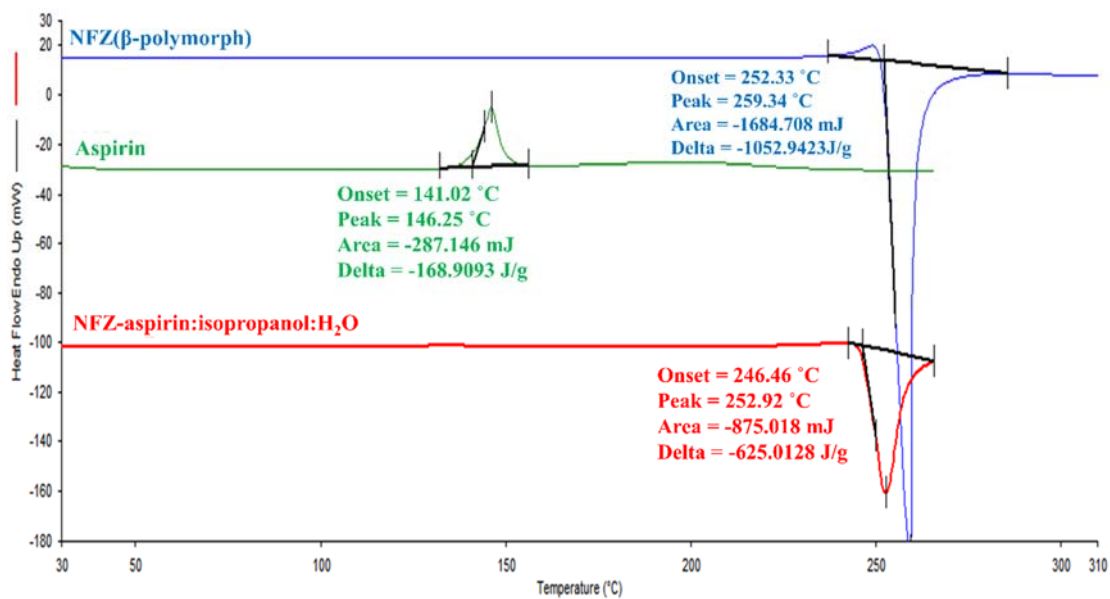


Figure A 31 DSC curves showing NFZ starting material and NFZ crystals obtained from aspirin:isopropanol:H₂O

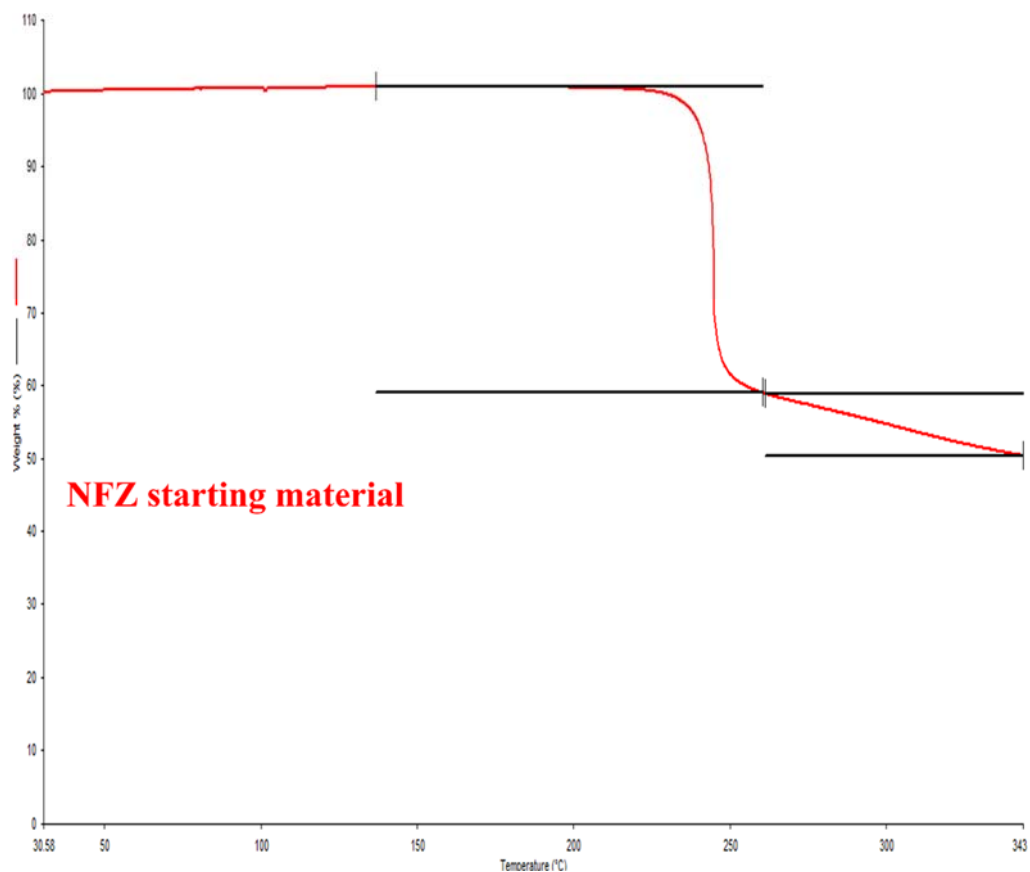


Figure A 32 Thermal analysis curve of NFZ starting material (β-polymorph)

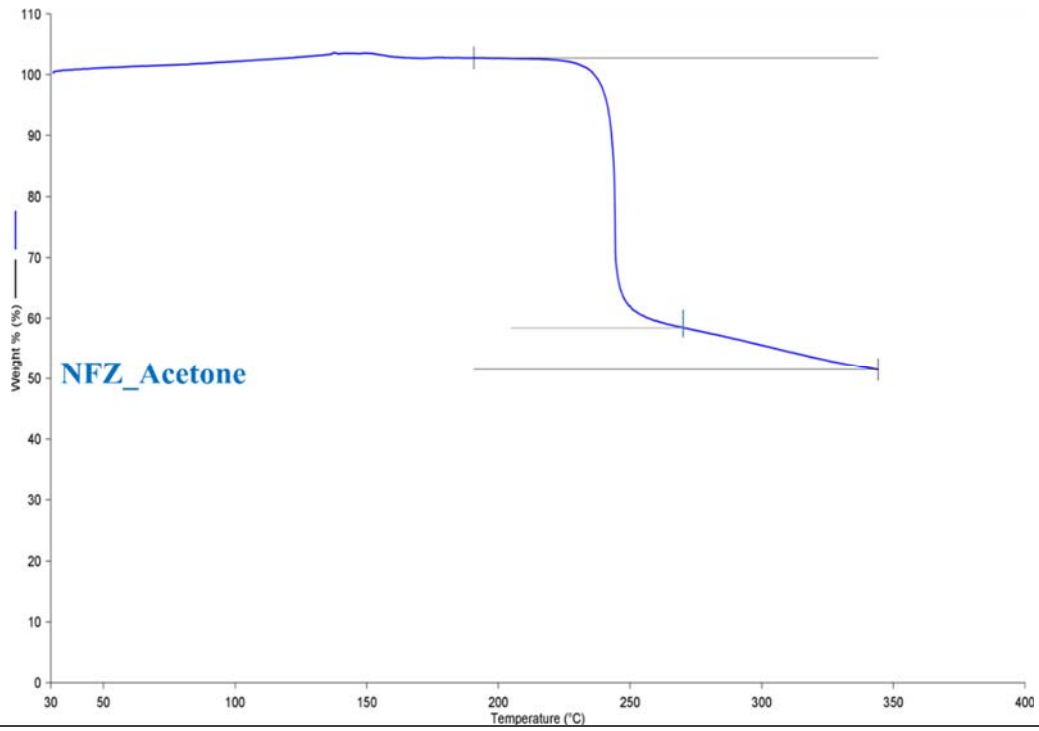


Figure A 33 Thermal analysis curve of NFZ_acetone crystals (α -polymorph)

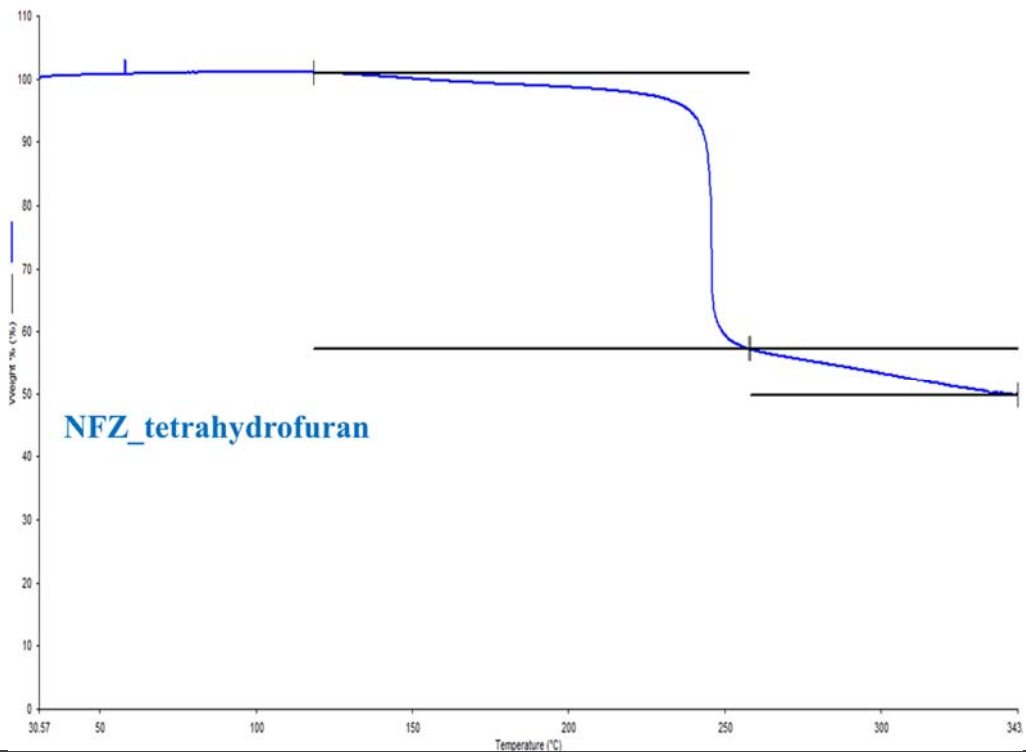
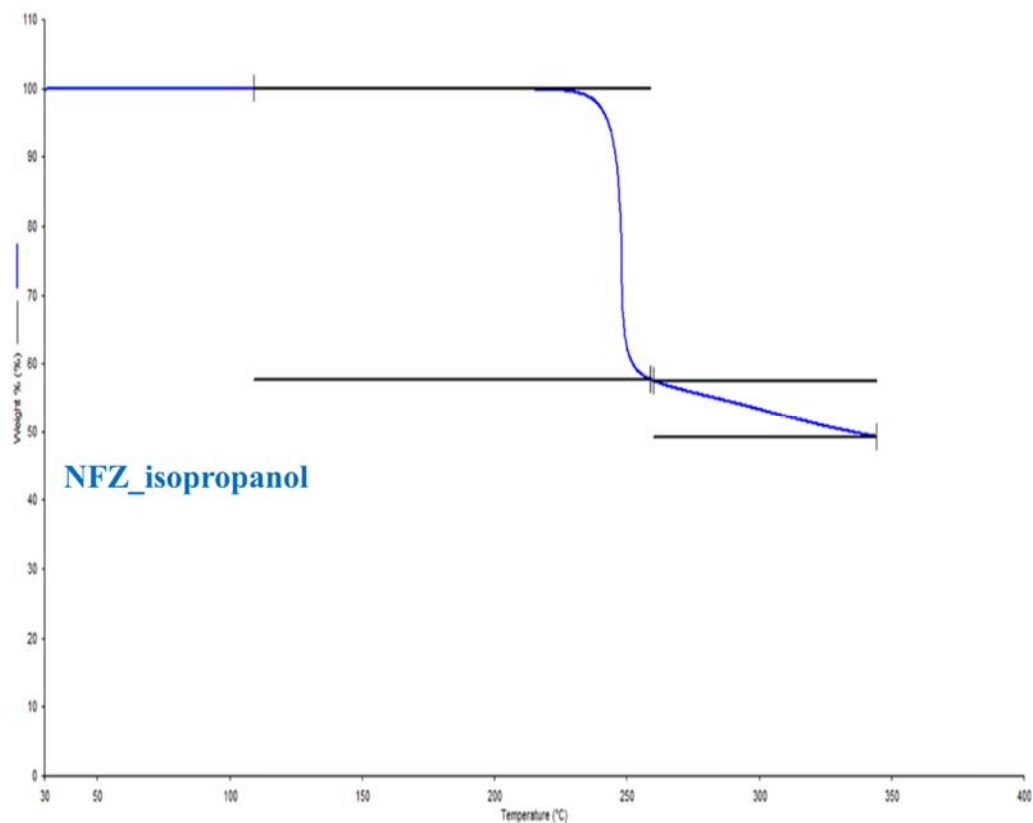
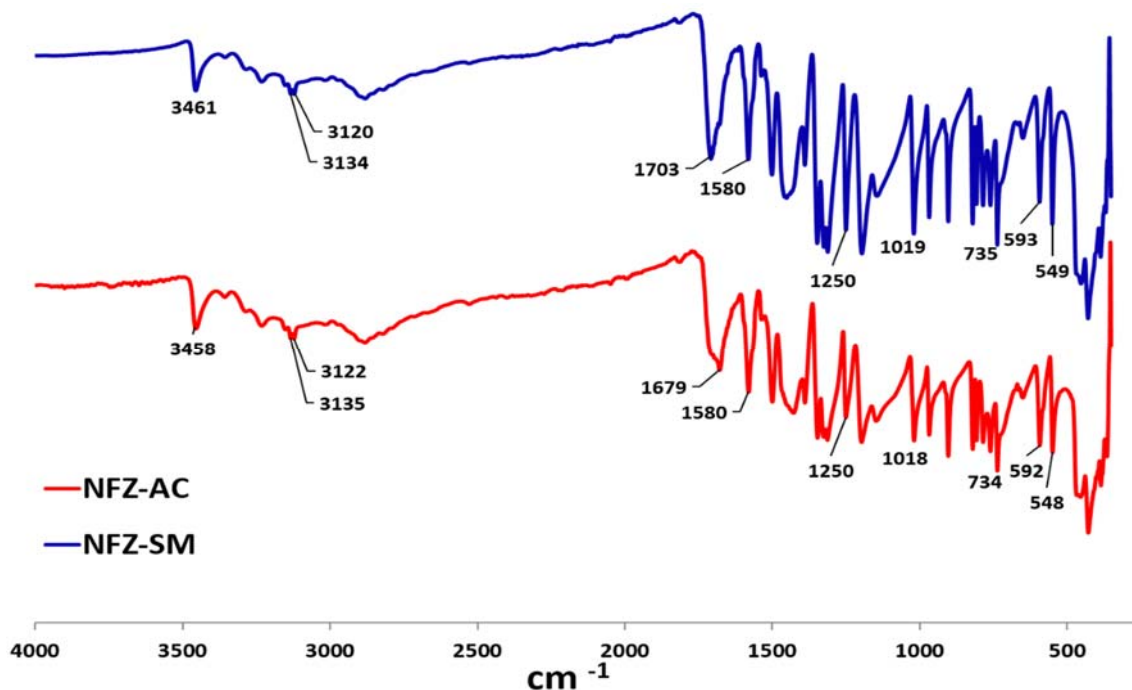


Figure A 34 Thermal analysis curve of NFZ_tetrahydrofuran crystals (β -polymorph)



NFZ_isopropanol

Figure A 35 Thermal analysis curve of NFZ_IPrOH crystals (γ -polymorph)



NFZ-AC

NFZ-SM

Figure A 36 Infra-red spectra of NFZ starting material and NFZ crystals obtained from acetone

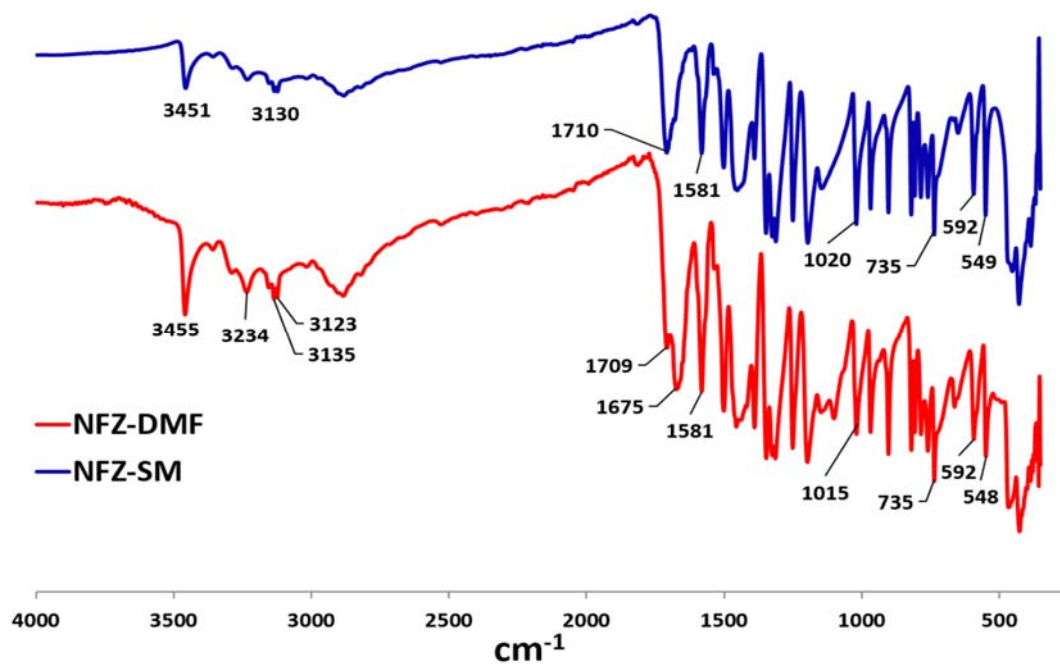


Figure A 37 Infra-red spectra of NFZ starting material and NFZ crystals obtained from dimethylformamide

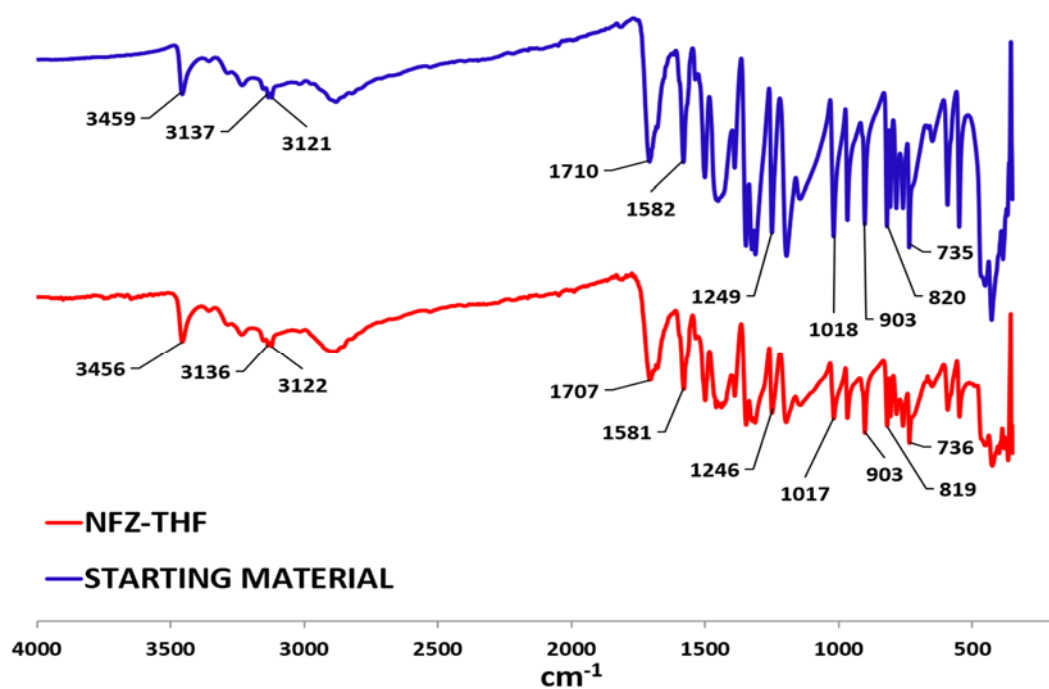


Figure A 38 Infra-red spectra of NFZ starting material and NFZ crystals obtained from tetrahydrofuran

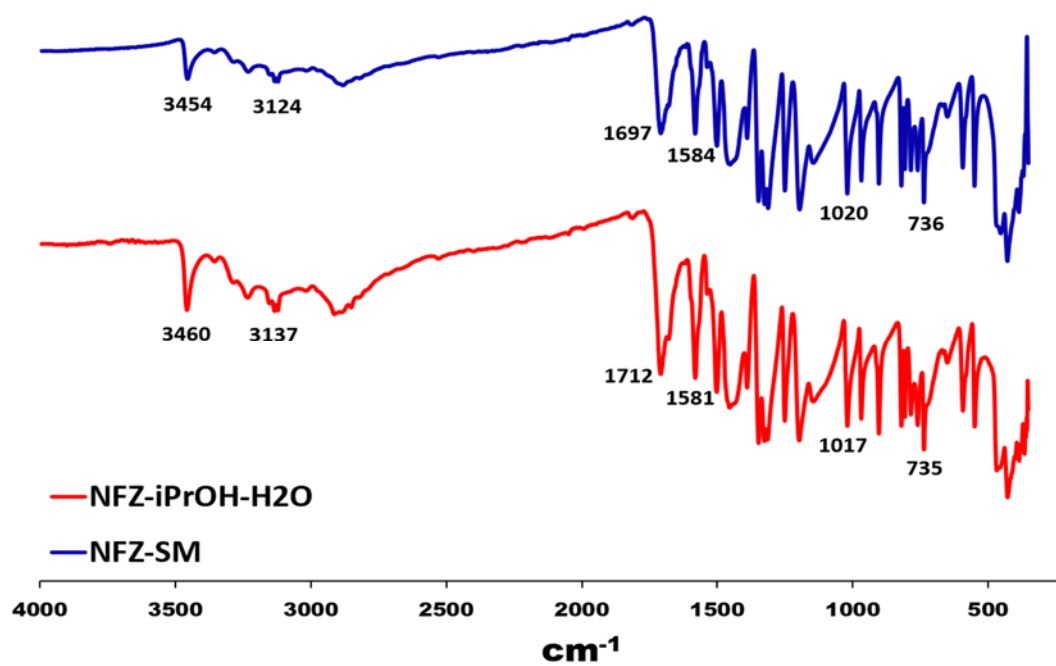


Figure A 39 Infra-red spectra of NFZ starting material and NFZ crystals obtained from isopropanol:H₂O